UNIVERSITAT DE BARCELONA

Primordial black holes and their implications for Inflation

Nikolaos Triantafyllou

Primordial black holes and their implications for Inflation

Nikolaos Triantafyllou

Supervisors: Jaume Garriga Torres and Vicente Atal

UNIVERSITAT DE BARCELONA

Departament de Física Quàntica i Astrofísica

Facultat de Física

Universitat de Barcelona

Primordial black holes and their implications for Inflation

Memòria presentada per optar al grau de doctor per la

Universitat de Barcelona

Programa de doctorat en Física

Autor: Nikolaos Triantafyllou

Directors: Jaume Garriga Torres i Vicente Atal

Tutor: Alberto Manrique Oliva

UNIVERSITAT DE BARCELONA

DECLARATION

This thesis is presented in accordance with the regulations of the University of Barcelona (*Aprovada pel CdG en sessió del 16 març de 2012 i modificada pel CdG de data 9 maig i 19 de juliol de 2012,29 de maig i 3 d'octubre de 2013, 17 juliol de 2014, 16 de juliol de 2015, 15 de juny i 21 de novembre de 2016, 5 de desembre de 2017, 4 de miag de 2018 i 15 de maig de 2019 i 22 de juliol de 2019*). The aforementioned regulations permit the submission and presentation of a PhD thesis as a "compendia of publications ". According to the regulations set by the University of Barcelona, the PhD thesis must be comprised of 3 publications. This thesis contains the necessary number of papers, rendering it eligible for submission and presentation.

Nikolaos Triantafyllou *Barcelona, July 2021*

ACKNOWLEDGEMENTS

It is exceptionally hard for a small section to contain the gratitude and respect I have for all of those people, who in one way or another, contributed to the completion of this thesis. Firstly, I would like to express how indebted I am to my PhD thesis advisor professor Jaume Garriga Torres and my co-director Dr. Vicente Atal for creating an ideal environment for me to grow as a physicist and as a person. Now, completing a PhD is mostly about one's hard word, devotion and dedication but in my case a major factor that played an instrumental part was the people with whom I shared my experiences as a pre-doctoral student. Therefore, I would like to thank my colleagues and friends, the inhabitants of office 4.10, Javi, Isa, Albert, Alan and Jairo for supporting me and mostly for putting up with my dancing around the room. Secondly, I would like to thank the foundation of Caixa not only for supporting me financially but also for granting me the opportunity to meet this extraordinary group of people: Milena, Albert, Katie and Sarah you brightened my days with your energy and laughters. I want to thank my friend Aaron for his unwavering encouragement and also for the hourly conversations we had about weird physical and mathematical topics while listening to techno. Additionally, although it may sound cliché, I would like to thank my friends Anastasis, Christos, Pantelis, Basilis, Thomas, Tasos for being there for me when I most needed it. Finally, this goes to my companion, Anna, for bearing with me every step of this long journey and to my beloved family for their unremitting support and encouragement over all these years.

Dedicated to my grandparents

ABSTRACT

The standard cosmological model, ΛCDM, with the addition of an early inflationary phase, provides an accurate description of a nearly flat and homogeneous Universe, at large scales, which expands at an accelerated rate. Despite its vindication, our knowledge of the components that trigger the early formation of structures and drive the accelerated expansion of the Universe, that is, dark matter (DM) and dark energy respectively, is severely limited, given their feeble interactions with the other components of the Universe. A number of candidates from particle physics, *e.g* weakly interacting massive particles (WIMPs) or axions, have been proposed to constitute DM, but so far there has been no evidence to support their existence. However, the detection of a signal from the merger of a binary of black holes of stellar masses, reinvigorated the interest in an old candidate for DM, namely primordial black holes (PBHs). These black holes behave as the ones sitting at the end of stellar evolution, with the distinctive differences that they may form in significant fractions even well before the appearance of the first stars, with masses that may range from the Planck mass, to the order of $M_{BH} \sim 10^{12}$ $M_{\odot}$. One possible formation mechanism involves perturbations originating from the fluctuations of a scalar field during inflation, that collapse after they re-enter the causal horizon in a radiation or matter domination era. The PBHs could easily form binaries in the early Universe and merge within our Hubble time, rendering them observable by the current detectors *LIGO/VIRGO*. The work presented in this thesis focuses on how such a population of PBHs could be utilised in order to elucidate certain spectral features of curvature perturbations characterizing the initial state of the Universe. Firstly, the effect of matter and radiation perturbations on the orbital parameter distributions of PBH binaries is studied. These perturbations are shown to provide a source of torque to the binary, particularly when their power spectrum is enhanced at the comoving scale of the binaries, leading to the suppression of the merger rate and subsequent relaxation of constraints on the PBH abundance. Secondly, the effect of primordial clustering on the distribution of orbital parameters of PBH binaries is investigated with the use of a phenomenological model of local non-Gaussianity. It is shown that due to the modal coupling of the perturbations,

the merger rate and the stochastic background of gravitational waves (SBGW) sourced by merging PBH binaries, are altered. An immediate result of clustering is that the observational constraint on the abundance of PBHs in DM is relaxed considerably, allowing for significant fractions, even close to totality. Thirdly, the possibility that the SBGW from the mergers of massive PBHs could provide an explanation for the recently detected isotropic signal by the *NANOGrav* collaboration is considered. The presence of non-Gaussianity, sourced from a phase of constant roll, is essential in order for such massive PBHs to evade the CMB μ-distortions constraints, in which case they may have formed in small abundances, of order 0.1% with respect to DM. The present work aims to provide a more robust modelling of the observational consequences of a population of PBHs in order to gain more insight into the spectrum of primordial perturbations at small scales and therefore into the initial conditions of the early Universe.

RESUMEN EN ESPAÑOL

El modelo cosmológico estándar, ΛCDM, con una temprana fase de inflación, nos proporciona una descripción precisa de un Universo casi plano y homogéneo a gran escala, que se expande a un ritmo acelerado. A pesar de las evidencias observacionales, nuestro conocimiento del 95% de la energía del Universo, es decir, la materia oscura (DM) y la energía oscura, está limitado por la falta de una detección directa, debido en parte a la poca interacción, aparte de la gravitacional, que tienen con el resto de la materia. La detección de la primera señal de un sistema binario de agujeros negros, revitalizó el interés por un viejo candidato a materia oscura, los agujeros negros primordiales (PBHs). Los PBHs han recibido atención dado que se pueden formar con abundancias importantes durante el Universo temprano y con una amplia gama de posibles masas. Esta tesis se centra en su empleo para explorar el espectro de potencias de las perturbaciones de curvatura a escala pequeña. Primero, se estudia el efecto de las perturbaciones cosmológicas sobre los parámetros orbitales de los sistemas binarios de PBHs. Cuando hay una meseta de amplitud considerable en el espectro de potencia en las escalas de los sistemas binarios, la tasa de fusión se ve afectada, relajando los limites de la abundancia de PBHs. Segundo, se muestra que debido al acoplamiento modal de las perturbaciones, introducido por la presencia de no-Gaussianidad, se alteran la tasa de fusión y el resultante fondo estocástico de las ondas gravitacionales (SBGW) y que esto tambien resulta en la relajación de las restricciones de la abundancia de PBH. Tercero, se considera la posibilidad de que el SBGW proveniente de los sistemas binarios de PBHs super masivos pueda proporcionar una explicación para la señal detectada por NANOGrav. La presencia de no-Gaussianidad es esencial para que estos PBHs masivos eviten las μ-distorsiones de la CMB y se puedan haberse formado en abundancias del orden $\sim 0,1\%$. Los PBHs constituyen una sonda única para explorar las condiciones iniciales del Universo y este trabajo pretende aportar un modelaje más robusto de las consecuencias observacionales de una población de PBHs.

Contents

1 Introduction

Understanding the forces that drive the evolution of the Universe as well as the intricate mechanisms that lead to the formation of the large structures we observe today, such as stars and galaxies, have been the prime quests of cosmology. The Hot Big Bang model offers a fairly accurate phenomenological description of the evolution of the Universe and the formation of subsequent large scale structures, from the moment of an initial singularity, to a radiation and then matter dominated era up to a late epoch where dark energy is accelerating the expansion. Although this description seems to offer a comforting picture, it does not address a number of features of the Universe, such as its flatness and homogeneity at cosmological scales. The introduction of a stage of accelerated expansion after the primordial singularity, though, provided the ideal mechanism in order to explain these properties. This mechanism is called inflation and it could also provide the primordial seeds of structure. In this Chapter, I will provide a simple layout of the fundamental ideas and principles of the cosmic inflation in its simplest form, namely the *slow-roll inflation* and how it could provide the initial conditions of the ΛCDM model. Also, I will discuss the natural embedding of primordial black holes in the picture of cosmological inflation.

1.1 The Cosmic Microwave Background Radiation and the Hot Big Bang model

The cosmic microwave background radiation, a coincidental detection by Penzias and Wilson in the 60s [1] that revolutionised the field of cosmology, offers us the first glance of the Universe in an infant stage of evolution. The CMB photons originated when the Universe started becoming transparent to radiation, around $t \sim 370.000$ years after the initial singularity, in the so called epoch of recombination.

At that moment the energy of the expanding Universe has sufficiently cooled down to scales of ~1 eV, allowing for the abundant formation of neutral hydrogen atoms and for the unhindered propagation of photons that have essentially decoupled from matter. The first mapping of the CMB radiation became available via the *Cosmic Background Explorer (COBE)* experiment [2], while in the years that followed surveys from the *WMAP* [3] and *Planck* [4, 5] collaborations, have corroborated the initial findings with increasing precision, pointing towards a black-body distribution of the CMB radiation, with a homogeneous temperature that has redshifted by today to $T \approx 2.7255$ K [4, 6]. These measurements implied that our Universe is homogeneous and flat at large cosmological scales ($k \lesssim 1$ Mpc^{-1}).

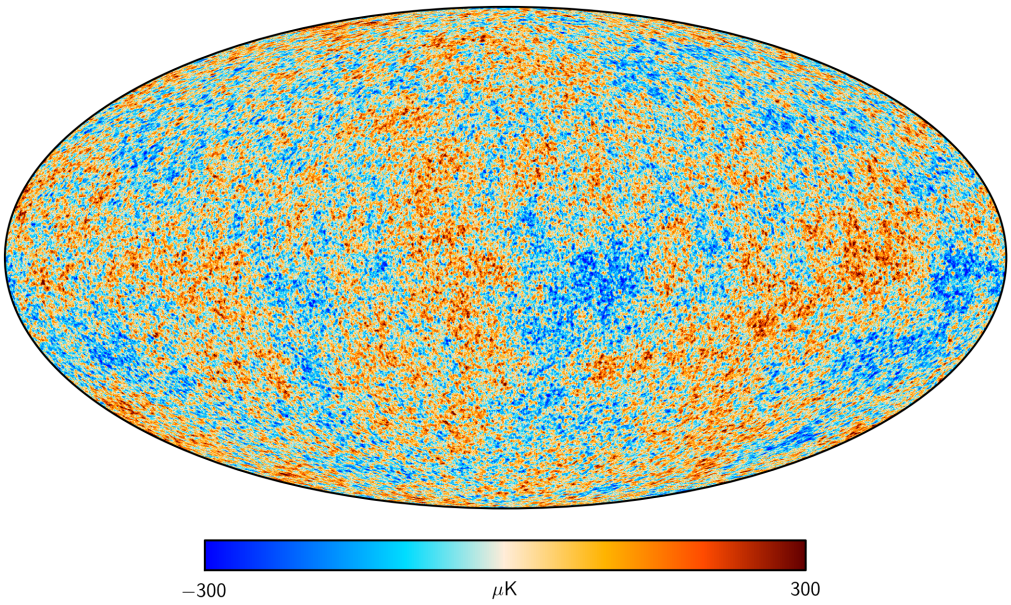

Figure 1.1: The map of temperature anisotropies in the CMB radiation as observed by Planck collaboration. The plot was adapted from [5].

Additionally, the CMB measurements revealed that there are deviations from the homogeneous and isotropic temperature distribution, of the order of $\Delta T/T \sim 10^{-5}$, as seen in Fig.1.1. The temperature anisotropies exhibited non-vanishing correlations at angles $\theta > 2\theta_{hor,rec} \sim 2.3°$, where $\theta_{hor,rec}$ measures the angle subtended by the comoving causal horizon at the time of recombination [7]. In what follows, I introduce the two main puzzles in the standard cosmological model, namely the *flatness* and the *horizon* problems. The standard Big Bang model, equipped with

a *Friedman-Robertson-Lemaître-Walker* (FRLW) metric, describes an expanding Universe, which is homogeneous and isotropic and has originated from a singularity around 13.7 billions years ago. Now, an important concept for the definition of the causal structure, is the particle horizon τ [1] , *i.e* the maximum comoving distance travelled by a photon from an initial time $t_i = 0$ up to a time t, given by

$$\tau = \int_0^t (aH)^{-1} d\,(\ln a), \tag{1.1}$$

where $a(t)$ is the scale factor and $H = \frac{\dot{a}}{a}$ is the Hubble rate. The particle horizon calculated at the present time t_0 can be thought of as a causal boundary between the observable and unobservable parts of our Universe. As the Universe expands, we expect the particle horizon to increase as well, meaning that we could receive information from larger comoving distances. This can be seen also if we look at the evolution of the comoving Hubble radius, $(aH)^{-1}$, given by

$$(aH)^{-1} \propto a(t)^{\frac{1}{2}(1+3w)}, \tag{1.2}$$

where $w = P/\rho$ is the equation of state of the dominant component of the Universe. For any type of matter that satisfies the strong energy condition, namely $\rho + 3P > 0$, the increasing comoving Hubble radius will lead to the expansion of the causal horizon τ, as

$$\tau \propto a(t)^{\frac{1}{2}(1+3w)}. \tag{1.3}$$

Now, the size of the particle horizon at the time of recombination will subtend an angle in the sky given by

$$\theta_{hor,rec} = \frac{\tau_{rec}}{\tau_0 - \tau_{rec}} \approx \frac{1}{\sqrt{1+z_{rec}}} \sim 2^\circ, \tag{1.4}$$

where $z_{rec} \sim 1100$. Therefore, regions in the sky that are separated by angles larger than $\theta_{hor} \gtrsim 2^\circ$, could not have been in causal contact at the time of recombination. The accurate measurements of the CMB have revealed, though, that points in the sky, separated by angles larger than θ_{hor}, exhibit a nearly homogeneous distribution of temperature, leading to the *horizon problem* of Big Bang cosmology, presented also in Fig.1.2.

[1] The particle horizon, with the speed of light c set to one is equivalent to the conformal time τ defined in Eq1.1. Basically, τ is the time required for a photon to reach the farthest observable distance of the Universe.

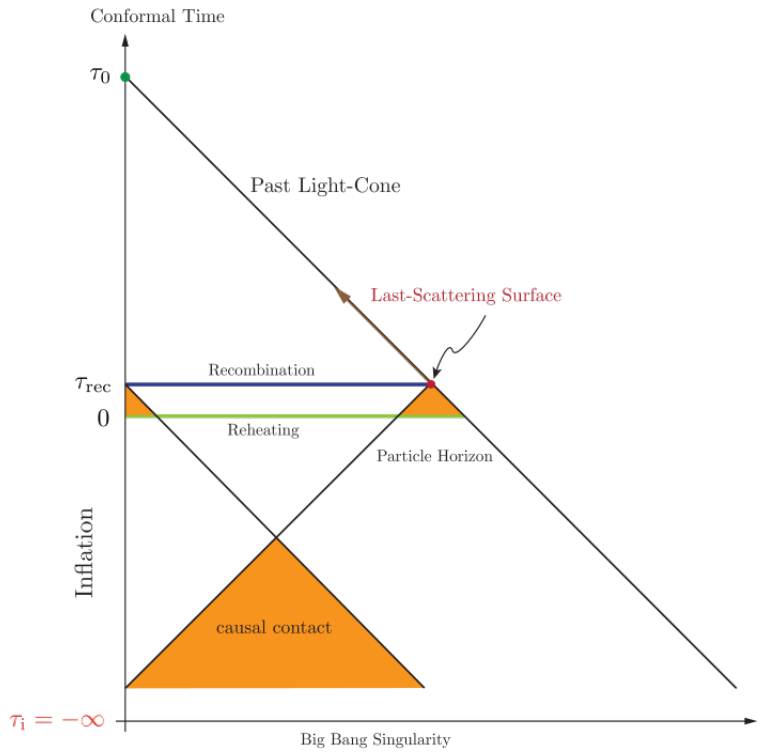

Figure 1.2: The horizon problem and its inflationary solution. The vertical axis represents the conformal time τ. The spacelike surface of recombination is represented here by the blue line. Note that two distant points on that surface couldn't have been in causal contact if the initial singularity was at $\tau = 0$. Instead, the decrease of the comoving Hubble radius during an era of cosmic inflation, ensures that the singularity is pushed to $\tau_{init} \to -\infty$ and now the green line at $\tau = 0$ represents the end of inflation and the onset of the reheating of the Universe. It is easy to see that any two points on the last scattering surface will have sufficient time to reach causal contact, thus resolving the puzzle of CMB homogeneity.

Another conundrum of the Big Bang cosmology involves the observed flatness of our Universe. In order to study the evolution of the spatial curvature of the Universe, the *Friedmann* equation needs to be introduced as

$$1 - \Omega(a) = \frac{-K}{(aH)^2}, \tag{1.5}$$

where $K = 0, +1, -1$ are the values for a flat, open or closed Universe respectively and $\Omega(a)$ is the normalised energy density parameter defined by

$$\Omega(a) = \frac{\rho(a)}{\rho_{crit}} \qquad \text{and} \qquad \rho_{crit} \equiv 3M_{PL}^2 H^2, \tag{1.6}$$

with ρ_{crit} being the critical density for the Universe to be flat and M_{PL} is the Planck mass. The measure of the curvature, $|1 - \Omega(a)|$, and its evolution are tightly connected with those of the comoving Hubble radius, $(aH)^{-1}$, as it is easy to note from Eq.(1.5). Now, we can see from Eq.(1.2) that if again the strong energy condition

is satisfied, $1+3w>0$, then the comoving Hubble radius grows, implying that for an initial value of $\Omega(a)>1$ the measure of curvature, $|1-\Omega(a)|$, would increase, whereas in the opposite case, $\Omega(a)<1$, it would decrease. Therefore, the fact that the spatial curvature of the Universe is observed to be of order $\mathcal{O}(0.001)$ [4], really close to being flat, poses an issue of initial conditions. By recasting Eq.(1.5) into the form

$$\frac{d\Omega}{d(\ln a)} = (1+3w)\Omega(a)(\Omega(a)-1)., \tag{1.7}$$

we can see that indeed $\Omega(a)=1$ is an unstable solution [7]. If $1+3w>0$, then the curvature $|1-\Omega(a)|$ would need to be a lot closer to one at earlier times, *e.g* $|1-\Omega(a_{GUT})| \lesssim 10^{-55}$, where a_{GUT} is the scale factor at the GUT energy scales [7]. This is the so called *flatness* problem.

A solution to both these problems that evades the need for any fine-tuning, is to introduce a stage in the evolution of the Universe where the comoving Hubble radius is shrinking [8, 9]. Such an era can be achieved via an early accelerated expansion of the Universe, a period called cosmological inflation. In Section 1.2 I will motivate how this solves the aforementioned problems and also how it provides an explanation for the CMB temperature anisotropies.

1.2 Cosmological Inflation

In this chapter I will present how cosmological inflation, specifically slow-roll inflation, provides a mechanism that not only solves the *horizon* and *flatness* problems but also produces an adiabatic, nearly scale-invariant power spectrum of Gaussian distributed primordial perturbations.

Before delving into the dynamics of inflation, I would briefly mention the conditions that need to be satisfied by matter in order to achieve such an accelerated expansion. As seen in Eqs.(1.1-1.3), the presence of a component that violates the strong energy condition, $1+3w<0$, will lead to the initial singularity being pushed to much earlier conformal times $\tau_{init}\rightarrow-\infty$ (see also Fig.1.2). Therefore, correlated regions on super-horizon scales at the time when the CMB radiation was emitted, could have been in causal contact earlier on. Similarly, the evolution of the curvature with the scale factor a, given in Eq.(1.7), shows that for $1+3w<0$, the Universe is attracted towards flatness, $\Omega(a)=1$. Therefore, the violation of the strong energy condition, could guarantee the resolution of both the *horizon* and *flatness* problem. Also, it is easy to note that if $1+3w<0$, then from Eq.(1.2) the comoving Hubble radius $(aH)^{-1}=(\dot{a})^{-1}$ is shrinking, which leads to $\ddot{a}>0$. Thus, if the dominant energy component has a sufficiently negative pressure, assuming a positive-definite energy density ρ, then this will lead to an accelerated expansion.

1.2.1 Single field inflation in the slow-roll regime

Inflation takes place at very early times when energies are extremely high [2]. One of the simplest ways to achieve such a phase of accelerated expansion is to assume that the energy density of the Universe is dominated by a scalar field, named "*inflaton*", that could have an equation of state obeying $1+3w<0$. The single-field inflationary model's predictions of a homogeneous, isotropic and flat Universe at large scales, exhibiting a spectrum of nearly scale-invariant, adiabatic Gaussian perturbations, match very closely the current CMB observations.

[2] Since inflation took place in the early Universe when energies were extremely high, it qualifies as a probe for high-energy physics that can not be accessed by terrestrial experiments, such as the ones taking place in the *Large Hadron Collider (LHC)*, but rather by surveys that intend to explore the cosmological scales.

We consider the field driving inflation to be minimally coupled to gravity and we write its action as

$$S = \int d^4x\sqrt{-g}\left[\frac{M_{PL}^2}{2}R - \frac{1}{2}g^{\mu\nu}\partial_\mu\partial_\nu\phi - V(\phi)\right], \tag{1.8}$$

where $g = det g_{\mu\nu}$, R is the *Ricci scalar* and $V(\phi)$ is the potential that is treated as an unknown function of the field ϕ. The liberty to choose the functional form of the potential, revealing our ignorance on the high-energy (UV) physics, has led to a plethora of models that currently can be tested by experiments, either by trying to map the anisotropies of CMB radiation, or by detecting the gravitational waves, sourced by tensor modes of the curvature fluctuations (see below in Section 1.32), or by any population of exotic inflationary byproducts, *i.e* domain walls, cosmic strings or primordial black holes [10, 11, 12].

Now, the evolution of the scalar field ϕ and the Hubble parameter H, are given by the Klein-Gordon and the Friedman equations, respectively defined as

$$\ddot{\phi} + 3H\dot{\phi} + V_{,\phi} = 0 \tag{1.9}$$

and

$$H^2 = \frac{1}{3M_{PL}^2}\left[\frac{1}{2}\dot{\phi}^2 + V(\phi)\right], \tag{1.10}$$

where the field ϕ is treated as a perfect fluid, homogeneous with no anisotropic pressure, $V_{,\phi} = \frac{dV}{d\phi}$ and the dot is the derivative with respect the time variable t. Assuming that the scalar field behaves as a perfect fluid, allows us to write its equation of state, defined below Eq.(1.2), as

$$w = \frac{\frac{1}{2}\dot{\phi}^2 - V(\phi)}{\frac{1}{2}\dot{\phi}^2 + V(\phi)}\,. \tag{1.11}$$

Then, it is easy to note that if the potential energy dominates the kinetic part, the the equation of state fulfills the condition in Eq.(**??**) and inflation takes place. For $V(\phi) \gg \frac{1}{2}\dot{\phi}^2$ we can think of the scalar field as slowly rolling from a plateau of the potential down to its minimum. In this slow-roll regime, the system of equations, given by Eq.(1.9) and Eq.(1.10), is reduced to a first order one,

$$3H\dot{\phi} \approx -V_{,\phi} \qquad \text{and} \qquad H^2 \approx \frac{V}{3M_{PL}^2}. \tag{1.12}$$

The solution $\phi(t)$ behaves as an attractor in the phase space $(\phi, \dot{\phi})$, called the *slow-roll attractor*, since its velocity $\dot{\phi} = \frac{d\phi}{dt}$ only depends on the shape of potential $V(\phi)$ and not on the initial conditions. The scale factor takes the form $a(t) \sim e^{Ht}$, with the Hubble parameter H slowly varying for the duration of inflation. This analytical solution resembles a *de Sitter* Universe, where the Hubble parameter is now exactly constant and $w = -1$. Any departure from such a *de Sitter* solution will be quantified using either the *Hubble slow-roll* parameters ϵ and η, or the equivalent *potential slow-roll* parameters ϵ_V and η_V defined correspondingly as

$$\epsilon \equiv -\frac{\dot{H}}{H^2} = \frac{\dot{\phi}^2}{2M_{PL}^2 H^2} \approx \frac{M_{PL}^2}{2}\left(\frac{V_{,\phi}}{V}\right)^2 \equiv \epsilon_V \quad \text{and} \quad \eta \equiv \frac{\ddot{H}}{H\dot{H}} - 2\frac{\dot{H}}{H^2} \approx \frac{M_{PL}^2}{2}\frac{|V_{,\phi\phi}|}{V} \equiv \eta_V, \tag{1.13}$$

where $V_{,\phi\phi} = \frac{d^2V}{d\phi^2}$ and as a time variable, we use the number of *e-folds* the Universe expanded during its inflationary phase, N [13, 7], defined as

$$N = \int_{a_i}^{a_f} d\ln a \approx \frac{1}{M_{PL}^2}\left|\int_{\phi_i}^{\phi_f} \frac{V(\phi)}{V'(\phi)\,d\phi}\right|, \tag{1.14}$$

where the approximate equality is a result of the use of (Eqs.1.13). Now, using the definitions in Eq.(**??**), it is easy to see that the necessary conditions for inflation to take place and the potential energy to dominate over the kinetic for sufficient time, thus resolving the *horizon* and *flatness* problems, are $\epsilon \ll 1$ and $\eta \ll 1$ (or equivalently $\epsilon_V \ll 1$ and $\eta_V \ll 1$). The comoving scale corresponding to our observable Universe has exited the horizon around $40-60$ *e-folds* before the end of inflation in order to explain the homogeneity of the Universe at large scale observed by CMB measurements.

1.2.2 The primordial power spectrum

The inflationary paradigm allows us to connect the quantum nature of the field, present during a phase of inflation, with the origin of structure at cosmological scales. The quantum nature of the inflaton field ϕ will give rise to differences, $\delta\phi(t,\mathbf{x}) = \phi(t,\mathbf{x}) - \bar{\phi}(t)$, where $\bar{\phi}(t)$ is the background value of the field. These fluctuations will be stretched to super-horizon scales, due to the accelerated expansion and consequent shrinking of the Hubble horizon during inflation, re-entering the

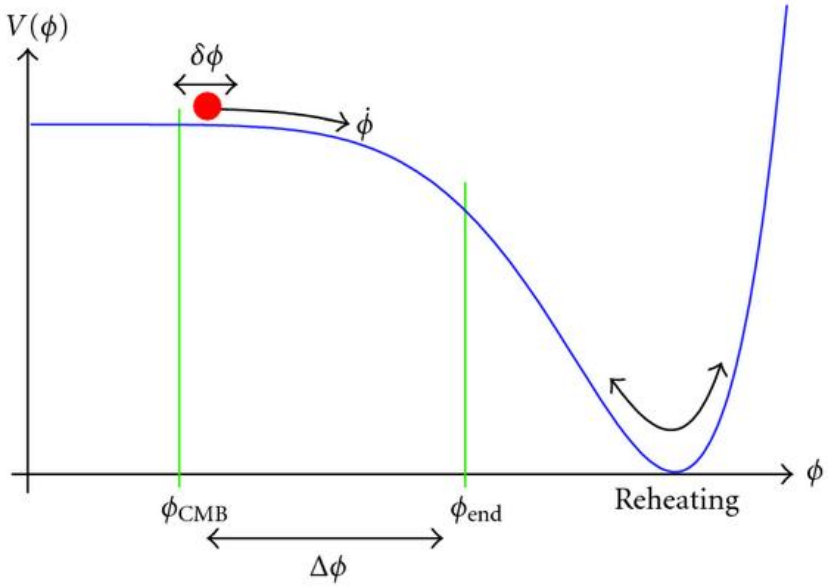

Figure 1.3: The inflationary potential $V(\phi)$ with the field ϕ slowly rolling from its plateau down to the true vacuum, where its kinetic energy will heat the universe, filling it with particles, a process called *reheating*. The primordial perturbations that have seeded the anisotropies we observe in the CMB power spectra, will have exited the causal horizon at the early stages of inflation when $\phi = \phi_{CMB}$ and they will keep exiting until slow-roll approximation breaks down, $\epsilon \sim 1$ and inflation ends. The plot was taken from [13].

causal patch at later times of radiation or matter domination [3]. This results in differences in the amounts of inflation experienced by different regions,

$$\delta N = -H\frac{\delta\phi(t,\mathbf{x})}{\dot{\phi}}, \tag{1.15}$$

that are subsequently translated into perturbations in the matter and radiation distributions and consequently seed the temperature anisotropies of the CMB radiation.

The generation and evolution of cosmological perturbations can be studied in the *Arnowitt-Deser-Misner (ADM) formalism* [7]. The spacetime is decomposed in 3-dimensional hypersurfaces and one time dimension, while the line element of the perturbed FRLW universe is written as

$$ds^2 = -N^2dt^2 + g_{ij}(dx^i + N^i dt)(dx^j + N^j dt), \tag{1.16}$$

[3] Note that when I mention that perturbations re-enter the causal horizon, I am referring to quantum fluctuations during inflation that are stretched to acausal distances, only to re-enter in the causal patch once the comoving Hubble radius matches their wavelength.

with $N(\mathbf{x})$ and $N_i(\mathbf{x})$ being the lapse and shift functions respectively and g_{ij} is the metric of the 3-dimensional hypersurfaces. Now, we can choose a gauge where the fluctuations in the inflaton are absorbed by the metric, $\delta\phi = 0$, and also write the metric with linearised perturbations as

$$g_{ij} = a^2(1-2\zeta)\delta_{ij} + a^2 h_{ij}, \tag{1.17}$$

where δ_{ij} is the 3-dimensional Kronecker symbol and h_{ij} is a traceless and transverse tensor that is related to the presence of primordial gravitational waves. The only physical scalar mode of the perturbations is identified with ζ, which represents the curvature of $\phi = const$ time slices. This definition is physical, therefore gauge-invariant. In a different gauge we can calculate ζ from the gauge invariant combination

$$\zeta = \mathscr{R} - \frac{aH}{\dot{\phi}}\delta\phi, \tag{1.18}$$

where $-4\nabla^2\mathscr{R}$ is the *Ricci scalar* of the new constant-time slices [7, 13]. In this discussion we have neglected the vector modes, since these are not generated to linear order in scalar field inflationary models.

Firstly, in order to study the scalar perturbations we have to expand the action Eq.(1.8) with respect to the physical degrees of freedom. Choosing ζ to represent the scalar modes of the perturbations is convenient, since the former remains constant on super-horizon scales, once the modes exit the causal horizon during a period of slow-roll inflation. Thus, ζ naturally relates the primordial fluctuations with the observed CMB anisotropies, opening a window to the early-time Universe. By expanding every term in Eq.(1.8) to the quadratic power of ζ and switching to the conformal time τ, the action takes the form

$$S = \frac{1}{2}\int d\tau d^3x\Big((v')^2 - (\partial_i v)^2 + \frac{z''}{z}\Big), \tag{1.19}$$

where $'$ is the differentiation with respect to τ and we have set $\mathrm{M_{PL}} = 1$, while using the Mukhanov-Sasaki variable $v = z\,\zeta$ with $z = a\sqrt{2\,\epsilon}$ [14, 15, 16]. Differentiating the quadratic action with respect to the variable v we arrive at the equation of motion in Fourier space written as

$$v_{\mathbf{k}}'' - \Big(k^2 - \frac{z''}{z}\Big)v_{\mathbf{k}} = 0. \tag{1.20}$$

The *Mukhanov-Sasaki equation*, as it is called, appears to be equivalent to the equation of motion of the harmonic oscillator with the only difference that the mass term, represented by

$$\frac{z''}{z} = \frac{H}{a\dot{\phi}} \frac{\partial^2}{\partial \tau^2} \frac{a\dot{\phi}}{H}, \tag{1.21}$$

induces a time dependence that reflects the interplay between the curvature perturbation and the time-dependent background. For modes with wavelengths larger than the comoving Hubble horizon and $k^2 \ll |z''/z|$, Eq.(1.20) has a growing solution $v_{\mathbf{k}} \propto \tau^{-1}$ resulting in $\zeta_{\boldsymbol{k}} = constant$. The next step in determining the solution of Eq.(1.20) involves the usual process of quantizing the harmonic oscillator by promoting the fields v and its conjugate momentum $\pi \equiv v'$ to quantum operators, $\hat{v}$ and $\hat{\pi}$ respectively. The operator $\hat{v}$ (the same expansion applies to $\hat{\pi}$ equivalently) can be expanded as follows

$$\hat{v} = \int \frac{d^3\mathbf{k}}{(2\pi)^{\frac{3}{2}}} \left[\hat{a}^-_{\mathbf{k}} v_k(\tau) e^{\imath \mathbf{k}\cdot\mathbf{x}} + \hat{a}^+_{\mathbf{k}} v^*_k(\tau) e^{-\imath \mathbf{k}\cdot\mathbf{x}} \right], \tag{1.22}$$

where $\hat{a_{\mathbf{k}}}^-$ and $\hat{a_{\mathbf{k}}}^+$ are the usual creation/annihilation operators that follow the equal-time commutation relations [4]

$$[\hat{a}^-_{\mathbf{k}}, \hat{a}^+_{\mathbf{k}'}] = \delta(\mathbf{k}-\mathbf{k}') \quad \text{and} \quad [\hat{a}^-_{\mathbf{k}}, \hat{a}^-_{\mathbf{k}'}] = [\hat{a}^+_{\mathbf{k}}, \hat{a}^+_{\mathbf{k}'}] = \delta(\mathbf{k}-\mathbf{k}') = 0. \tag{1.23}$$

The mode functions $v_k(\tau)$, $v^*_k(\tau)$ are solutions to the *Mukhanov-Sasaki equation* such that the *Wronskian* is normalised to $W(v_k, v^*_k) = v'_k v^*_k - v'^*_k v_k = -\imath$. In time-independent spacetimes, such as Minkowski, there is a unique way of defining a ground state by demanding that the vacuum expectation value of the Hamiltonian [5] is minimised. Such a construction is not so useful when dealing with a time-dependent background, *e.g* the *quasi de-Sitter* spacetime of slow-roll inflation, where $\omega_{\mathbf{k}} = k^2 - z''/z$, because for each conformal time $\tau = \tau_o$ there is a different state that minimises the Hamiltonian, thus introducing a degree of uncertainty when choosing the physical vacuum state. If we consider, though, that at very early times, during inflation, $|k\tau| \gg 1$, then the time dependence of the frequency ω_k is lifted and the *Mukhanov-Sasaki equation* reduces to the one for Minkowski space,

[4] These commutation relations are derived from $[\hat{v}(\tau,\mathbf{x}), \hat{\pi}(\tau,\mathbf{y})] = \imath\,\hbar\,\delta(\mathbf{x}-\mathbf{y})$ and $[\hat{v}(\tau,\mathbf{x}), \hat{v}(\tau,\mathbf{y})] = [\hat{\pi}(\tau,\mathbf{x}), \hat{\pi}(\tau,\mathbf{y})] = 0$.

[5] The Hamiltonian is written as $\hat{H} = \frac{1}{2}\int d^3\mathbf{x} \left[\hat{\pi}^2 + (\partial_i \hat{v})^2 - \frac{z''}{z}\hat{v}^2 \right]$.

which is

$$v_k'' + k^2 v_k = 0. \tag{1.24}$$

The solution that minimises the vacuum expectation value in Minkowski space is $v_k = \frac{1}{\sqrt{2k}} e^{-\imath k\tau}$. Therefore, in the inflationary quasi-de Sitter space, by picking the mode functions that satisfy the condition

$$\lim_{\tau\to-\infty} v_k(\tau) = \frac{1}{\sqrt{2k}} e^{-\imath k\tau}, \tag{1.25}$$

a unique vacuum state is defined, the *Bunch-Davies vacuum state*. Once the initial conditions are unequivocally defined, the zero-point fluctuations of the quantized scalar field v are given by

$$\langle \hat{v}_{\mathbf{k}} \hat{v}_{\mathbf{k}'} \rangle = \langle 0|\hat{v}_{\mathbf{k}} \hat{v}_{\mathbf{k}'}|0\rangle = \langle 0|(a^-_{\mathbf{k}} v_k + a^+_{-\mathbf{k}} v_k^*)(a^-_{\mathbf{k}'} v_{k'} + a^+_{-\mathbf{k}'} v_{k'}^*)|0\rangle = P_v(k)\delta(\mathbf{k}+\mathbf{k}'), \tag{1.26}$$

where $P_v(k) = |v_k|^2$ is the power spectrum of the perturbations of the field v. Switching variables to $v = z\,\zeta$, allows us to exploit the fact that ζ is constant on super-horizon scales in order to define the dimensionless power spectrum of primordial perturbations at horizon crossing ($k \sim aH$)

$$P_\zeta(k) = \frac{k^3}{2\pi^2 z^2} P_v(k) = \frac{1}{4\pi^2} \frac{H^4}{\dot{\phi}^2}\bigg|_{k=aH} = \frac{1}{8\pi^2} \frac{H^2}{\epsilon}\bigg|_{k=aH}. \tag{1.27}$$

Since $P_\zeta(k)$ is only a function of k that varies slowly, it is customary to use a power-law fit $P_\zeta(k) = A(k_0)\left(\frac{k}{k_0}\right)^{n_s-1}$, with the scale k_0 being chosen as the pivot scale where the errors coming from observations are minimised (for the measurements of the CMB anisotropies the pivot scale is $k_0 = 0.05 Mpc^{-1}$) [4] and the *spectral index* is defined as

$$n_s - 1 \equiv \frac{d\ln P_\zeta}{d\ln k}. \tag{1.28}$$

Now, for a quasi-de Sitter space, if we expand Eq.(1.20) with respect to the slow-roll parameters $\epsilon \ll 1$ and $\eta \ll 1$, keeping only the first order in the super-horizon limit ($|k\tau| \gg 1$), we find that the spectral index is given by

$$n_s - 1 = -2\epsilon - \eta. \tag{1.29}$$

This equation exemplifies how the slow-roll parameters quantify the deviation of the Universe from a scale-invariant ($n_s = 1$) de Sitter space. WMAP [3] and lately the Planck collaboration [4], having conducted a very precise measurement of

the CMB temperature anisotropies, were able to detect such departures with a red-tilted ($n_s < 1$) power spectrum for the curvature perturbations and also place stringent bounds on its spectral index at the 1-σ level, $n_s = 0.966 \pm 0.004$ [4, 5].

Besides the scalar perturbations, we have also tensor modes described by the traceless and transverse tensor h_{ij}, defined below Eq.(1.16). Similarly, we can expand the action Eq.(1.8) up to second order for h_{ij} and write

$$S = \sum_{\gamma} \frac{1}{2} \int d\tau d^3\mathbf{k} \Big[(v'_{\mathbf{k},\gamma})^2 - \big(k^2 - \frac{a''}{a}\big) v^2_{\mathbf{k},\gamma} \Big]. \tag{1.30}$$

The sum is over the polarisation of the tensor field $\gamma = (+, \times)$ and the normalised field $v_{\mathbf{k},\gamma} = \frac{a(t)}{2} M_{PL} h_{\mathbf{k},\gamma}$ is used instead of the Fourier modes $h_{\mathbf{k},\gamma}$. The equations of motion of these tensor modes have the same form as Eq.(1.20), meaning that the dimensionless power spectrum of the primordial gravitational waves calculated at horizon crossing can be written as

$$P_t(k) = \frac{2}{\pi^2} \frac{H^2}{M^2_{PL}} \Big|_{k=aH}. \tag{1.31}$$

We note that $P_t(k) = 2P_h(k)$ is the sum of the power spectra for the modes with the two distinct polarisations and it only depends on the Hubble parameter at horizon crossing. An important observational quantity that relates the amplitudes of both scalar and tensor perturbations and can be used as a discriminator between the predictions of various inflationary models, namely the tensor-to-scalar ratio, is defined as

$$r = \frac{P_t(k)}{P_\zeta(k)} = \frac{8}{M^2_{PL}} \frac{\dot{\phi}^2}{H^2} = 16\,\epsilon, \tag{1.32}$$

where the Eq.(1.27) and Eq.(1.31) were used. Furthermore, the fact that the power spectrum of tensor modes depends only on the Hubble rate at horizon crossing, renders gravitational waves an ideal probe for the energy scale of inflation since we have that

$$V^{1/4} \sim \Big(\frac{r}{0.01}\Big)^{1/4} \; 10^{16} \text{ GeV}. \tag{1.33}$$

The fact that the tensor-to-scalar ratio, as seen in Eq.(1.32), depends on ϵ, implies that inflation produces an amplitude of the tensor modes that is subdominant to the scalar one, a prediction that is corroborated by Planck measurements of the CMB, where values of $r < 0.1$ are favoured by the data, also seen in Fig.1.4.

One way to probe the existence of these modes involves looking at the signatures of both scalar and tensor perturbations on the CMB linear polarisation field. In general, the linear polarisation field of the CMB radiation can be decomposed into two modes, in particular into the so called the E and B modes. It was found that the scalar and tensor modes leave distinct imprints on the angular CMB power spectra, with the former creating only *E-modes* while the latter generating *B-modes* as well. Now, the presence of primordial *B-modes* reveals the existence of primordial tensor modes. Such a signal, however, has not been detected, possibly due to its inherently small amplitude and to various sources of background noise and foreground contamination. Nonetheless, the combined data of temperature and *E-polarisation* anisotropies from Planck [17] and the *B-polarisation* measurements from *BICEP/Keck Array (BK15)* [18] have placed the tightest bounds on the tensor-to-scalar ratio at the pivot scale $k_{pivot} = 0.002$ Mpc^{-1}, reporting an upper limit of $r < 0.056$ at the 95% confidence level. This immediately translates into an upper bound on the energy scale of inflation $V^{1/4} < 1.6 \cdot 10^{16}$ GeV, given by Eq.(1.33). Furthermore, the values for $n_s - r$ coming from Planck, *Baryon Acoustic Oscillations (BAO)* and *BICEP/Keck Array*, have already disfavoured some models with a power-law potential, such as the chaotic models of inflation, pointing towards concave potentials (where $\frac{d^2V}{d\phi^2} < 0$ when CMB scales exit the horizon), as depicted in Fig.1.4. Future measurements of CMB radiation by experiments such as PIXIE [19] and LiteBIRD [20], aim to probe the tensor-to-scale ratio down to values of $r \sim \mathcal{O}(10^{-3})$. On the other hand, a non-detection of primordial waves by those experiments will disfavour models that have been allowed by current observations of CMB, such as the Starobinsky model [20].

1.3 Primordial black holes as dark matter

Despite the undoubted success of the ΛCDM model to describe the Universe at cosmological scales $k \lesssim 1$ Mpc^{-1}, we still lack an accurate miroscopic description of dark energy and dark matter (DM), the two components that constitute almost 95% of the energy density of the Universe. The former has a negative pressure that drives the accelerated expansion of the late Universe, whereas the latter one is

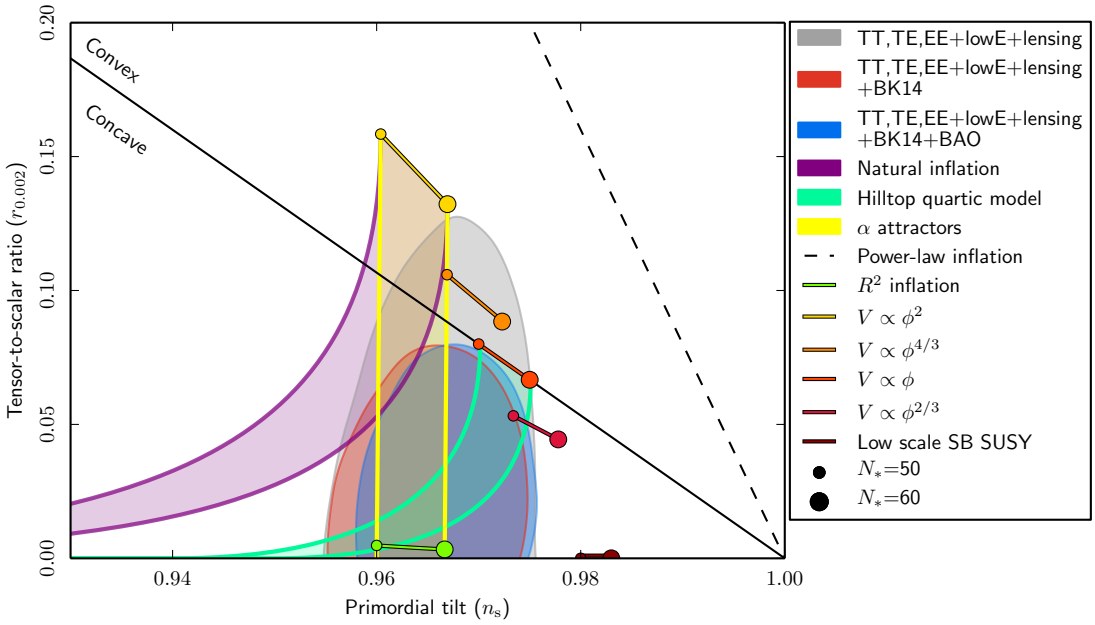

Figure 1.4: Constraints on the tensor-to-scalar ratio r in terms of the spectral index n_s at the 95% confidence level measured at the pivot scale $k = 0.002\ Mpc^{-1}$. A ΛCDM model with negligible running of the spectral index $\left(\frac{dn_s}{d\ln k} \approx 0\right)$ and a nearly scale-invariant power spectrum of the tensor modes (satisfying the consistency relation $n_t = -r/8$) is assumed. The grey shaded region is the constraint coming from Planck while the red and blue ones are due to $(BK15)$ and BAO accordingly. The coloured solid lines indicate the theoretical predictions of a sample of inflationary models allowing for an uncertainty in the number of e-folds until the end of inflation, $50 < N_* < 60$. The plot is adapted from [5].

responsible for seeding the formation of the observable large scale structure as well as explaining the features of the CMB, seen in Fig.1.5.

One of the first indications of such a dark component of matter was found in the rotation curves of stars or galaxies that were observed to stay flat even for large distances from the galactic center or from the center of the cluster respectively. *Zwicky* [21] in the 1930's was one of the first to point that the inexplicably fast orbits of the galaxies in the *Coma cluster* could be explained if there was a dark matter component in order to create a larger gravitational pull. But it was not until the systematic study of the orbits of stars in the Andromeda Nebula by *Rubin* [22], revealing the same flat pattern in the rotation curves, that dark matter started being considered as an essential component of the cosmological paradigm.

A supplementary observational method used to probe the fraction in dark matter is the use of weak-gravitational lensing. Mapping how the photon trajectories,

coming from distant and bright sources as active galactic nuclei (AGN) or quasars, are bent by massive sources, such as galaxies or clusters of galaxies, has aided to the unveiling of the spatial distribution of dark matter. These lensing data sets, along with radio and X-ray emissions from the intergalactic hot gas, demonstrated that galaxies are more massive than previously thought, with most of their mass residing in the dark matter halo extending up to 200 kpc [23, 24, 25]. Also, more investigations in the years that followed, unveiled the rich structure of galaxies [26], where clusters of galaxies are connected via filamentary tubes that could span up to a few Mpcs [27, 28], corroborating the cosmic web picture of structure predicted by the standard ΛCDM model.

The observations of the distribution of dark matter at intergalactic scales are consistent with the former behaving as a cold, non-relativistic fluid with a dust-like equation of state $w = 0$, interacting mainly gravitationally with standard matter. Because of its pressurless nature, it started forming clumps before the time of recombination, providing the primordial potential wells. This so called recombination time marks the era until when photons and baryons were tightly bound in a highly energetic plasma. Now, the perturbations of the plasma that entered the comoving Hubble horizon at $z > z_{rec}$ exhibit an oscillatory behaviour, with a decreasing amplitude, resulting in the distinctive peaks of the CMB power spectrum shown in Fig.1.5. On the other hand, the dark matter component, which is unaffected by the suppression from interactions with the baryon-photon plasma, starts clumping [6] and gravitating regular matter, thus kickstarting the evolution of structure at cosmological scales [30].

Currently, the two most prominent particle candidates for dark matter, from the particle physics perspective, are the weakly interacting massive particles (*WIMPs*) and the axions (or axion-like particles). The former, with masses of order GeV – 10 TeV, have a freeze-out relic abundance that matches pretty closely the dark matter one (*WIMP miracle*), thus they were readily considered as a viable candidate for dark

[6] The study of the evolution of perturbations of the cold dark matter component in a radiation dominated background on sub- and superhorizon scales reveals that the amplitude of the fluctuations that enter in the causal horizon before radiation-matter equality will increase logarithimically before matter equality at $z_{eq} \sim 3400$, while afterwards it will start growing proportionally to the scale factor. [29]

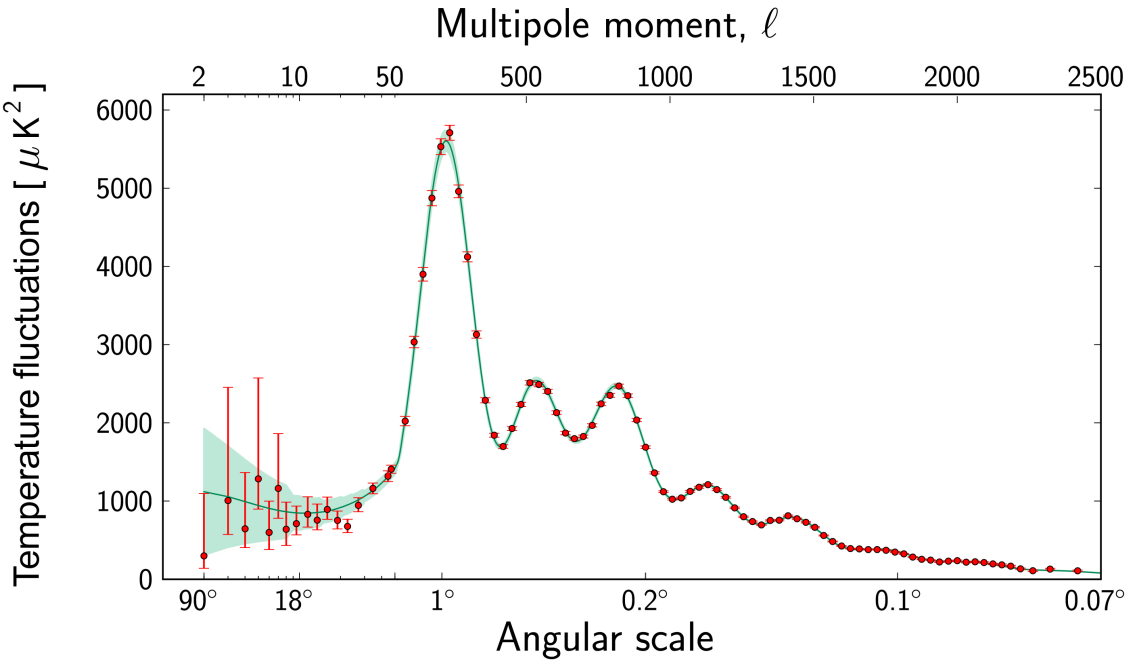

Figure 1.5: The power spectrum of the fluctuations in the temperature of the cosmic microwave background radiation as observed by the ESA and Planck collaboration. The measured red points follow perfectly the green curve, representing the predictions of the ΛCDM model, particularly for the angular scales smaller than 6°, whereas there is a 10% deviation for the larger distances due to the cosmic variance effect. The shaded green region shows all the configurations of ΛCDM allowed by the Planck data. The position of the first peak around $\sim 1°$ is consistent with a flat Universe, while the position of the second and third ones do agree with a baryon density of $\sim 5\%$ and dark matter density around $\sim 25\%$. Note the suppression of the acoustic peaks for angular scales smaller than 0.2°, originating from *Silk damping* and free-streaming effects due to the mixture of energetic photons. The plot is taken from [31, 32].

matter [33, 23, 34]. Although such weakly interacting particles have stimulated a great deal of interest, since they could be found in supersymmentric extensions of the Standard model (*SUSY*), their existence still eludes any conclusive observational confirmation. The second most prominent particle candidate for dark matter is the axion. The axion is a pseudoparticle produced after the spontaneous breaking of a $U(1)$ symmetry, introduced by *Peccei* and *Quinn* [35] in order to resolve the strong-CP problem of quantum chromodynamics (*QCD*). Since that initial proposal, various axion-like particles have been introduced (see [36, 37] and references within for a review of the axion landscape) with a mass spectrum spanning numerous orders of magnitude. Despite the persistent efforts, there

has not been any conclusive direct [38, 39] or indirect [40, 41] detection of any such particle, same as for WIMPs, but instead stringent limits have been placed on their possible ranges of mass as well as on the strength of their interactions with Standard model particles or nuclei [34, 42].

Lastly, another prominent candidate for dark matter is a population of stellar remnants (namely white dwarfs or neutron stars), faint stars (brown dwarfs) or any other compact object that could reside in the haloes of the galaxies. Although this seemed an intriguing possibility, the bounds on the *baryon-to-photon ratio* n, derived from the measurement of the abundances of light nuclei that formed during the era of Big Bang Nucleosynthesis (BBN), prevent dark matter from totally consisting of a population of massive halo compact objects (*MACHOs*). Apart from the constraints set by BBN, the abundance of MACHOs is further limited by surveys of gravitational lensing. Since these faint objects were theorized to populate a significant fraction of the halo of each galaxy, they could pose as possible 'dark' sources of lensing. In order to test this idea, the fraction of our galaxy's halo in MACHOs was probed by observing the rate at which the light of stars in Milky Way was lensed [43]. Since then, numerous surveys for microlensing events along the line of sight of neighbouring satellite galaxies, *i.e Large Maggelanic Clouds (LMCs)* or *M31*, such as the *EROS* [44] / *MACHO* [45, 46] collaborations, have been conducted, successfully constraining said abundance over a fairly large mass span, $10^{-7}\ \mathrm{M}_{\odot} \lesssim M \lesssim 10\mathrm{M}_{\odot}$. However, since the detection of $M_{BH} \sim \mathcal{O}(10)\ M_{\odot}$ merging black holes by the LIGO/VIRGO collaboration [47], the interest for dark matter being comprised of MACHOs, and more concretely in the form of primordial black holes, has heightened once again. The advantage of dark matter being composed of PBHs over stellar MACHOs lies in the fact that the former evade the bounds from BBN, since they could originate from the collapse of adiabatic density perturbations, which are made mainly of radiation and not so much of baryons.

It was Novikov and Zeldovich [48] along with Hawking and Carr [49, 50, 51], who first envisioned that inhomogeneities in the energy density of the early Universe could overcome the radiation pressure and collapse under their own gravity forming primordial black holes. The mass of the collapsing region is of the order of the

mass included in the comoving horizon at the moment of formation and is given by the following approximate relation [52]

$$M_{PBH} \sim 10^{15}\left(\frac{t}{10^{-23}s}\right) \text{gr.} \tag{1.34}$$

PBHs forming around the *QCD* phase transition ($t \sim 10^{-5}$ s) would have masses of the order of our Sun ($M \sim 1\ M_{\odot}$), whereas the one with a mass of 10^{15}gr would have evaporated by now [49] via Hawking radiation [53]. Additionally, the fact that Eq.(1.34) offers mass support in the so called gaps of the mass distribution of stellar black holes, could be utilised as a strong observational indication for the primordial origin of said size [54, 55]. More concretely, PBHs could populate the lower mass gap set between the heaviest neutron stars and the lightest astrophysical black hole, $2 \lesssim M_{PBH}/M_{\odot} \lesssim 5$ [7] as well as the upper mass gap, $45 \lesssim M/M_{\odot} \lesssim 135$ set by pair production instabilities in the collapsing star [56, 57]. The *LIGO/VIRGO* collaboration has detected mergers [54, 55], where the mass of one or both of the binary components is found to fall within either mass gap, enforcing the idea that their progenitors could consist of primordial black holes. Due to the observational difficulties of disentangling the different channels of binary formation and statistically inferring the parameters of each of the components, there is still ambiguity in determining the nature of the colliding objects, allowing for either a primordial [58] or an astrophysical origin [59, 60, 61].

Generally, there is a plethora of mechanisms that could produce a cosmologically interesting abundance of PBHs. These could range from inflationary curvature fluctuations that collapse after they re-enter the horizon either during an early matter [62, 63] or a radiation dominated era [64] in a single or multi-field inflationary scenario[65, 66, 67], to phase transitions in the early Universe [68, 69, 70], the collapse of topological defects of phase transitions, such as domain walls [71, 72, 73, 74] and collisions of bubbles of false-vacuum [75, 76, 77]. In this thesis, I will focus mainly on PBHs originating from the first formation channel, *e.g*

[7] The lower mass limit is called the *Tolman-Oppenheimer-Volkoff* (TOV) limit for a non-rotating neutron star and it is an analogue of the *Chandrasekhar* bound for the mass of white dwarves. Its precise value is not known since it depends on the equation of state of the neutron star but recent and more accurate estimations place it between $2.2 < M_{TOV}/M_{\odot} < 2.9$. Observations of the mass of neutron stars have shown that neutron stars seem to approach the TOV limit, having masses of the order $M_{NS} \sim 2.4\ M_{\odot}$. Therefore, the possibility that neutron stars could populate that mass gap could point to new physics.

adiabatic curvature fluctuations with an amplitude above a certain threshold, of order $\zeta \sim \mathcal{O}(1)$ that collapse soon after re-entering the horizon. But before I discuss in more detail the general characteristics of such a population of PBHs, I would like to briefly mention how they are embedded into the whole inflationary picture and more concretely into the single-field scenario.

As mentioned above, the amplitude of the power spectrum of curvature perturbations, defined in Eq.(1.27), has been tightly constrained over the years by CMB temperature anisotropies measurements (around the scale $k_0 = 0.05\ \mathrm{Mpc}^{-1}$) and large scale structure surveys, to a value $P_\zeta = 2.1 \cdot 10^{-9}$ [4] at $k \lesssim 1\ \mathrm{Mpc}^{-1}$. Now, we know that the collapse of the overdensity under its own gravity is a non-linear process that requires large values for the amplitude of the curvature perturbations. Thus, in order for PBHs to match the DM abundance, the power spectrum of the curvature perturbations needs to take a value $P_\zeta(k_{PBH}) \sim 10^{-2}$ [78, 79, 80] for $k_{PBH} \gtrsim 10^7\ \mathrm{Mpc}^{-1}$. Since the power spectrum at the cosmological scales is of order $P_\zeta(k_{CMB}) \sim 10^{-9}$, we note that it needs to grow considerably, close to seven orders of magnitude. That rapid amplification of the amplitude at small scales could not be achieved by a single field slowly rolling down the inflationary potential. The reason is that the slow roll parameters vary slowly, thus resulting in a nearly constant primordial power spectrum (see also the discussion below Eq.(1.21)). This, however, could be achieved in inflationary models where the slowly-rolling inflaton field ϕ reaches an inflection point [48, 81, 82, 83], where $V_{,\phi} \to 0$. Once the field reaches either a flat region or a local maximum of the potential , its trajectory enters in an ultra-slow-roll regime (USR) [84, 85] or a transient constant-roll phase (CR) [86] (see Fig.1.6). There, the field's velocity $\dot{\phi}$ decreases exponentially leading to an enhancement of the primordial power spectrum, in the shape of a spiky feature, as seen in Eq.(1.27) and depicted in Fig.1.7. This amplification will inevitably lead to a violation of the slow-roll approximation at least at an order of $\mathcal{O}(1)$ [87, 81, 88]. Another effect that will further contribute to the amplification of the power spectrum involves the evolution of the modes of $\zeta_{\mathbf{k}}$ once they exit the comoving horizon. More concretely, if the field ϕ reaches the plateau or local maximum, then the acceleration term in the *Klein-Gordon* equation, Eq.(1.9), cannot be neglected,

as it is assumed in the slow-roll approximation, since now it is compensating for the friction term that drives the field evolution. In order to see that a spatially flat direction of the potential and the field following a non-attractor trajectory (*i.e* the ultra-slow-roll regime) for an adequate number of e-folds, can lead to the enhancement of the power spectrum, we need to rewrite the *Mukhanov-Sasaki* equation, Eq.(1.20), with respect to $\zeta_{\mathbf{k}}$ and N (given in 1.14) in the form [89]

$$\frac{d^2\zeta_{\mathbf{k}}}{dN^2} + (3-\epsilon+\eta)\frac{d\zeta_{\mathbf{k}}}{dN} + \left(\frac{k}{aH}\right)^2 \zeta_{\mathbf{k}} = 0. \tag{1.35}$$

For super-horizon scales, where $k \ll aH$, the third term in Eq.(1.35) is negligible and the solution is given by

$$\zeta_{\mathbf{k}} = C_1 + C_2 \int e^{-3N+\ln H-\ln\epsilon} dN. \tag{1.36}$$

Now, in slow-roll inflation the second term of Eq.(1.36) is exponentially suppressed, leaving the curvature perturbations constant as soon as they exit the causal horizon, as mentioned above. If the field enters an USR or a CR regime, then $\eta \lesssim -6$ [85, 90] (where the equality is for USR), implying that $3-\epsilon+\eta < 0$. Therefore, the second term in Eq.(1.36) corresponds to a growing mode of the solution once it exits the comoving Hubble horizon, thus leading to the enhancement of the primordial power spectrum.

Now that the mechanism for the amplification of the power spectrum is introduced, we can proceed with the description of the formation of PBHs. Generally, the probability of PBH formation is reasonably well understood when the curvature perturbation ζ_G is Gaussian distributed and the power spectrum has a sharp spike at a particular scale $k_\star$. The power spectrum need not be strictly monochromatic, since the spike could exhibit certain width. Now, provided that the IR and UV tails fall off sufficiently, we can employ peak theory [91] in order to determine the typical profile of high peaks, defined as

$$\psi_G(r) \propto \langle \zeta_G(0)\zeta_G(r)\rangle. \tag{1.37}$$

This typical profile is proportional to the two-point function for $\zeta_G(r)$, and thus can be calculated for any given spectrum. Although there are fluctuations around the typical profile, these are of the order of the r.m.s. fluctuations of the Gaussian

random field. Hence, if we are considering peaks that are several standard deviations high above the mean, as required in order not to overproduce PBHs, the fluctuations will be subdominant. In this sense, the high peaks are approximately spherically symmetric too.

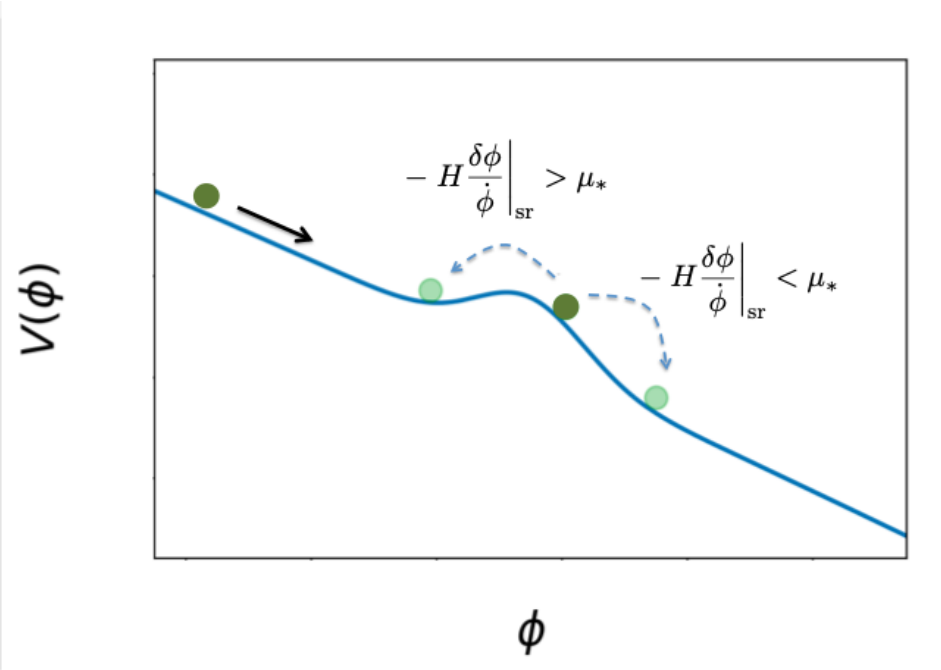

Figure 1.6: An inflationary potential exhibiting a small barrier on its slope. As the background field surpasses the barrier, it undergoes a transient phase of constant-roll with $\ddot{\phi}/H\dot{\phi} \approx const. < -3$, which significantly enhances the power spectrum of curvature perturbations to the necessary amplitude for an abundant production of PBHs. Here, $\delta\phi$ denotes the perturbation of the inflaton field calculated in the flat gauge and it is evaluated at the time when the field overshoots the barrier and enters into the slow-roll regime. Perturbations with $-H\delta\phi/\dot{\phi}|_{SR} > \mu_*$, where $\mu_* = 5/(6f_{NL})$, could impede some regions, with the size of the comoving horizon, from surpassing the local maximum of the potential, resulting in the formation of false vacuum bubbles [86]. Naturally, the local relation in Eq.(1.39) breaks down beyond that point. From the perspective of an observer inside the bubble, these regions continue to inflate at a high rate, while for an external observer, these bubbles will lead to the formation of PBHs, as soon as they enter the comoving horizon during the radiation dominated epoch. The plot is adapted from [86, 92].

Note also that if the curvature perturbation ζ is not Gaussian, we can still calculate the profile of the perturbation and formation probability, provided that the non-Gaussianity is of the local type. This corresponds to the case where the curvature perturbation ζ is a local function of a Gaussian distributed random field, already defined as ζ_G,

$$\zeta = F[\zeta_G]. \tag{1.38}$$

In the inflationary context, and for the models we shall be interested in, ζ_G is basically proportional to the inflaton field perturbation on flat slicings, as noted also in Eq.(1.18) for $\mathscr{R} = 0$, whose wavefunction is approximately Gaussian. Once the profile $\psi_G(r)$ has been determined, we can simply find the non-Gaussian profile as $\psi(r) = F[\psi_G(r)]$.

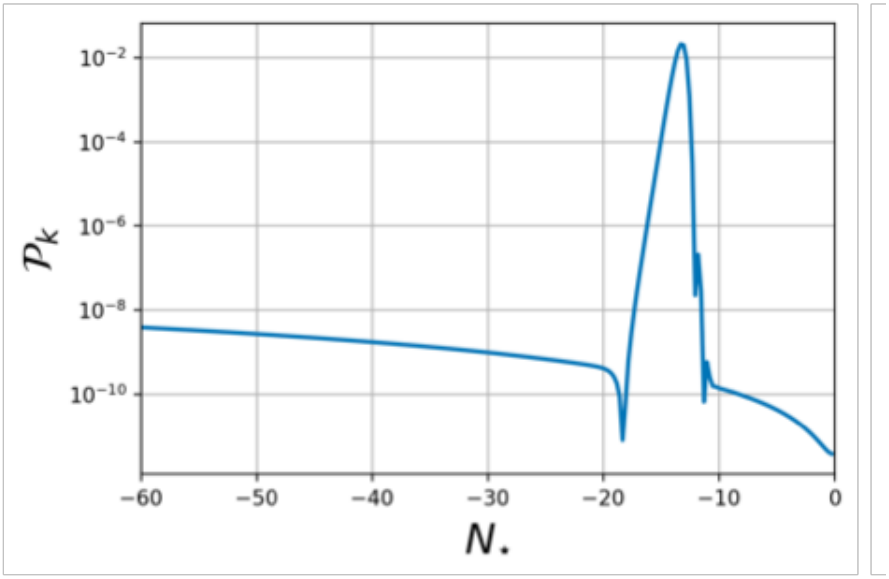

Figure 1.7: The power spectrum of curvature perturbations from the constant roll potential, given in Fig.1.6, showing a strong enhancement at the comoving scale of PBHs. The plot is adapted from [86].

As an example, a phase of constant-roll, where the inflaton overcomes a small barrier on its way down the potential, also shown in Fig.1.6, leads to a non-linear relation of the form [92]

$$\zeta = -\frac{5}{6f_{NL}} \ln\left(1 - \frac{6f_{NL}}{5}\zeta_G\right), \tag{1.39}$$

where f_{NL} is determined in terms of the curvature of the potential at the barrier [85, 93] as

$$f_{NL} = \frac{5}{12}\left(-3 + \sqrt{9 - 12\eta}\right) \tag{1.40}$$

In an expansion at quadratic order, f_{NL} is the well known local non-Gaussianity parameter, but in the present context, the non-linear completion Eq.(1.39) plays a significant role. In the case of CR, where the filed transverses a maximum of the potential, there is a well defined exit of that phase, given by the moment in which the field crosses the potential barrier (which can be modelled with a simple

quadratic function). Now, in the case of an USR phase, the way that the field exits that regime in order to enter into a slow-roll one, needs to be further specified [94]. If the transition is smooth, $f_{NL} = 0$ (this is a limit of the CR non-linear completion for $V_{,\phi\phi} = 0$). If the transition between the USR and subsequent slow-roll phase is abrupt(non-continuous), then $f_{NL} = 5/2$.

The next issue that needs to be considered involves the probability of PBH formation. For this purpose, it is useful to introduce the so-called compaction function [95, 96, 97] as

$$C(r) = \frac{1}{3}\left[1 - (1 - r\zeta')^2\right], \tag{1.41}$$

where the prime $'$ denotes the radial derivative and spherical symmetry is also assumed. At superhorizon scales ζ is conserved and that also translates into a time-independent compaction function. Physically, it can be shown that this function is related to the volume averaged density contrast $\overline{\delta}$ as

$$C(r) = \frac{1}{2}(HR)^2\,\overline{\delta} \tag{1.42}$$

Here, R is the aereal radius corresponding to the comoving coordinate radius r. Note that $\overline{\delta}$ itself depends on time, but such dependence is cancelled by the growth of the aereal radius with the scale factor. Therefore, at the time of horizon crossing, $HR = 1$ and $C = \overline{\delta}/2$, so we can think of the compaction function as the averaged overdensity at the time of horizon crossing.

Furthermore, numerical simulations of the non-linear evolution of perturbations and the subsequent formation of a PBH [98, 99, 100, 97] revealed that this phenomenon is critical. Critical collapse is usually studied in terms of the compaction function, since it provides a robust measure of the perturbation's amplitude. Now, for a given profile $\psi(r)$ of the overdensity, it is useful to introduce the radius at which the compaction function exhibits a maximum, r_m. Then, critical collapse occurs when $C(r_m)$ exceeds a certain threshold C_{th}. It was soon realized that the threshold lies in the narrow range $0.2 < C_{th} < 0.33$ [8] [78, 97, 100], with the dispersion resulting from the dependence on the profile $\psi(r)$ of the curvature perturbation. Noticeably, it was shown that by taking another spatial average of the compaction

[8] The lower limit coincides with the analytical estimation known as the *Harad-Yoo-Kohri threshold* [101].

function over a volume defined by r_m, as

$$\overline{C} \equiv \frac{3}{r_m^3} \int_0^{r_m} R^2 C(r)\, dR, \tag{1.43}$$

the threshold for formation exhibited a universal behaviour for a broad class of profiles of the perturbations [102, 92], taking the value

$$\overline{C}_{th} \approx \frac{1}{5}. \tag{1.44}$$

The criticality of the formation of a PBH is manifested in its mass, that follows a scaling law

$$M_{PBH} = \mathrm{K}(\zeta - \zeta_c)^{\gamma} M_H, \tag{1.45}$$

where M_H is the mass of the horizon at the time of formation t_{form}. The constants K and γ depend on the profile of the high peak as well as on the equation of state w and have values $\gamma \approx 0.36$ for $w = \frac{1}{3}$ and $1 \lesssim \mathrm{K} \lesssim 10$ respectively, for a a range of broad and peaked profiles [103, 104]. Here, the curvature perturbation ζ is proportional to the profile $\psi(r)$. In Eq.(1.45), ζ stands for the curvature perturbation at the center of the overdensity, and ζ_c is the critical value for which $C(r_m) = C_{th}$. Thus, the criticality of gravitational collapse will lend support to a low mass tail, even for a narrowly spike in the power spectrum.

Now that the critical formation of a PBH is introduced, we can proceed to define the fraction of the Universe's energy content in such objects at the time of their formation t_{form} as

$$\Omega_{PBH}|_{t_{form}} = \int_{\zeta_c}^{\infty} \frac{M_{PBH}(\zeta)}{M_H} n(\zeta) d\zeta, \tag{1.46}$$

where $n(\zeta)$ is the number density of peaks of a height ζ and the term $\frac{M_{PBH}}{M_H}$ accounts for the aforementioned criticality.

Now, if we assume a Gaussian probability distribution of the perturbations, then $n(\zeta)$ is given by [91, 78]

$$n(\nu) = \frac{k_\star^3}{4\pi^2} \nu^3 e^{-\nu^2/2} \theta(\nu - \nu_c). \tag{1.47}$$

where $\nu = \frac{\zeta_c}{\sigma_{M_{PBH}}}$ and the variance of the perturbations, $\sigma_{\mathrm{M}_{PBH}}$, is defined by [105, 106]

$$\sigma^2_{\mathrm{M}_{PBH}} = \int d(\ln k) P_\zeta(k). \tag{1.48}$$

Given that PBHs may form at different epochs, the relevant observational quantity, is the abundance of PBHs at the present time, $\Omega_{PBH}\Big|_{t_0}$, described by the relation [96]

$$\Omega_{PBH}\Big|_{t_0} = \left(\frac{M_{eq}}{M_H}\right)^{1/2} \Omega_{PBH}\Big|_{t_{form}}, \tag{1.49}$$

where M_{eq} is the mass of the horizon at matter-radiation equality and time of formation is parametrised via the horizon mass M_H. The factor $\left(\frac{M_{eq}}{M_H}\right)^{1/2}$ accounts for the fact that the energy density of matter evolves with the scale factor until matter-radiation equality. Now, the mass function is defined as [96, 107]

$$f(M_{PBH}) = \frac{1}{\Omega_{PBH}} \frac{d\Omega_{PBH}}{dM_{PBH}}. \tag{1.50}$$

Effects such as the critical collapse in Eq.(1.45) or a broadening of the spike in the power spectrum would skew and broaden the mass function to lower masses; keeping in mind that there is an upper limit on the PBH mass set by the mass contained in the comoving Hubble horizon, when the physical scale of the perturbation re-enters. On the other hand, late-time processes, such as PBHs accreting on baryonic matter or on their DM haloes and hierarchical binary mergers in dense globular clusters, would potentially shift the mass function towards its higher tail.

Additionally, the profile of the initial mass function of PBHs depends on the formation channel as well. For example, the mass function of PBHs that originate from the collapse of enhanced perturbations with a smooth and symmetric spike in the power spectrum, is often parametrised as a lognormal function [108, 109, 110], whereas other mechanisms, such as the collapse of scale-invariant perturbations [51] or of cosmic strings [111, 112], results in a mass function that follows a power-law $f(M_{PBH}) \propto M^{\theta}$ between the masses (M_{min}, M_{max}), with the exponent θ depending on the equation of state [109].

A more refined formulation of the initial mass function and its evolution as well as more accurate estimates of the mass fraction of PBHs, $f(M_{PBH})$, is essential if we want to accurately map the constraints on their abundance, $\Omega_{PBH}|_{t_0}$, to bounds on the small-scale power spectrum, P_ζ. In general, the constraints on the mass fraction span a wide range of masses (for updated summaries of constraints see [113, 114, 52, 111]) but here I will only list some of the most robust ones. For $M_{PBH} < 10^{15}$ gr

the evaporation of PBHs and their contributions to the galactic and extragalactic γ-ray backgrounds place tight limits of the order $\Omega_{PBH}|_{t_0} < 10^{-11}$, whereas black holes of $\mathcal{O}(10\,M_\odot)$ have been restricted by the *LIGO/VIRGO* merger rates and the Planck measurements of CMB anisotropies to abundances of order $\sim 0.1\%$. Lastly, the gravitational and tidal effects of massive PBHs, with $M_{PBH}/M_\odot > 10^4$, on the formation of large structures, such as globular clusters, as well as the accretion limits from X-ray binaries, narrow the possible observational windows that could accommodate PBHs as a viable candidate for the totality of DM. The refined and more systematic treatment of several observational constraints, particularly the ones coming from femtolensing of γ-ray bursts [115] or optical microlensing events along the sight of the Maggelanic clouds [116] and from the interaction of PBHs with main-sequence stars (white dwarfs and neutron stars) [113], has reintroduced the scenario that PBHs with masses in the asteroid-Earth range, $10^{-16} \lesssim M_{PBH}/M_\odot \lesssim 10^{-10}$ could constitute all of dark matter [117]. A reappraisal of the bounds on the PBH abundance, at masses around $1 \lesssim M_{PBH}/M_\odot \lesssim 10^2$, is also needed since effects, such as an enhanced power spectrum of cosmological perturbations [118] or primordial clustering [119], could relax considerably said constraints. I will expand more on these two last models on Chapter 2, where the aforementioned publications are presented.

1.4 Overview of the thesis

This manuscript is a collection of the research conducted throughout my PhD. Its goal is to employ PBHs in order to probe the primordial power spectrum and thus the early-time Universe. Particularly, I explore how different features of such a power spectrum, such as an enhanced plateau at the comoving size of binaries at the time of their formation or a strong enhancement at the scale of solar mass PBHs, as well as the modal coupling between the long and short wavelengths, could mitigate the severe bounds on the abundance of intermediate-mass PBHs set from *LIGO/VIRGO*. Furthermore, the possibility that supermassive PBHs could provide an explanation for the recently detected isotropic signal by the *NANOGrav* collaboration [120] is considered.

The thesis has the following structure. In Section 2.1 of Chapter 2, I study how cosmological perturbations in radiation and matter could alter the distributions of orbital parameters by providing torque to the PBH binaries. In order to achieve that, three different templates for an enhanced power spectrum of cosmological perturbations at scales larger than $k > 1$ Mpc^{-1} are employed. Firstly, it is shown that perturbations in matter and radiation with an amplified plateau in their power spectrum at scales $k \sim 10$ Mpc^{-1} are the primary source of torque to the binary for any value of the abundance f_{PBH}, whereas for a power spectrum that increases monotonically up to the comoving sizes of the binaries at the time of their formation, the perturbations provide enough torque to relax the bounds on the abundance of 30 $M_\odot$ PBHs sgnificantly. Lastly, a power spectrum that rises up to scales smaller than the comoving size of the binary, exhibiting a narrow or a broad strong enhancement at the 30 $M_\odot$ PBH formation scale, is considered. The contribution of the cosmological perturbations to the peculiar velocities of PBHs is not found to be significant for any relevant abundance of PBHs, unless the enhancement is rather broad. Additionally, I present how an observable quantity, the universality coefficient α, which is agnostic to the initial mass function of PBHs but associated with their binary merger rate, could provide insight into not only the amplitude and spectral index of the primordial power spectrum but also into the mechanisms that affect the binary formation and evolution. These results can be found in the publication [118].

In Section 2.2, I study how primordial clustering affects the distribution of orbital parameters of binary systems consisting of 30 $M_\odot$ PBHs. More precisely, the primordial clustering is induced by the presence of a local type of non-Gaussianity, which will lead to different modes of the curvature perturbations being coupled. It is found that for abundances of order 0.1% the clustering will have as an effect the circularisation of the PBH binaries and the subsequent exponential suppression of their merger rate observed at present time. This suppression inevitably relaxes the constraints on the abundances of 30 $M_\odot$ PBHs set by *LIGO/VIRGO* observations. An interesting feature of our phenomenological model for primordial clustering is that the suppression of the merger rate gives rise to degeneracies in the model's parameters, meaning that two different populations of PBHs are producing the

same merger rate. By considering the evolution of the merger rate with redshift as well as the stochastic background of gravitational waves (SBGW) we manage to lift these degeneracies and disentangle the different PBH populations. The results of this chapter are found in the publications [118] and [119] respectively.

In Chapter 3, I focus on the idea that PBHs, particularly the ones that are extraordinarily massive, having a mass around $\sim 10^{12} M_{\odot}$, could provide an explanation for the isotropic signal that was detected in the pulsar timing data provided by the NANOGrav collaboration. More concretely, we show that the peak of the NANOGrav signal can be explained with the stochastic background of gravitational waves sourced from the mergers of stupendously massive PBHs, with masses of order $\sim 10^{11} - 10^{12}$ $M_{\odot}$, finding that it could be explained by a PBH abundance of $\sim 0.1\%$. In order for such supermassive PBHs to exist, the bounds from the non-detection of CMB spectral distortions need to be evaded. Since the amplitude of the curvature perturbations needed in order to achieve a certain abundance of PBHs decreases as f_{NL} increases, we show that for a single-field inflationary model with a transient phase of constant roll and for $f_{NL} > 3$, the constraints from μ-distortions can be evaded. The results of this Chapter can be found in the publication [121]. Lastly, Chapter 4 gathers the results and presents possible pathways that can be followed in order to expand upon said work.

2 Solar mass PBHs and the LIGO/VIRGO mergers

The detection of merging black holes with masses of order ~ 30 $M_\odot$ by the *LIGO/VIRGO* collaboration, reinvigorated the interest in PBHs, both as a candidate of DM but also as a viable explanation for a fraction of the aforementioned mergers. Since the first successfully detected pair of colliding black holes [47] and the subsequent addition of 10 more merging events by the *LIGO/VIRGO* collaboration in the first two runs (*O1/O2*) [122], another 34 confirmed events [123] (only of black hole mergers)[1], were added after the end of the third run (*O3a*) in 2019. Generally, there are two prominent astrophysically-motivated models for binary formation [127] and evolution, namely the channel of the isolated binary evolution in galactic fields and the dynamical capture channel of formation in dense clusters, *i.e* globular clusters. They respectively predict an aligned and isotropic distribution of effective spins for the merging BHs, but both models' estimations of the magnitudes are plagued by uncertainties having to do with supernova natal kicks, angular momentum transfer and tidal effects [128, 129]. These channels of binary formation fail though to completely account for the statistically inferred tendency of the merging population towards low values of the effective spin χ_{eff} [2] and masses of $\sim \mathcal{O}(10)\ M_\odot$, features that seem to be consistent with a significant fraction of these mergers being primordial.

Now, the fact that PBHs from the collapse of inflationary fluctuations are shown

[1] More events with astrophysical significance $p_{astro} > 0.5$ have been reported in [124, 125, 126].

[2] The spin variable measured with the least ambiguity is $\chi_{eff} = \frac{\vec{J}_1/M_1 + \vec{J}_2/M_2}{M_1+M_2} \cdot \vec{L}$ [130, 131, 132], where $(\vec{J}_1, \vec{J}_2)$ are the angular momentum vectors, the masses (M_1, M_2) and $\vec{L}$ is the orbital angular momentum.

to exhibit an isotropic distribution of small spin amplitudes [133, 134], qualifies them as a possible candidate for said coalescing population (except for a few high mass events that have been confirmed to have a non-negligible spin values [124, 125, 130]). Various hierarchical Baysesian analyses have been conducted in order to discriminate between the different populations. These analyses employed the posterior probability density functions of the effective spins and chirp masses M_{chirp}, inferred from the growing catalogue of *LIGO/VIRGO* mergers and showed that a single PBH population is disfavoured by the *GWTC-2* data [135, 136, 137]. More refined investigations, based on a mixed-population approach that encompasses also the different astrophysical models, such as the isolated and dynamical capture channels mentioned above, demonstrated that there is a statistical significance that a fairly considerable number of mergers, up to $\sim 27\%$, detected so far could be of primordial origin [3] [141, 142, 143].

Additionally, another quantity that could be employed, besides the effective spin, chirp mass and the mass ratio ($q = M_2/M_1$), in order to discern the different populations, is the merger rate's evolution with redshift. For PBHs, the rate increases monotonically with redshift, whereas for the astrophysical one, there is a peak around $z \sim 10$ [141, 144] due to coalescences of *Population III* stars. The advent of the third generation ground-based interferometric detectors, such as the *Einstein Telescope* [145] and the *Cosmic Explorer* [146], will aid towards disentangling the various binary formation channels and shed more light onto their origin, since they will be able to probe the evolution of the merger rate up to redshifts $z \sim 50$, despite the increasing uncertainty for higher values of z [147], for masses of $\mathcal{O}(10\ M_\odot)$. Therefore, it is imperative to update and refine our phenomenological modeling of the PBH merger rate in order to exploit the breadth of the incoming data. Accounting for a DM dress around a PBH binary [148], the effect of early clustering structures on the merger rate [149, 150, 151] or the impact of early accretion on the evolution of the spin distribution [152] are few of the effects that could be incorporated in our modelling of the evolution of PBH binaries, in an effort to reevaluate

[3] A direct detection of PBHs by the *LIGO/VIRGO* collaboration or any other ongoing or planned experiment would have immediate consequences for the viability of the particle candidate of DM, *i.e WIMPs*, since the existence of the former may restrain the latter to abundances that are cosmologically negligible [138, 139, 140].

their contribution to the *LIGO/VIRGO* rate and thus to the energy content of the Universe at present time [153, 154].

The papers presented in this Chapter [118, 119] introduce two effects that need to be acknowledged, since they shape the surroundings within which the binary is evolving. In the first paper, I present how enhanced perturbations, both in matter and radiation, at binary scales could relax the tight *LIGO/VIRGO* constraints on the PBH abundance, while the observational prospect of a parameter that carries information about the different mechanisms that can induce torque on the binary, is discussed. In the second paper, a phenomenological model of clustering of PBHs is presented, where the modal coupling between the short and long wavelengths of the perturbations, sourced from the presence of a local type non-Gaussianity, causes a suppression on the merger rate, relaxing considerably the bounds on their abundance.

2.1 Primordial black holes and enhanced cosmological perturbations

Journal of Cosmology and Astroparticle Physics
An IOP and SISSA journal

Enhanced cosmological perturbations and the merger rate of PBH binaries

Jaume Garriga and Nikolaos Triantafyllou

Departament de Física Quàntica i Astrofísica, Institut de Ciències del Cosmos, Universitat de Barcelona, Martí i Franquès 1, 08028 Barcelona, Spain

E-mail: jaume.garriga@ub.edu, nitriant@icc.ub.edu

Received July 30, 2019
Accepted August 27, 2019
Published September 20, 2019

Abstract. The rate of merger events observed by LIGO/Virgo can be used in order to probe the fraction f of dark mater in the form of primordial black holes (PBH). Here, we consider the merger rate of PBH binaries, accounting for the effect of cosmological perturbations on their initial eccentricity e. The torque on the binaries may receive significant contributions from a wide range of scales, that goes from the size of the horizon at the time when the binary forms, down to the co-moving size of the binary. Extrapolating the observed plateau in the power spectrum $P_\Phi \approx 10^{-9}$ from cosmological scales down to the co-moving size of binaries, the torque from perturbations is small. In this case, for $f \gtrsim 10^{-2}$, the distribution of eccentricities is dominated by tidal torques from neighboring PBHs. On the other hand, in scenarios where PBH are formed from adiabatic perturbations, it is natural to expect an enhancement of P_Φ at small scales, where it is poorly constrained observationally. The effect can then be quite significant. For instance, a nearly flat spectrum with amplitude $P_\Phi \gtrsim 10^{-7}$ on scales smaller than $\sim 10\,\mathrm{Mpc}^{-1}$ gives a contribution $\langle j^2\rangle \sim 10^3 P_\Phi$, where $j = (1-e^2)^{1/2}$ is the dimensionless angular momentum parameter of the binaries. This contribution can dominate over tidal torques from neighboring PBHs for any value of f. Current constraints allow for a power spectrum as large as $P_\Phi \sim 10^{-5}$ at the intermediate scales 10^3–$10^5\,\mathrm{Mpc}^{-1}$, comparable to the co-moving size of the binaries at the time of formation. In particular, this can relax current bounds on the PBH abundance based on the observed LIGO/Virgo merger rate, allowing for a fraction $f \sim 10\%$ of dark matter in PBH of mass $\sim 30 M_\odot$. We investigate the differential merger rate $\Delta\Gamma(m_1, m_2)$, as a function of the masses of the binary components, and the corresponding "universality" coefficient [1] $\alpha = -(m_1+m_2)^2\partial^2 \ln\Delta\Gamma/\partial m_1 \partial m_2$. For an enhanced power spectrum with spectral index p we find that $\alpha \approx 30/(32-7p)$ for $0 < p \lesssim 2$, and $\alpha \approx 5/3$ for $p \gtrsim 2$. Such values may lie well outside the narrow range $\alpha \approx 1 \pm 0.05$ characteristic of tidal forces from neighboring PBHs. We conclude that, given a large enough sample of events, merger rates may provide valuable information on the spectrum of primordial cosmological perturbations at currently uncharted lengthscales.

Keywords: primordial black holes, cosmological perturbation theory, power spectrum, inflation

ArXiv ePrint: 1907.01455

https://doi.org/10.1088/1475-7516/2019/09/043

JCAP09(2019)043

Contents

1 Introduction

The detection of gravitational waves (GWs) from merging black hole binary systems has revived interest in the idea that primordial black holes (PBHs) may be a viable candidate for dark matter (DM). The abundance of PBHs is severely constrained for a wide range of masses (see e.g. [2] and references therein), but it could still be significant both for sublunar and stellar masses. In particular there is an active debate on wheter PBHs in the mass range recently detected by LIGO/Virgo collaboration could account for a sizable fraction of DM [3, 4].

The observed merger rate [5–8] $\Gamma \approx 10\text{–}100\,\mathrm{Gpc}^{-3}\,\mathrm{yr}^{-1}$ in the range $\sim 5\text{–}100 M_\odot$ has recently been used in order to place limits on the PBH abundance [4, 9]. In such estimates, it has been assumed that PBH are spatially uncorrelated at the time of formation, and that the dominant contribution to the orbital angular momentum of the binaries originates from tidal forces exerted by other black holes in the neighborhood, around the time when the binary decouples from the Hubble flow [1, 11, 12]. With these assumptions, the observational upper bound on the merger rate limits the fraction of PBHs in DM to $f \lesssim 1\%$. Several refinements to this estimate have been considered, including initial spatial correlations of the PBHs [13–16], tidal forces from non-relativistic matter perturbations [9, 10, 17], as well as the effect of a dark matter dress around the PBHs [18], with similar results for the bound on the PBH abundances. In ref. [19], the effect of infalls of neighboring PBHs on the binary has been studied, with the conclusion that this may significantly reduce the observed merger rate. Also, N-body simulations for the formation and evolution of binaries [19] indicate that for high $f \sim 1$, the rate may be significantly reduced by disruption, through the interaction of binaries with compact N-body systems.

JCAP09(2019)043

In this paper, we consider the effect of primordial cosmological perturbations on the angular momentum of PBH binaries during the radiation dominated era. We note that, even for a scale invariant spectrum of density perturbations, there is a wide range of scales contributing to the torque. Moreover, the amplitude of the power spectrum P_Φ is poorly constrained beyond the scale of $10\,\mathrm{Mpc}^{-1}$, and it could be significantly larger than it is on cosmological scales. In the present context this possibility seems rather natural, since some scenarios for PBH formation[1] rely on a prominent enhancement or "bump" in the power spectrum at relatively short wavelengths, corresponding to the co-moving size of the horizon at the time when PBHs form. In the inflationary context, the height and location of the bump depend on specific features in the inflaton potential. For instance, in one field models, the field may undergo a short period of ultra-slow roll or constant roll as it encounters local extrema on its way down the potential [20–27]. While the amplitude of perturbations on cosmological scales is of order $P_\Phi \sim 10^{-9}$, the r.m.s. amplitude at the bump should be much larger, $P_\Phi \sim 10^{-3}$–10^{-2}, so that PBHs can form in significant abundance. This is a strong departure from scale invariance, and it seems plausible that in generic models of this sort the power spectrum might be enhanced also at the scales interpolating from the cosmological plateau down to the PBH scale, including the intermediate scales comparable to the co-moving size of the binaries. Here, we shall be agnostic about the specific inflationary dynamics, and will simply explore the consequences of an enhanced spectrum which we shall model as a (piecewise) power law $P_\Phi(k) \propto k^p$. As we shall see, such an enhancement may have potentially observable consequences. In particular, it may affect the differential merger rate of binaries as a function of the component masses.

The paper is organized as follows. In section 2 we briefly review the formation of PBH binaries and the distribution of orbital parameters, taking into consideration the effect of neighbouring black holes but ignoring cosmological perturbations. It is in this context that the universality coefficient α, which charaterizes the dependence of the merger rate on the masses of the components, was first introduced [1]. Hence, this will be a useful reference case. We also comment on PBH infalls and their effect on α.

In section 3 we discuss the effect of cosmological perturbations on the dimensionless orbital angular momentum parameter j. In contrast with earlier analysis, here we include the perturbations in radiation, whose effect dominates over that of matter perturbations for binaries which decouple from the Hubble flow deep in the radiation era. For an enhanced P_Φ these tend to dominate the distribution of j.

In section 4 we consider the merger rates in three different scenarios: the nearly scale invariant cosmological plateau (Case A), an enhanced spectrum at intermediate scales with a moderate spectral index $0 < p \lesssim 2$ (Case B), and a rather steep power spectrum $p > 2$, peaked at scales smaller than the binary size (Case C). Our conclusions are summarized in section 5.

Throughout the paper f will denote the fraction of dark matter in the form of PBHs, and s will denote the cosmological scale factor, while a will denote the semi-major axis of binaries. We adopt the convention that $s = 1$ at the time of matter-radiation equality. The speed of light is set to $c = 1$.

[1]Not all scenarios for PBH formation require a bump in the power spectrum. For instance, PBH could be created by active seeds such as relic domain walls or false vacuum bubbles produced during inflation [28–30], rather than adiabatic perturbations. In such alternative scenarios, an enhancement in the spectrum of cosmological perturbations does not seem to be a necessary feature. The same is true for PBH formation at post-inflationary phase transitions (see e.g. [31–34] and references therein).

JCAP09(2019)043

2 PBH binary formation and universality

In this section, we briefly review the case where the angular momentum of binaries is due to the tidal torque from other PBHs in the vicinity, neglecting cosmological perturbations. We also introduce the universality coefficient α [1], and we discuss how this may be affected by the infall of neighboring PBH on binaries.

2.1 Initial orbital parameters and the life-time of binaries

Following [4, 11], let us assume a uniform distribution of PBHs, without any initial spatial correlations.[2] From a given PBH, the probability of finding the nearest neighbour at a certain distance is given by

$$dP = e^{-X} dX. \tag{2.1}$$

Here $X = nV$ is the product of the co-moving number density n times the co-moving volume $V = (4/3)\pi x^3$, where x is the co-moving distance. We adopt the convention that the cosmological scale factor is $s = 1$ at the time of matter-radiation equality.

We shall also assume that the PBH mass function is not too broad,[3] allowing however for some spread in the masses within an order of magnitude or so. The co-moving number density takes the form $n = f\rho_{\rm eq}/(2\bar{m})$, where f is the fraction of DM in the form of PBHs, $\rho_{\rm eq}$ is the density at the time of equality, and $\bar{m}$ is the average mass in the distribution. We may then write

$$X = nV = \left(\frac{x}{\bar{x}}\right)^3,$$

where

$$\bar{x} = \left(\frac{3\bar{m}}{2\pi f \rho_{\rm eq}}\right)^{1/3}. \tag{2.2}$$

In a spherical region of radius $\bar{x}$ we expect to find one PBH, on average, so the length scale $\bar{x}$ can also be thought of as a typical separation between PBHs.

A pair of black holes forms a binary when the relative kinetic energy due to the Hubble flow becomes comparable to the gravitational binding energy between the two objects [4],

$$\frac{1}{2}\mu H^2 s^2 x^2 \sim \frac{G m_1 m_2}{s x}. \tag{2.3}$$

Here, $\mu = m_1 m_2/M$ is the reduced mass, where $M = m_1 + m_2$ is the total mass of the binary. The above relation has to be satisfied before the end of the radiation era, since both sides will scale as s^{-1} during matter domination. For $x \lesssim \bar{x}$, and taking into account that $\rho \approx \rho_{\rm eq}/(2s^4)$ in the radiation era ($s \ll 1$), the relation (2.3) is satisfied when the cosmological scale factor s is of order $s \sim \lambda(\bar{m}/M) \leq 1$, where we have introduced

$$\lambda \equiv \frac{X}{f}. \tag{2.4}$$

[2] The effect of such an initial correlation has been discussed in refs. [14, 16].

[3] This is expected when PBH are formed from very high peaks of a Gaussian random field of density perturbations [35, 36], even if the enhancement in the power spectrum has a sizable width. Unless the power spectrum involves different explicit scales, high peaks of the random field tend to have a well defined shape, which leads to a relatively narrow range of masses after gravitational collapse.

JCAP09(2019)043

More precisely, parametrizing the physical distance as $d = \chi(\eta; \lambda)x_0$, where x_0 is the initial co-moving separation, we may write

$$x = |\vec{x}| = \frac{\chi(s)}{s} x_0. \tag{2.5}$$

The numerical analysis in refs. [9, 19] shows that, that for binaries forming deep in the radiation era (i.e. $\lambda \ll 1$), the function χ is self-similar

$$\chi(s; \lambda) = \lambda \chi(s/\lambda; 1). \tag{2.6}$$

Initially, the two PBH are following the Hubble flow, so that $\chi \approx s$, $\vec{x} \approx \vec{x}_0$ is approximately constant, and the physical distance grows linearly in s. However, when the scale factor reaches the value

$$s \approx s_b = \frac{\lambda}{3} \left(\frac{2\bar{m}}{M} \right), \tag{2.7}$$

the physical distance turns around and a bound system is formed with semi-major axis given by [9]

$$a = 3\beta s_b \frac{x}{2} = \frac{\beta}{2} \left(\frac{2\bar{m}}{M} \right) \left(\frac{3\bar{m}}{2\pi\rho_{\rm eq}} \right)^{1/3} \lambda^{4/3}, \tag{2.8}$$

where $\beta \approx 0.2$. Introducing the dimensionless average mass parameter

$$m \equiv \frac{\bar{m}}{M_\odot}, \tag{2.9}$$

we have

$$a \approx 1.8 \cdot 10^{-7} \lambda^{4/3} m^{1/3} \left(\frac{2\bar{m}}{M} \right) H_{\rm eq}^{-1}, \tag{2.10}$$

where we have used $H_{\rm eq}^{-1} \approx 0.9 \cdot 10^{18}\, km$.

In an environment with no external forces and torques, two PBHs which are initially at rest would collide head-on due to gravitational attraction in a very short time-scale

$$\Delta t \sim a^2 (GMa)^{-1/2} \sim H_b^{-1} \lesssim t_{\rm eq}, \tag{2.11}$$

comparable to the Hubble radius H_b^{-1} at the time when the binary forms. However, the binary system is immersed in a local tidal field, created by density perturbations and by other PBHs in the neighborhood. These forces will exert a torque on the binary, giving it an orbital angular momentum which avoids the head-on collision. The binary will then slowly radiate its energy by emitting gravitational waves in a much longer timescale, before the final merger occurs.

For a binary with initial orbital angular momentum ℓ per unit reduced mass, the life-time is given by Peters formula [37]

$$t = t[j, a] \equiv \frac{3}{85} \frac{a^4}{G^3 m_1 m_2 M} j^7, \tag{2.12}$$

where dimensionless parameter j, is defined as

$$j \equiv \frac{\ell}{\sqrt{GMa}}. \tag{2.13}$$

JCAP09(2019)043

For an elliptic orbit with semi-minor axis b, we have $j = b/a = \sqrt{1-e^2}$, where e is the eccentricity. Note that $j < 1$. Using $t = t_0 \approx 1.3 \cdot 10^{23}\, km$, we find that the binaries which are merging today are characterized by

$$j = j_0(\lambda) \approx 1.6 \cdot 10^{-3} \lambda^{-16/21} m^{5/21} \left(\frac{M}{2\bar{m}}\right) \left(\frac{4m_1 m_2}{M^2}\right)^{1/7}, \tag{2.14}$$

where we have used eq. (2.8) with $\beta \approx 0.2$. The distribution of j in the ensemble of binaries depends on the specific mechanisms which give the binaries their angular momentum.

2.2 Merger rates

In general, the differential number density of binaries per unit volume is given by

$$dn_{\rm bin} = dn_M d^2\mathcal{F}. \tag{2.15}$$

Here

$$d^2\mathcal{F} \equiv d\mathcal{F}(m_1) d\mathcal{F}(m_2), \tag{2.16}$$

where $d\mathcal{F}$ is the PBH mass distribution function, and $dn_M(m_1, m_2, X, j)$ is the distribution of binaries with masses m_1 and m_2, initial separation of the partners characterized by X and orbital angular momentum parameter j. The variable X is distributed as (2.1), so using $X = f\lambda$, we have

$$dn_M = \Theta\left(M - \lambda\bar{m}\right)\ f^2 \frac{\rho_m(t_0)}{2\bar{m}} e^{-f\lambda} dP(j;\lambda) d\lambda, \tag{2.17}$$

where $dP(j;\lambda)$ is the distribution of j for given λ, $f\rho_m(t_0)/\bar{m}$ is the number density of PBH at the present time, ρ_m is the current matter density, and we have inserted a factor of $1/2$ to avoid double counting of binaries. The Heavyside function restrics the range of λ since, according to our earlier discussion around eq. (2.3), a given PBH will only be part of a binary if the distance to the nearest PBH satisfies

$$\lambda \lesssim \frac{M}{\bar{m}}. \tag{2.18}$$

Otherwise the Hubble flow velocity always remains larger than the binding energy. If the distribution of masses is not too wide, we have $M \sim 2\bar{m}$, and for $f \ll 1$ the exponential factor $e^{-f\lambda}$ can be approximated by 1.

The intrinsic merger rate[4] of PBH binaries per unit time and volume can be written as

$$d\Gamma(t_0, m_1, m_2) = \Gamma_M(t_0) d^2\mathcal{F} \tag{2.19}$$

where the rate at fixed total mass $M = m_1 + m_2$ is given by

$$\Gamma_M(t_0) = \int \delta\left(t_0 - t[j,a]\right) dn_M. \tag{2.20}$$

Using (2.12) in the argument of the delta function, we can perform the j integration to obtain

$$\Gamma_M(t_0) = f^2 \frac{\rho_m}{14\bar{m}t_0} \int_{\lambda_{\rm min}}^{M/\bar{m}} W(\lambda) d\lambda. \tag{2.21}$$

[4]Here, and for the rest of this paper, we consider intrinsic merger rates, ignoring effects due to time delay of events which occur at high redshift. These can be incorporated along the lines of ref. [19].

JCAP09(2019)043

Here, we have dropped the factor $e^{-f\lambda}$, since as mentioned above this can be approximated by unity in the relevant range of parameters. Also, we have introduced

$$W(\lambda) = j \left. \frac{dP(j;\lambda)}{dj} \right|_{j=j_0}, \tag{2.22}$$

where j_0 given by eq. (2.14) is the value of j for which the lifetime of the binary coincides with the present age of the universe t_0. The integral in (2.21) is in the range

$$\lambda_{\rm min} < \lambda \lesssim M/\bar{m}, \tag{2.23}$$

where the lower limit[5] $\lambda_{\rm min} \sim 2 \cdot 10^{-4} m^{5/16}$ is determined from (2.14), taking into account that we must have $j_0 \leq 1$.

The distribution $dP(j;\lambda)$ depends on the mechanism which gives angular momentum to the binaries. In general,

$$j = |\vec{j}_{nb} + \vec{j}_{cp}| \tag{2.24}$$

is the added contribution from torques due to neighboring PBHs, and from torques due to cosmological perturbations. For the rest of this section we concentrate on j_{nb}, while the effect of cosmological perturbations will be discussed in the following sections.

2.3 Tidal torque due to neighboring black holes

Let us start by considering the effect of a single neighboring PBH, producing a tidal torque on the binary. By integrating the torque over time, we have,

$$\vec{j} \sim (\vec{x} \times \Delta\vec{g}) \frac{\Delta t}{\sqrt{GMa}}, \tag{2.25}$$

where Δt is given in eq. (2.11). Here, and for the rest of this section, we suppress the subscript nb from $\vec{j}$, since we are only dealing with the effect of neighboring PBHs. In eq. (2.25), $\vec{x} = \vec{x}_2 - \vec{x}_1$ is the relative co-moving separation between the members of the binary and

$$\Delta\vec{g} = \vec{\nabla}\Phi(\vec{x}_1) - \vec{\nabla}\Phi(\vec{x}_2), \tag{2.26}$$

is the tidal acceleration, expressed in terms of the Newtonian potential Φ created by the neighboring PBH. If the gradients vary on a length scale much larger than the separation $\vec{x}$, the tidal acceleration can be expanded in powers of $\vec{x}$ and the leading term is given by $\Delta g^k = -\Phi_{,kl}\, x^l$, where the spatial derivatives are with respect to the co-moving coordinates. If the 3rd black hole has a mass m_3, and is at a co-moving distance $y \gtrsim x$, then $\Phi \approx Gm_3/(s_b x)$, where s_b is the scale factor around the time when the binary forms. The co-moving gradients can then be estimated as $|\Phi_{,ij}| \sim (Gm_3/s_b y^3)(3y^i y^j - \delta_{ij})$, and Substituting in (2.25) with $a \sim s_b x$ we obtain

$$j = |\vec{j}| = \gamma \frac{j_X}{Y}. \tag{2.27}$$

Here we have introduced the variable $Y \equiv (y/\bar{x})^3$, characterizing the distance to the nearest third PBH, and

$$j_X = (\bar{m}/M) X. \tag{2.28}$$

[5] In the expressions which are given only by order of magnitude, and in the interest of brevity, we will often omit the explicit dependence on the individual masses, assuming they are within one order of magnitude or so from each other.

JCAP09(2019)043

Since the position of the third black hole is random, the distribution for Y is also given by

$$dP(Y) = e^{-Y} dY. \tag{2.29}$$

The coefficient γ is given by

$$\gamma \approx 1.5 \, |\sin 2\theta_3| \frac{m_3}{\bar{m}}, \tag{2.30}$$

where θ_3 is the angle between the relative coordinate $\vec{x}$ and the position of the third black hole $\vec{y}$, that is, $\cos\theta_3 = \hat{x} \cdot \hat{y}$. The overall numerical factor in this expression is determined by taking into consideration the time dependence in eq. (2.5) as the binary forms [1, 9, 12, 19]. Note that the average of γ over angle and mass distribution function is

$$\bar{\gamma} \approx 1.$$

Following [1], we keep γ as an undetermined random variable of order one, over which we can integrate at the end of the computation, if needed.

Taking into consideration (2.27) and (2.29), we have

$$dP^{(1)}(j;\lambda) = \gamma \frac{j_X}{j^2} \exp\left(-\gamma \frac{j_X}{j}\right) dj. \tag{2.31}$$

Here, the superindex in the probability distribution indicates that, for the time being, we are considering the effect of the nearest neighboring PBH only. Then, we have

$$W^{(1)}(\lambda) = j \left.\frac{dP^{(1)}(j;\lambda)}{dj}\right|_{j=j_0} = Y_0(\lambda) e^{-Y_0(\lambda)}, \tag{2.32}$$

where

$$Y_0(\lambda) \equiv \gamma \frac{j_X}{j_0(\lambda)} = \gamma \left(\frac{\lambda}{\lambda_*}\right)^{37/21}. \tag{2.33}$$

The characterisctic value

$$\lambda_* \approx 3.7 \cdot 10^{-2} f^{-21/37} m^{5/37} \left(\frac{M}{2\bar{m}}\right)^{42/37} \left(\frac{4m_1 m_2}{M^2}\right)^{3/37}, \tag{2.34}$$

is essentially the peak of the function $W^{(1)}(\lambda)$. The rate (2.21) is plotted in figure 1 for a range of values of f, and for different values of the mass $\bar{m}$, assuming that $m_1 = m_2 = \bar{m}$ and $\gamma \approx 1$. The curves have a knee which separates two different regimes with a power law behaviour in f. This can easily be understood analytically. The behaviour of the merger rate depends on whether λ_* is large or small, and this in turn depends on the value of f.

The behaviour of the merger rate below the knee ($\lambda_* \gg 1$) corresponds to a low fraction of DM in PBH, $f \ll f_*$, where

$$f_* \sim 3 \cdot 10^{-3} m^{5/21}. \tag{2.35}$$

Since $\lambda \lesssim M/\bar{m} \sim 1 \ll \lambda_*$, we have $Y_0 \ll 1$, and we may then neglect the exponential dependence of the integrand in (2.21),

$$\int_0^{\frac{M}{\bar{m}}} d\lambda W^{(1)} \approx \gamma \int_0^{\frac{M}{\bar{m}}} \left(\frac{\lambda}{\lambda_*}\right)^{37/21} d\lambda. \tag{2.36}$$

JCAP09(2019)043

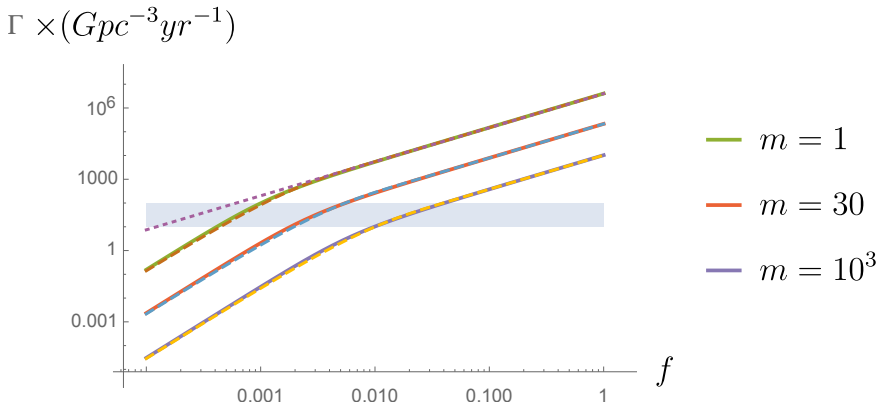

Figure 1. The dashed lines represent the merger rate $\Gamma_M^{(1)}$ of PBH binaries [given by eq. (2.21) with eq. (2.32)], as a function of f for different values of the mass. This estimate assumes that the initial angular momentum is due to the closest neighbouring black hole, and naively counts all binaries with the appropriate initial conditions for merging at the present time, as if they were in complete isolation. The thick lines represent the merger rate $\Gamma_M^{(\infty)}$ [given by eq. (2.21) with eq. (2.44)], where torques from all neighboring PBH are included. Solid and dashed curves nearly coincide, in agreement with the notion that it is the closest PBH that gives the dominant contribution to the torque. The gray shaded region corresponds to the merger rates observed by LIGO/Virgo. The approximation eq. (2.41) is also shown as a dotted line for $m = 1$. Unless otherwise stated, we will use $m_1 = m_2 = \bar{m}$ in all figures.

Since the lower limit of integration $\lambda_{\rm min} \sim 10^{-4}$ does not play a role, we have set it to zero for simplicity. This leads to the estimate

$$\Gamma_M^{(1)} \sim \frac{1.6 \cdot 10^{11}}{\mathrm{Gpc}^3\,\mathrm{yr}} \gamma f^3 m^{-26/21} \left(\frac{M}{2\bar{m}}\right)^{16/21} \left(\frac{M^2}{4m_1 m_2}\right)^{1/7}, \quad (\text{low } f) \tag{2.37}$$

where we have used

$$\frac{\rho_m}{M_\odot t_0} \approx 3 \cdot 10^9\,\mathrm{Gpc}^{-3}\,\mathrm{yr}^{-1}. \tag{2.38}$$

For an approximately monochromatic PBH mass function, the observational bound $\Gamma \lesssim 10^2\,\mathrm{Gpc}^{-3}\,\mathrm{yr}^{-1}$ then leads to

$$f \lesssim 0.85 \cdot 10^{-3} m^{26/63}. \tag{2.39}$$

We conclude that, if the third black hole is the dominant source of orbital angular momentum, then solar mass black holes, with $m \sim 1$, can only account for a very small fraction of dark matter, with $f \lesssim 10^{-3}$. This is in agreement with the analysis of refs. [1, 4]. Note that, even in the case $m \sim 1$ the upper limit of the observational bound (2.39) satisfies the condition $f \lesssim f_*$ only marginally.

Hence, let us now consider the complementary limit $f \gtrsim f_*$. For $\lambda \gg \lambda_*$ we have $Y_0(\lambda) = \gamma(\lambda/\lambda_*)^{37/21} \gg 1$, and due to the factor e^{-Y_0} the integral (2.21) is effectively cut-off at $\lambda = \lambda_* \ll 1$. Therefore it is a good approximation to remove the upper limit of integration, which doesn't play a role, and then the integral scales as λ_*,

$$\int_0^{\frac{M}{\bar{m}}} W^{(1)} d\lambda \approx \int_0^\infty d\lambda Y_0 e^{-Y_0} \approx \frac{21}{37}\Gamma\left(\frac{58}{37}\right)\gamma^{-21/37}\lambda_*. \tag{2.40}$$

JCAP09(2019)043

The rate can then be approximated as

$$\Gamma_M^{(1)} \sim \frac{4\cdot 10^6}{\mathrm{Gpc}^3\,\mathrm{yr}} f^2(\gamma f)^{-21/37} m^{-32/37} \left(\frac{M}{2\bar{m}}\right)^{42/37} \left(\frac{4m_1m_2}{M^2}\right)^{3/37}. \quad \text{(higher } f\text{)} \tag{2.41}$$

The observational bound $\Gamma \lesssim 10^2\,\mathrm{Gpc}^{-3}\,\mathrm{yr}^{-1}$ then leads to the condition

$$f \lesssim 0.6\cdot 10^{-3} m^{32/53}, \tag{2.42}$$

where, as in eq. (2.39), in this inequality we assume a nearly monochromatic PBH mass function. In the mass range of LIGO/Virgo detections, $m \sim 30$, the bound on the fraction f of DM in PBH is limited to $\sim 0.5\%$, again in good agreement with [1, 4]. The analytic estimate (2.41) is plotted in figure 1 as a dotted line for $m = 1$.

The previous considerations can be extended to the case where we include the torque of all neighboring black holes, and not just the closest one. An expression for $dP^{(\infty)}(j)$ due to the cumulative effect of all PBHs in the neighborhood was derived in [1, 9, 19]. This has the form of a power law distribution with a break at $j_X \equiv (\bar{m}/M)X = (\bar{m}/M)f\lambda$:

$$j\frac{dP^{(\infty)}(j;\lambda)}{dj} = \frac{(j/j_X)^2}{(1+(j/j_X)^2)^{3/2}}. \tag{2.43}$$

Note that at large j, the behaviour of (2.43) is similar to (2.31), where only the nearest PBH is considered. However, at small j the distribution (2.31) vanishes exponentially in $1/j$, while (2.43) has the form $dP^{(\infty)} \propto jdj$. As pointed out in [1], the reason is that in the case of a single PBH, the only way to reduce the torque on the binary is to place the PBH sufficiently far. The probability for that decays exponentially in $1/j$ for large distance. On the other hand, when many neighboring PBHs are involved, their added torques may randomly produce a small effect, with a probability which is only phase space suppressed. The dimensionless angular momentum $\vec{j}$ is in the plane orthogonal to the initial relative separation $\vec{x}$, so the corresponding measure is two dimensional $d^2\vec{j} = 2jdj$, and the behaviour $dP \propto jdj$ is expected. In conclusion, the distribution (2.31) does not provide a very good description at small j, even if it is true that the nearest PBH gives the dominant contribution to the torque.

Using (2.43) in (2.22) we have

$$W(\lambda) = \frac{\bar{Y}_0}{(1+\bar{Y}_0^2)^{3/2}}, \tag{2.44}$$

where

$$\bar{Y}_0 = \frac{j_X}{j_0} = \left(\frac{\lambda}{\lambda_*}\right)^{37/21}, \tag{2.45}$$

is the same as Y_0 given in (2.33), with the coefficient γ replaced by its averaged value over masses and directions, $\bar{\gamma} = 1$.

At low f, where $\lambda_* \gg 1$, we have $\bar{Y}_0 \ll 1$ throughout the range of integration in (2.21). Hence, $W \approx \bar{Y}_0$, and the rate will be given by eq. (2.37). In other words, the inclusion of the effect of an infinite number of neighbours does not change the merger rate:

$$\Gamma_M^{(\infty)} \approx \Gamma_M^{(1)}, \quad \text{(low } f\text{)} \tag{2.46}$$

JCAP09(2019)043

Also, at high f, where $\lambda_* \ll 1$, the integral is dominated by $\lambda \sim \lambda_* \ll M/\bar{m}$, so we can approximate by extending the range of integration to infinity and evaluating in terms of Euler's Gamma function. Then one finds

$$\Gamma_M^{(\infty)} \approx 0.95\Gamma_M^{(1)}, \quad \text{(higher } f\text{)} \tag{2.47}$$

and the difference between the two cases is only by a very small change in the overall numerical factor. In fact, the distributions (2.32) and (2.44) produce integrated merger rates which are almost indistiguishable from one another (also for intermediate values of $f \sim 10^{-3}$), in agreement with the notion that the nearest PBH gives the dominant contribution to the torque (See figure 1). More importantly, the dependence of the merger rate on binary masses is basically unaffected by the inclusion of an infinite number of neighbours. Let us now turn to the characterization of such mass dependence.

2.4 Universality in the mass dependence of the merger rates

In principle, we cannot predict the mass dependence of the merger rates unless the initial mass distribution function $d\mathcal{F}(m_i)$ is known. Unfortunately, the latter is model dependent. However, a very interesting observation was made in ref. [1] which may bypass this difficulty. Noting that the rate in a given mass interval Δm_1, Δm_2 is given by $\Delta\Gamma(m_1, m_2) = \Gamma_M(m_1, m_2)\Delta\mathcal{F}(m_1)\Delta\mathcal{F}(m_2)$, the expression

$$\alpha \equiv -M^2 \frac{\partial^2}{\partial m_1 \partial m_2} \ln[\Delta\Gamma(m_1, m_2)] \tag{2.48}$$

is independent of the unknown distribution funcion $\mathcal{F}$. It was argued in [1] that with a sufficiently large sample of PBH merger events, of order 10^3, the coefficient α can be determined observationally with accuracy of order 15%. This makes it a very attractive observable, within reach of existing and upcoming gravitational wave detectors [38].

If neighboring PBHs are the only source of angular momentum for the binaries, the coefficient α can readily be found from the expressions (2.37) and (2.41). The powers of $m_1 m_2$ in these expressions for the merger rate do not contribute to α, since after taking the logarithm and the two derivatives with respect to m_1 and m_2 such terms drop out. This is the same reason why α does not depend on the initial mass distribution functions $\mathcal{F}$. The only contributions to α come from powers of the total mass M. Hence, from (2.37), we have

$$\alpha = 22/21, \quad (\text{low} f) \tag{2.49}$$

and from (2.41) we have

$$\alpha = 36/37. \quad (\text{higher} f) \tag{2.50}$$

This leads to the prediction of a "hidden universality" in the merger rate [1], where the parameter α should be in the narrow range

$$0.97 \lesssim \alpha \lesssim 1.05. \tag{2.51}$$

As we shall see, this universality coefficient can be altered by different effects [see figure 9]. This may convey useful information about the actual circumstances surrounding binary formation and evolution.

JCAP09(2019)043

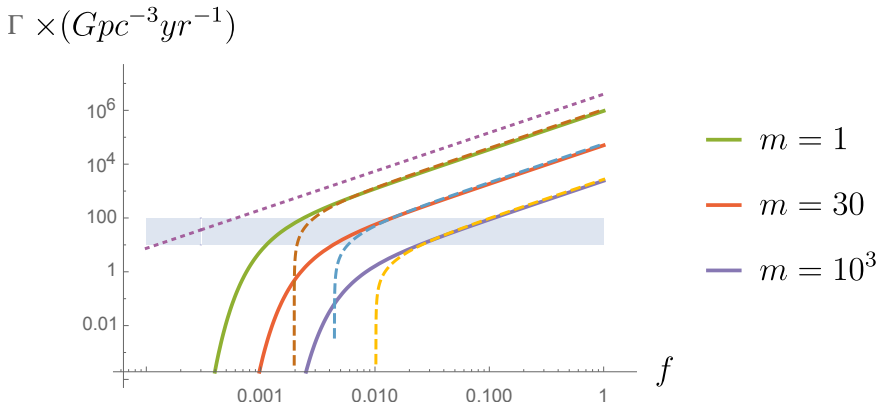

Figure 2. The effect of PBH infalls onto binaries. The plot is the same as figure 1, but now excluding all binaries with $Y < Y_{\rm min} = 2$ since these are likely to be disrupted by the infall of neighbouring PBHs. For comparison, the approximation eq. (2.41) is also shown as a dotted line for $m = 1$. Dashed lines correspond to the crude approximation where only the closest PBH contributes to the torque, whereas solid lines include the torque from all neighboring PBHs. Generally, the rate is suppressed at large f by a factor of order $e^{-Y_{\rm min}}$. At low f the rate drops rather dramatically since it is hard to give the binaries the necessary angular momentum unless there is a neighbour close enough to the binary. However, as we shall see, this dramatic drop is avoided when the torque from cosmological perturbations is included (see e.g. figure 4).

2.5 PBH infalls and the universality coefficient

Eq. (2.21) includes all binaries which have the appropriate initial conditions to merge at the present time, provided that they remain in isolation for the rest of cosmic history. It has been argued in [19] that this overestimates the rate, because some of the binaries may be affected by the infall of neighboring PBHs, which could disturb the eccentricity or even disrupt the binary. Note that binaries merging at the present time have a very low j, which is given by eq. (2.14), $j \sim 10^{-3}$. PBH infalls would increase this value by a large factor, making the life-time of the binary much larger than the age of the universe. On the other hand, if the closest neighbour is at a distance such that $Y \gtrsim M/\bar{m}$, then the binary is in an underdense region, and the neighbouring PBHs will not decouple from the Hubble flow to fall onto it [12, 19].

To illustrate the potential impact of infalls as a function of f, let us start by using a crude approximation where only the closest PBH contributes to the torque. Within this approximation, we may compare the naive rate given by eq. (2.21) with the merger rate of "pristine" binaries which are unaffected by infalls. This is achieved by restricting the integration to the range where, say,

$$Y > Y_{\rm min} = \frac{M}{\bar{m}}. \tag{2.52}$$

The result is illustrated in figure 2 (dashed lines). For that comparison, we assume a monochromatic mass spectrum, and the lower limit of the integral in eq. (2.21) is taken to be the value of λ that corresponds to $Y_0(\lambda) = M/\bar{m} = 2$. For very low $f \sim 10^{-3}$, the lower limit of integration becomes of order one, and for lower f the range of integration completely disappears. This causes the sudden drop of the dashed curves in figure 2. On the other hand the effect is not so dramatic for higher $f \gtrsim 10^{-3}$, amounting only to a moderate overall factor of order 10 or so. The reason is simple to understand. According to the analysis of

JCAP09(2019)043

subsection 2.3, for f above the knee in the curves of figure 1, the rates are dominated by binaries where the closest neighbor is at a distance $Y_0(\lambda_*) \sim 1$. In this case the factor $e^{-Y_0(\lambda)}$ acts as the effective cut-off of the integral (2.21) at the value $\lambda_* \lesssim 1$. Hence, the effect of restricting the range of integration to $Y > Y_{\rm min} = 2$ is only a mild suppression by a factor of order $\exp[-(Y_{\rm min} - Y(\lambda_*))]$, where the exponent is of order 1.

Since PBH infalls have a sizeable impact on the merger rates, it important to consider the overall effect of all neighboring PBH under the assumption that all of them are outside the basin of attraction of the binary. This issue was considered in generality in ref. [19], where the distribution $dP(j;\lambda,Y_{\rm min})$ was calculated, by taking into account *all* neighboring PBHs, and assuming that these are at a distance larger than $Y_{\rm min}$ from the binary. The result was found in closed form in terms of integrals of Hypergeometric functions, and it is somewhat cumbersome in general. However, the expression greatly simplifies in the limits $Y_{\rm min} \to 0$ and $Y_{\rm min} \gg 1$, which are of our primary interest. For $Y_{\rm min} \to 0$, eq. (2.43) is recovered, as expected, since in this case we do not exclude any of the binaries from the count. On the other hand, for $Y_{\rm min} \gg 1$, it was found that the distribution can be approximated as a Gaussian

$$dP(j;\lambda,Y>Y_{\rm min}) \approx \exp\left(-\frac{j^2}{\sigma_{nb}^2}\right)\frac{2jdj}{\sigma_{nb}^2}, \quad (Y_{\rm min}\gg 1) \tag{2.53}$$

with variance

$$\sigma_{nb}^2 = \frac{K}{Y_{\rm min}} j_X^2. \tag{2.54}$$

Here, $K = 6\langle m^2\rangle/(5\bar{m}^2) \sim 1$, where the brackets indicate average over the mass distribution. The approximation is already quite accurate for $Y_{\rm min} \gtrsim 2$, which is the range of our interest.

The differential merger rate is therefore given by

$$W(\lambda) = j\frac{dP(j;\lambda,Y>Y_{\rm min})}{dj}\bigg|_{j=j_0} e^{-Y_{\rm min}}, \tag{2.55}$$

where the factor $e^{-Y_{\rm min}}$ accounts for the probability that the closest neighboring PBH is further than $Y_{\rm min}$. Here, and in what follows, we restrict attention to the regime where $f \gtrsim f_*$, which seems most relevant for observations. Then, we can approximate (2.21) by removing the upper limit of integration and we have

$$\int_0^\infty W d\lambda \approx \frac{21}{37}\Gamma\left(\frac{53}{74}\right)(K\bar{\gamma}^2)^{-21/74}\lambda_* Y_{\rm min}^{21/74} e^{-Y_{\rm min}}, \tag{2.56}$$

where we have used (2.45). The corresponding merger rate is plotted in figure 2 (solid lines), for different values of the mass.

Let us now consider the universality coefficient α. If $Y_{\rm min}$ were independent of the masses, then (2.57) would scale like λ_*, just like in eq. (2.40). In that case, we would recover the value $\alpha = 36/37$. However, since heavier binaries have a larger basin of attraction, $Y_{\rm min}$

JCAP09(2019)043

scales as (2.52), and we have[6]

$$\alpha = \frac{36}{37} + \frac{21}{74} \approx 1.26. \tag{2.58}$$

The second term comes from $M^{21/74}$ in (2.56). It is interesting to note that the factor $e^{-Y_{\rm min}}$, which is exponential in M, does not contribute to the parameter α, since it drops out after taking two derivatives of $\log\Gamma$ with respect to the masses. We conclude that the effect of infalls of neighboring PBHs onto binaries produces a significant shift of α towards a higher value.[7] Let us now turn our attention to the effect of cosmological perturbations. As we shall see, the parameter α can also be sensitive to these.

3 Cosmological perturbations

In this section we consider the effect of cosmological perturbations on the eccentricity of PBH binaries. In contrast with previous work, we include the effect of density perturbations in radiation, which can be dominant for binaries with $\lambda \ll 1$, decoupling from the Hubble flow deep in the radiation era.

Let us assume that primordial density perturbations are adiabatic and Gaussian. These are completely characterized by the primordial power spectrum of a single scalar variable, such as the temporal component of the metric perturbation in the longitudinal gauge [39], often denoted by Φ. This variable plays the role of the Newtonian potential in the non-relativistic limit. In Fourier space the gravitational potential is expressed as

$$\Phi(\vec{x},\eta) = (2\pi)^{-3/2} \int \Phi_{\vec{k}}(\eta) e^{i\vec{k}\cdot\vec{x}}\, d^3k. \tag{3.1}$$

For perturbations with $k\eta_{\rm eq} \gg 1$, entering the horizon well before equality($\eta \ll \eta_{\rm eq}$), radiation dominates over dark matter and baryons. Neglecting the decaying mode on supercurvature scales, the time dependence of such modes for $\eta \ll \eta_{\rm eq}$ is then given by [39]

$$\Phi_{\vec{k}}(\eta) \approx \Phi^0_{\vec{k}} \left[G(k\eta/\sqrt{3}) + \kappa s(\eta) H(k\eta/\sqrt{3}) \right], \tag{3.2}$$

where $\kappa = \Omega_{DM}/\Omega_M \approx 0.84$ is the fraction of non-relativistic matter in the form of dark matter, and the time dependence is given in terms of

$$G(x) \equiv \frac{3}{x^2}\left[\frac{\sin x}{x} - \cos x\right], \qquad H(x) \equiv \frac{9}{2x^2}\left[\mathbf{C} - \frac{1}{2} + \ln x\right]\Theta(x-1). \tag{3.3}$$

[6] An analogous computation considering only the effect of the nearest PBH produces a somewhat different answer,

$$\int W d\lambda \approx \int Y_0 e^{-Y_0} d\lambda \approx \frac{21}{37}\gamma^{-\frac{21}{37}}\lambda_* \int_{Y_{\rm min}}^{\infty} Y_0^{\frac{21}{37}} e^{-Y_0} dY_0 = \frac{21}{37}\gamma^{-\frac{21}{37}}\lambda_* \Gamma(58/37, Y_{\rm min}). \tag{2.57}$$

Approximating $\Gamma(58/37, Y_{\rm min}) \approx 1.25\, Y_{\rm min}^{21/37} e^{-Y_{\rm min}}$ for $Y_{\rm min} \gtrsim 2$, and using (2.52) we find $\alpha = (36+21)/37 \approx 1.54$. However, it should be noted that here we are considering large Y, which corresponds to small j, and in this regime it is not a good approximation to neglect the contribution from all other PBHs, as explained in the paragraph following eq. (2.43).

[7] Aside from infalls, the simulations in ref. [19] also indicate that, for $f \gtrsim 0.1$, binaries can be disrupted during the matter dominated era by interaction with compact N-body systems. This effect can be particularly important for $f \sim 1$, where a sizable fraction of the binaries undergo interactions even before the time of recombination. This effect is also likely to suppress the rates at high f, and further work is needed to assess what fraction of the binaries may ultimately remain unaffected. In what follows, we shall simply ignore this possibility, assuming that f is low enough for this effect to be unimportant.

JCAP09(2019)043

Here, $\mathbf{C} \approx 0.577$. The initial amplitudes $\Phi^0_{\vec{k}}$ of the gravitational potential on superhorizon scales are Gaussian distributed, with variance given by

$$\langle \Phi^0_{\vec{k}} \Phi^0_{\vec{k}'} \rangle = \sigma^2_\Phi(k) \delta^{(3)}(\vec{k} + \vec{k}'). \tag{3.4}$$

The functions G and H represent the contribution of radiation and matter density perturbations, respectively. Which one dominates the torque will depend on the time η_b when binaries decouple from the Hubble flow, which in turn is related to the co-moving binary size [see eq. (2.7)]. At early times, matter is subdominant, and the contribution of matter perturbations to Φ is suppressed by the scale factor $s = (\eta/\eta_{\rm eq})$ in front of H in eq. (3.3). The factor $\Theta(x-1)$ in H should not be taken too literally, it is just meant to indicate that the expression is only valid after the modes cross the horizon, $k\eta_{\rm eq} \gg 1$, and the logarithmic growth begins.

The angular momentum per unit reduced mass of the binary, $\vec{\ell}$, can be written as a time integral of the tidal torque exerted by the gravitational potential. Denoting by $\vec{x}_1(\eta)$ amd $\vec{x}_2(\eta)$ the co-moving positions of the two members of the binary, we have:

$$\vec{\ell} = -\int \vec{x}(\eta) \times [\vec{\nabla}\Phi(\vec{x}_2, \eta) - \vec{\nabla}\Phi(\vec{x}_1, \eta)]\, s(\eta) d\eta, \tag{3.5}$$

where $\vec{x}(\eta) = \vec{x}_2 - \vec{x}_1$ is the relative co-moving coordinate, which is time dependent from the time η_b when the binary decouples from the Hubble flow [see eq. (2.5)].

In order to calculate the variance of the angular momentum, we will work at lowest order in the gravitational potential, so that inside the integrand in eq. (3.5) we can use the unperturbed head-on trajectory, which we shall take along the z axis, with relative coordinate:

$$\vec{x} = x \hat{e}_z. \tag{3.6}$$

Assuming that the center of mass is at the origin of coordinates, the positions of the two PBHs are given by $\vec{x}_2 = (m_1/M)\vec{x}$ and $\vec{x}_1 = -(m_2/M)\vec{x}$. Using (3.4) and (3.5) we have

$$\langle \ell^i \ell^j \rangle = \frac{\epsilon^{zmi}\epsilon^{znj}}{2\pi^3} \int \sigma^2_\Phi(k) k_m k_n F^* F d^3\vec{k}, \tag{3.7}$$

where the indices i, j, m, n can only take values x or y and

$$F = \frac{1}{2}\int_0^{\eta_{\rm eq}} d\eta s(\eta) x [G(k\eta/\sqrt{3}) + \kappa s(\eta) H(k\eta/\sqrt{3})] \left(e^{ik_z x \frac{m_1}{M}} - e^{-ik_z x \frac{m_2}{M}} \right). \tag{3.8}$$

Introducing spherical coordinates in momentum space, $k_x = k\sin\theta\cos\phi$, $k_y = k\sin\theta\sin\phi$, $k_z = k\cos\theta$, and integrating over ϕ, we have

$$\langle \ell^2 \rangle = \frac{1}{\pi^2} \int dk k^4 \sigma^2_\Phi(k) \int_{-1}^{1} dw (1-w^2) |F(k, x_0, w)|^2, \tag{3.9}$$

where we have used $\langle \ell^2 \rangle = \langle \ell^i \ell^j \rangle \delta^{ij} = 2\langle \ell^x \ell^x \rangle$ and we have introduced the change of variable $w = \cos\theta$.

To estimate the integral F we first note that the radiation G, and matter H terms make their contribution at very different times. Consider a binary with initial separation x_0 that decouples from the Hubble flow at the conformal time η_b. From (2.8) and (2.10), these two scales are widely separated, and parametrically related by

$$k_0^{-1} = x_0 \sim 5.4 \cdot 10^{-6} m^{1/3} \lambda^{-2/3} \eta_b \ll \eta_b. \tag{3.10}$$

JCAP09(2019)043

In general, all perturbations make their contribution to the torque at times $\eta \lesssim \eta_b$. After that, the binary starts oscillating, its co-moving size shrinks, and tidal gradients decay in inverse proportion to the scale factor. Perturbations in radiation start oscillating once they enter the horizon, and make most of their contribution to the torque at $\eta \sim k^{-1} \lesssim \eta_b$, while matter perturbations make their contribution near the time $\eta \sim \eta_b$, regardless of their wavelength.

3.1 Perturbations in radiation

Let us start by considering small binaries, for which $\lambda \ln(k_0\eta_b) \ll 1$. These form deep in the radiation dominated era, at the time when $s = s_b(\lambda) \sim \lambda \ll 1/\ln(k_0\eta)$. In this case, perturbations in radiation dominate over matter perturbations. From eq. (3.10), and assuming masses in the stellar range, the logarithm is of order 10, and so this condition requires $\lambda \ll 0.1$. In this regime, we can neglect $s(\eta)H(k\eta/3)$ relative to $G(k\eta/3)$ for $\eta \lesssim \eta_b$, and we have

$$F \approx \frac{x_0}{2}\left(e^{ikwx_0\frac{m_1}{M}} - e^{-ikwx_0\frac{m_2}{M}}\right)\int_0^{\eta_{\rm eq}} d\eta\, s\, G\left(\frac{k\eta}{\sqrt{3}}\right). \quad (k\eta_b \gtrsim 1) \tag{3.11}$$

Due to the oscillating nature of G for $\eta \gg k^{-1}$, the integral is dominated by early times $\eta \ll k^{-1} \lesssim \eta_b$, where $x = x_0\chi(\eta)/s$ is approximately constant, $x \approx x_0$, and can be taken out of the integral (3.8). Noting that

$$\int_0^{\eta_b} d\eta s G\left(\frac{k\eta}{\sqrt{3}}\right) = \frac{9}{k^2\eta_{\rm eq}}\left[1 - \mathrm{sinc}\left(\frac{k\eta_b}{\sqrt{3}}\right)\right], \tag{3.12}$$

it is clear that the contribution of modes outside the horizon at the time of binary formation, $k\eta_b \ll 1$, is suppressed. For modes with $k\eta_b \gg 1$ we can approximate

$$|F|^2 \approx \frac{81x_0^2}{k^4\eta_{\rm eq}^2}\sin^2\left(\frac{kwx_0}{2}\right). \tag{3.13}$$

Substituting in (3.9), and using

$$\int_{-1}^{1} dw(1-w^2)\sin^2\left(\frac{kwx_0}{2}\right) = \frac{2}{3}[1 - G(kx_0)], \tag{3.14}$$

where the function G is defined in (3.3), we have[8]

$$\sigma^2_{cp(rad)} \equiv \langle j^2_{cp}\rangle = \frac{\langle \ell^2\rangle}{GMa} \approx 2.2\cdot 10^3 \int \frac{dk}{k}\, P_\Phi(k)\left[\frac{1-G(kx_0)}{(kx_0)^2}\right]\left[1 - \mathrm{sinc}\left(\frac{k\eta_b}{\sqrt{3}}\right)\right]^2. \tag{3.16}$$

The subindex in j_{cp} indicates that this is due to cosmological perturbations, as opposed to the neighboring black holes which we considered in the previous section. Here we have introduced the standard expression for the primordial power spectrum

$$P_\Phi(k) = \frac{\sigma_\Phi^2 k^3}{2\pi^2}. \tag{3.17}$$

[8] In determining the numerical coefficient in front of (3.16), we have used, from (2.2) and (2.8),

$$GMa = G\beta\lambda\bar{m}x = G\beta\bar{m}\frac{x_0^4}{f\bar{x}^3} = \beta x_0^4\frac{2\pi G}{3}\rho_{\rm eq} = \frac{\beta}{4}x_0^4 H_{\rm eq}^2 \approx \frac{x_0^4 H_{\rm eq}^2}{20}. \tag{3.15}$$

Also, we have used $H_{\rm eq}^2\eta_{\rm eq}^2 \approx 1$. Note that we are using the convention where the scale factor is equal to unity at the time of equality.

JCAP09(2019)043

In standard slow-roll inflationary scenarios, $P_\Phi(k)$ is nearly independent of k. In that case, the two factors in square brackets in eq. (3.16) play the role of the infrared and ultraviolet cut-off which regulate the logarithmic behaviour of the integral. Note that

$$\frac{1-G(kx_0)}{(kx_0)^2} \approx \begin{cases} \frac{1}{10}, & (kx_0 \ll 1) \\ \frac{1}{(kx_0)^2}. & (kx_0 \gg 1) \end{cases} \tag{3.18}$$

while

$$1 - \mathrm{sinc}\left(\frac{k\eta_b}{\sqrt{3}}\right) \approx \begin{cases} \frac{(k\eta_b)^2}{18}, & (k\eta_b \ll \sqrt{3}) \\ 1. & (k\eta_b \gg \sqrt{3}) \end{cases} \tag{3.19}$$

Therefore, for a nearly flat power spectrum, the integral will be dominated by the range $\eta_b^{-1} \lesssim k \lesssim k_0 = x_0^{-1}$,

$$\langle j_{cp}^2 \rangle \approx 2.2 \cdot 10^2 \int_{\sqrt{3}\eta_b^{-1}}^{k_0} \frac{dk}{k} P_\Phi \approx 2.2 \cdot 10^2 \ln\left(\frac{k_0\eta_b}{\sqrt{3}}\right) P_\Phi, \tag{3.20}$$

where

$$\ln\left(\frac{k_0\eta_b}{\sqrt{3}}\right) \approx 9.6 + \ln\left[\left(\frac{\lambda}{0.3}\right)^{2/3}\left(\frac{m}{30}\right)^{-1/3}\right]. \tag{3.21}$$

In the last approximate equality, we have used (3.10).

It may seem counterintuitive that the dispersion in j receives contributions from a wide range of scales, since at the time η_b when the binary forms, the amplitude of the gravitational potential for modes within the horizon falls off as k^{-2}. However, the torque at wavelenths larger than x_0 depends on second derivatives of the potential, which brings in a factor of k^2. As a result, the contribution is independent of scale in the range we are considering. Physically, the effect takes place well before the binary decouples from the Hubble flow, at the time $\eta \lesssim k^{-1}$. Hence, it seems appropriate to refer to this as the contribution of the peculiar velocities of the PBHs to the orbital angular momentum at the time when the binary forms.

It is also worth noting that the prefactor in front of the logarithm is independent of the parameters characterizing the binary. Each decade in wavelength gives the same contribution to $\langle j^2 \rangle$, and the dependence on parameters such as massess and semi-major axis, is only through the range of scales contributing to the logarithm. This is in contrast with the contribution from matter perturbations, which we now review.

3.2 Adding matter perturbations

Matter perturbations can be included along similar lines. One difference is that their effect on the binary occurs near the time $\sim \eta_b$ when the binary starts oscillating, and we cannot ignore the time dependence of the separation x in the integral (3.8) which gives $F(k, x_0, w)$. For $kx_0 \gg 1$, this has a dependence on m_1 and m_2 which, unlike the radiation case, is hard to disentangle in general.

For $kx_0 \ll 1$, we may use the approximation

$$e^{ikwx\frac{m_1}{M}} - e^{-ikwx\frac{m_2}{M}} \approx ikwx, \tag{3.22}$$

JCAP09(2019)043

in the integral (3.8). With this approximation, the dependence on masses disappears and we obtain the total contribution of radiation and matter perturbations as[9]

$$F \approx ikw\frac{9x_0^2}{k^2\eta_{\rm eq}}\left\{1+0.38\lambda\left(\frac{2\bar{m}}{M}\right)[L_0+\ln(kx_0)]\right\}, \tag{3.23}$$

where

$$L_0 \equiv \ln(k_0\eta_b/\sqrt{3}) + \mathbf{C} - (1/2) \approx 9.7. \tag{3.24}$$

Here, we have used (3.21), neglecting the small logarithmic dependence in λ and m.

Substituting (3.23) in (3.9) and performing the w integration, we immediately find the total variance of the orbital parameter due to long wavelength cosmological perturbations:

$$\sigma_{cp}^2 \equiv \langle j_{cp}^2\rangle \approx 2.2\cdot 10^2 \int_{\sqrt{3}\eta_b^{-1}}^{k_0}\frac{dk}{k}\left[1+0.38\lambda\left(\frac{2\bar{m}}{M}\right)[L_0+\ln(kx_0)]\right]^2 P_\Phi(k). \tag{3.25}$$

The first term in the square brackets in (3.23) corresponds to radiation, while the second one, accompanied by the factor of λ, corresponds to matter perturbations. The latter become subdominant for sufficiently small $\lambda \lesssim 0.27$. In view of our earlier discussion in subsection 2.3, for $f \gg 3\cdot 10^{-3}$ the rates are dominated by small binaries, with $\lambda \lesssim \lambda_* \ll 1$. Hence, it appears that perturbations in radiation may be as relevant for observations as the matter perturbations which have been considered in earlier analysis.

Let us now turn to a discussion of the effect of such perturbations on the merger rates.

4 Effect of perturbations on the merger rates

The size of binaries at the time of formation (shaded in gray in figure 3) is at intermediate co-moving scales which are much smaller than those probed by CMB temperature anisotropies or large scale structure. Indeed, from eqs. (2.8) and (2.10), we have

$$k_0 = \frac{1}{x_0} \approx 0.5\cdot 10^6 (m\lambda)^{-1/3} k_{\rm eq}. \tag{4.1}$$

Taking into account that λ is in the range (2.23), for stellar mass black holes $m \sim 1$–100 we have $k_0 \sim (10^5$–$10^7)k_{\rm eq}$, which corresponds to the present co-moving scale in the range[10] $\bar{k} \sim (10^3 - 10^5)\,{\rm Mpc}^{-1}$.

The angular momentum of PBH binaries may be affected by the power spectrum P_Φ of cosmological perturbations over a very wide range of scales. As illustrated in figure 3, such power spectrum is poorly constrained on scales smaller than $3\,{\rm Mpc}^{-1}$, and here we would like to explore the consequences this uncharted territory might have on the merger rate of

[9] In order to obtain the numerical coefficient in front of the matter contribution, we have used [9, 19] $\int_0^1 ds(\chi^2/s^2) \approx 0.3\lambda(2\bar{m}/M)$ to do the intergral of the second term in (3.8). Also, we have used $\kappa \approx 0.84$ for the ratio of dark matter density to the total non-relativistic matter density, and we have ignored the slow logarithmic dependence in η. Since the integral is dominated by $\eta \sim \eta_b$, we have used the value $\eta = \eta_b$ inside the logarithm in the mode function H.

[10] Throughout this paper, we adopt the convention that the scale factor s is equal to 1 at the time of equality. Thus, to avoid confusion, we will refer to the present day wave number by $\bar{k} = z_{\rm eq}k$. Note that relations such as eq. (4.1) between k_0 and $k_{\rm eq}$ are valid in both conventions, since the factor of $z_{\rm eq}$ applies to both sides of the equation.

JCAP09(2019)043

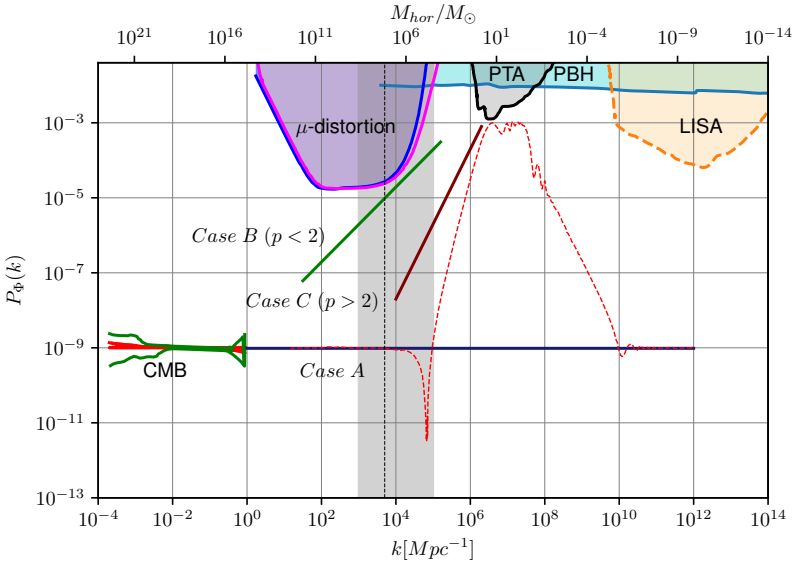

Figure 3. Current bounds on the power spectrum P_Φ of cosmological perturbations (see e.g. [40, 41]). Aside from the constraints from $\mu-$distorsions of the CMB, we also display the pulsar timing array (PTA) and LISA bounds, which constrain the production of gravitational waves from scalar perturbations at second order in perturbation theory. The PBH bound near the top of the figure is intended to represent the level at which the probability of PBH formation would high enough to be in conflict with current constraints on their cosmic abundance. We consider the effect of cosmological perturbations on the merger rate of PBH binaries in three different cases, labeled as case A, B and C, consistent with the observational constraints. The vertical shaded band corresponds to the scales k_0 characteristic of binaries which would be merging at the present time, in the mass range $m \sim 1$–100. The vertical dashed line corresponds to the pivot scale $k_B \approx 5 \cdot 10^3\,\mathrm{Mpc}^{-1}$ in eq. (4.8). For illustration, in dashed red line we plot the power spectrum of an inflationary model, which raises steeply with spectral index $p \approx 4$ up to a scale $k_C \approx 3 \cdot 10^6\,\mathrm{Mpc}^{-1}$, leading to a rather broad peak spanning one order of magnitude or so. This corresponds to a model [41] where the inflaton goes from slow roll to fast roll and then back to slow roll, through a discrete sequence of values of the second slow roll parameter η (see figure 10 of [41]).

binaries.[11] For this purpose, let us consider three distinct behaviours which may capture the generic effect of an enhanced power spectrum at small scales. These are labeled case A, B and C in figure 3. Let us consider them in turn.

4.1 Case A: nearly scale invariant cosmological perturbations

Consider a nearly scale invariant power spectrum of the form

$$P_\Phi \approx A_\Phi \left(\frac{k}{k_*}\right)^{n_s-1} . \tag{4.2}$$

This is consistent with observations of the CMB and large scale structure on cosmological scales, down to $\bar{k} \sim 3\,\mathrm{Mpc}^{-1}$, with $n_s \approx .97$, $A_\Phi \approx .97 \cdot 10^{-9}$ and $\bar{k}_* \approx 0.05\,\mathrm{Mpc}^{-1}$ [42]. A minimal assumption we can make, consistent with standard slow roll inflationary models, is

[11] In figure 3, we are ignoring bounds which are related to the abundance of ultra-compact mini-halos. Such constraints depend on the nature of dark matter, and could be absent in certain models (e.g. if dark matter belongs to a hidden sector). For a recent discussion, see [40] and references therein.

JCAP09(2019)043

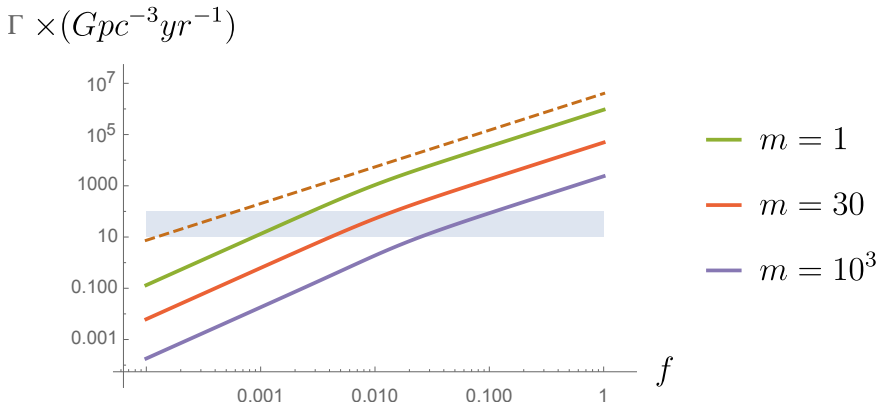

Figure 4. Here we plot the merger rate as a function of f (thick lines) for different values of m, assuming a scale invariant spectrum of cosmological perturbations with amplitude $P_\Phi \sim 10^{-9}$ (Case A). At small f, cosmological perturbations control the angular momentum of binaries merging today. The knee at $f \sim 10^{-2}$ arises because at higher f the effect of neighboring PBHs becomes dominant. Here we have used $Y_{\rm min} = 2$ for the infall radius. For comparison, we include the dotted line, corresponding to the analytic estimate (2.41) which ignores cosmological perturbations and binary infalls (here we use $m = 1$).

that the nearly flat spectrum can be extrapolated down to the co-moving size of binaries. Since the tilt is rather small, we may approximate $P_\Phi \approx const.$ over the range of interest.

Using (3.25) we then find

$$\sigma_{cp}^2 = \langle j_{cp}^2 \rangle \approx 2.1 \cdot 10^3 \left[1 + 3.7\lambda \left(\frac{2\bar{m}}{M} \right) + 4.5\lambda^2 \left(\frac{2\bar{m}}{M} \right)^2 \right] P_\Phi . \tag{4.3}$$

Assuming the CMB normalization $P_\Phi \approx 10^{-9}$, we have $\sigma_{cp}^2 \sim (2\text{–}9)10^{-6}$. Hence, for moderate values of λ, cosmological perturbations may easily provide an angular momentum comparable to j_0, given in (2.14), necessary for binaries to have a life-time comparable to the age of the universe. Still, neighboring PBH contribute to j with variance given by (2.54) [19],

$$\sigma_{nb}^2 \approx \frac{K}{4Y_{\rm min}} f^2 \lambda^2 \left(\frac{2\bar{m}}{M} \right)^2 , \quad (Y_{\rm min} \gtrsim 2), \tag{4.4}$$

where we are excluding binaries which may be disrupted by a PBH at distances smaller than $Y_{\rm min}$. Thus, at low f the effect of neighboring PBHs on the angular momentum is negligible compared to that of cosmological perturbations, while the latter effect can become important only at higher f. This is illustrated in figure 4.

To better understand the relative importance of the two effects, it is illustrative to look at the differential merger rate in the integrand in eq. (2.21):

$$W(\lambda) = 2\frac{j_0^2}{\sigma^2} e^{-\frac{j_0^2}{\sigma^2}} e^{-Y\rm min}, \tag{4.5}$$

where $\sigma^2 = \sigma_{nb}^2 + \sigma_{cp}^2$.

The function $W(\lambda)$ for Case A is plotted in thick lines in the left pannel of figure 5, for different values of f, and $m = 30$. At low $f \lesssim 10^{-2}$, the effect of neighboring PBHs is negligible. This corresponds to the values below the knee in figure 4. In this case figure 5 shows

JCAP09(2019)043

that for the low amplitude cosmological plateau with $P_\Phi \approx 10^{-9}$ the dominant contribution to W is at $\lambda \sim 1$. This value corresponds to a time of binary formation $\eta_b \sim \eta_{\rm eq}$. Even at this relatively late time the effect of relativistic matter perturbations has a noticeable effect on the position of the peaks. For comparison, we plot in dotted lines the case where perturbations in radiation are ignored. At higher $f \sim 10^{-1}$ we see from figure 5 that the rate is dominated by lower $\lambda \sim 0.1$. For such values of λ, binaries decouple earlier in time, when perturbations in radiation would be more important than those in non-relativistic matter. But in fact, both are negligible, since for such low values of f, the variance in j is dominated instead by the torque from neighboring PBHs. The situation is different when we consider an enhanced power spectrum (Case B), which is plotted in the right pannel of figure 5.

Before moving on to a discussion of enhanced power spectra, let us consider the parameter α in the presence of the standard scale invariant spectrum of cosmological perturbations (4.2). Note that the variance (4.4) dominates at high f, whereas the last term in (4.3) dominates at low f. Both terms have exactly the same dependence on λ and on the masses. They only differ in the explicit dependence of the variance on $Y_{\rm min}$, which is absent at low f. Hence, by the same argument which lead us to eq. (2.58), it is straightforward to conclude that

$$\frac{36}{37} < \alpha < \frac{36}{37} + \frac{21}{74}, \tag{4.6}$$

where the lower and upper bounds correspond to the limiting behaviours for low and high f respectively.

4.2 Case B: enhancement of the power spectrum at intermediate scales

Bounds on the amplitude of the power spectrum above $\bar{k} \sim 10\,{\rm Mpc}^{-1}$ are rather loose. The absence of CMB spectral distortions gives an upper bound at intermediate scales in the range $\bar{k} \sim 10$–$10^5\,{\rm Mpc}^{-1}$ [40, 45]

$$P_\Phi \lesssim 10^{-5}, \tag{4.7}$$

several orders of magnitude higher than the nearly scale invariant plateau observed on cosmological scales.

Hence, let us consider a generic power spectrum of the form

$$P_\Phi(k) = B_\Phi \left(\frac{k}{k_B}\right)^p, \quad (0 \leq p < 2) \tag{4.8}$$

where for convenience we choose the pivot scale to be $k_B = 5 \cdot 10^5 k_{\rm eq}$, corresponding to the present co-moving scale of $5 \cdot 10^3\,{\rm Mpc}^{-1}$. From eq. (4.1), this is by order of magnitude the co-moving size of the binaries, and we see from figure 3 that the power spectrum can be rather high at those scales, allowing for an enhanced amplitude up to $B_\Phi \lesssim 10^{-5}$. Let us now discuss the impact of this enhancement as a function of p. Here we focus on $p < 2$, leaving the discussion of steeper power spectra for the next subsection.

The case $p = 0$ is special, since the variance σ^2_{cp} depends logarithmically on the width of the plateau in the power spectrum. For illustration, let us consider a scale invariant spectrum of amplitude B_Φ between the scale $k_{\rm min} = 10^3 k_{\rm eq}$ and $k_{\rm max} \gtrsim 10^7 k_{\rm eq}$. Then, using (3.25), we find[12]

$$\sigma^{2\,(p=0)}_{cp} = \langle j^2_{cp} \rangle \approx 1.2 \cdot 10^3 \left[1 + 5.2\lambda \left(\frac{2\bar{m}}{M}\right) + 7.5\lambda^2 \left(\frac{2\bar{m}}{M}\right)^2\right] B_\Phi. \tag{4.9}$$

[12] In this estimate, we neglect a small subleading dependence in λ and m, assuming $|\ln[(\lambda/0.3)(m/30)]| \ll 16$.

JCAP09(2019)043

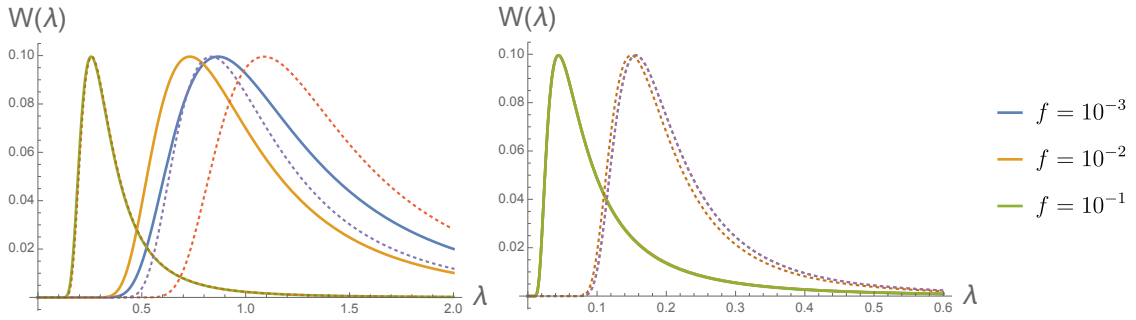

Figure 5. The left pannel shows the differential rate W in the integrand of eq. (2.21), for $m = 30$ and different values of f, in the case of a scale invariant spectrum of cosmological perturbations with amplitude $P_\Phi = 10^{-9}$ (Case A). The curves move from right to left with increasing values of f. At low $f \lesssim 10^{-2}$, cosmological perturbations give the dominant contribution to j,, while for higher f, cosmological perturbations are subdominant compared with the effect of neighboring PBHs. The thick curves include both matter and radiation perturbations, while perturbations in radiation are ignored in the dotted curves. We see that perturbations in radiation cause a shift of the peak towards smaller λ, which means that the binaries which are merging today decouple from the Hubble flow somewhat earlier. The right pannel corresponds to an enhanced power spectrum, which is nearly scale invariant at intermediate scales (Case B). In this case, cosmological perturbations provide the dominant contribution to the angular momentum of binaries which are merging today, for all values of f. The differential rate W is plotted for a power spectrum amplitude $B_\Phi = 10^6$ and three different values of f in thick lines. The three cases are degenerate, which implies that cosmological perturbations, and not the neighboring PBHs, provide the dominant torque. Note that W peaks at $\lambda \sim 0.05$. This corresponds to binaries which decouple from the Hubble flow deep in the radiation dominated era, when perturbations in non-relativistic matter are small relative to the perturbations in the radiation fluid. This is confirmed by the curves in dotted lines, where perturbations in radiation have been ignored, and which are quantitatively different (the curves with $f \lesssim 10^{-2}$ are degenerate in this case). Dominance of radiation perturbations grows even stronger at higher values of B_Φ.

Comparing with (4.4), it is clear that for $f \lesssim 0.1$ cosmological perturbations will dominate over the effect of neighboring PBH for amplitudes $B_\phi \gtrsim 10^{-7}$, which are well within the range allowed by observational constraints. This is illustrated in the right pannel in figure 5, where we see that the rate is dominated by $\lambda \lesssim 0.1$ Hence, we may approximate

$$\sigma_{cp}^{2\,(p=0)} \approx 1.2 \cdot 10^3 B_\Phi. \quad (B_\Phi \gtrsim 10^{-7}) \tag{4.10}$$

Using (2.14) we then have

$$\frac{j_0^2}{\sigma^2} \approx \left(\frac{\lambda}{\lambda_B^{(p=0)}} \right)^{-32/21}, \tag{4.11}$$

where

$$\lambda_B^{(p=0)} = \left[\frac{2.1 \cdot 10^{-9}}{B_\Phi} \left(\frac{M}{2\bar{m}} \right)^2 \left(\frac{4 m_1 m_2}{M^2} \right)^{2/7} \right]^{21/32} m^{10/32}. \tag{4.12}$$

For sufficiently high $B_\phi \gtrsim 10^{-7}$ we have $\lambda_B^{(p=0)} \ll 1$, and we can ignore the upper limit of integration in (2.21). Then we have:

$$\Gamma_M(t_0) \approx \frac{\rho_m}{M_\odot t_0} \frac{f^2}{14 m} \frac{21}{32} \Gamma\left(\frac{11}{32} \right) \lambda_B^{(p=0)} e^{-Y_{\rm min}}, \tag{4.13}$$

JCAP09(2019)043

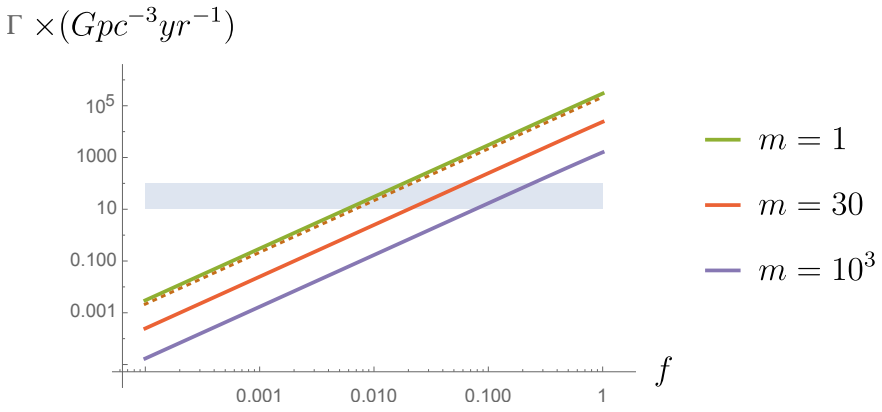

Figure 6. The thick lines represent the rates corresponding to a nearly scale invariant spectrum which is enhanced to the saturate the observational bound, $P_\Phi \lesssim 10^{-5}$, at the intermediate scales 10–$10^5\,\mathrm{Mpc}^{-1}$. This corresponds to Case B with $p \approx 0$, discussed in subsection 4.2, and we have used $Y_{\rm min} = 2$. The dotted line shows the analytic expression (4.17) for $m = 1$.

and using (2.38) and (4.10) we have

$$\Gamma_M(t_0) \approx \frac{7.8\cdot 10^4 f^2}{\mathrm{Gpc}^3\,\mathrm{Yr}} \frac{m^{-11/16}}{\sigma^{21/16}} \left(\frac{M}{2\bar{m}}\right)^{\frac{21}{16}} \left(\frac{4m_1m_2}{M^2}\right)^{3/16} e^{-Y_{\rm min}}. \tag{4.14}$$

We note that the same parametric dependence is obtained if we simply assume that all binaries are born equal, with the same initial dimensionless angular momentum[13] $j_* \sim \sigma$. From (4.14) we have $\Gamma_M \propto M^{15/16} e^{-Y_{\rm min}}$, and therefore

$$\alpha = \frac{15}{16} \approx 0.93, \quad (p = 0) \tag{4.16}$$

which is significantly lower than the values in the range (4.6), corresponding to the cosmological plateau. The difference comes from the fact that for the enhanced spectrum, perturbations in radiation dominate over matter perturbations, and this changes the mass dependence of merger rates. For $P_\Phi \approx 10^{-5}$, and for a monochromatic spectrum, we have

$$\Gamma(t_0) \approx 1.6\cdot 10^6 f^2 m^{-11/16} e^{-Y_{\rm min}}\,\mathrm{Gpc}^{-3}\,\mathrm{yr}^{-1}. \quad (p = 0) \tag{4.17}$$

This turns out to be an excellent approximation to the numerical result which is plotted in figure 6. In the mass range 30–100 solar masses, the LIGO bound on the merger rate requires $f \sim 5$–9%, where we have used $Y_{\rm min} \approx 2$. Hence, the bound on f is significantly relaxed compared to the case without cosmological perturbations.

[13]Indeed, if all binaries have the same $j = j_*$, then the rate is determined by those binaries whose semi-major axis is such that $j_0(\lambda) = j_*$. Assuming, for simplicity, a monochromatic PBH mass spectrum, this determines $\lambda = \lambda_0 = 1.3\cdot 10^{-4} j_*^{-21/16} m^{5/16}$. Hence, we have

$$\Gamma(t_0; j_*) = \frac{f\rho_m}{4\bar{m}} \int \delta(t_0 - t[a; j_*]) e^{-X} dX \approx 1.8\cdot 10^4 f^2 \frac{m^{-11/16}}{j_*^{21/16}}\,\mathrm{Gpc}^{-3}\,\mathrm{yr}^{-1} e^{-Y_{\rm min}}, \tag{4.15}$$

where we used $t \propto a^4 \propto \lambda^{16/3}$ and $X = \lambda f$ in order to do the integration over X by using the Dirac delta function. This matches eq. (4.14) for $j_* \approx 0.33\,\sigma$.

JCAP09(2019)043

For $0 < p < 2$, the integral in (3.25) is dominated by $k \approx k_0$. As we have just seen for the case of $p = 0$, when the amplitude of cosmological perturbations is enhanced, it is the perturbations in radiation that dominate, and in this case we know that the contribution of modes with $k \gtrsim k_0$ can also be important. This is given by eq. (3.16). Defining

$$\psi(p) = \int_0^\infty \frac{dk}{k} \left(\frac{k}{k_0}\right)^p \left[\frac{1 - G(kx_0)}{(kx_0)^2}\right] = 3\cos\left(\frac{\pi p}{2}\right) \frac{\Gamma[p-3]}{p-5}, \tag{4.18}$$

and using (4.8) in (3.16) we have

$$\sigma_{cp}^2 \approx 2.2 \cdot 10^3 \psi(p) \left(\frac{k_0}{k_B}\right)^p B_\Phi \left[1 + 3.7\lambda \left(\frac{2\bar{m}}{M}\right)\right]^2. \tag{4.19}$$

For the purpose of keeping track of the relative importance of radiation versus matter perturbations, here we have included the effect of matter perturbations up to the time $\eta = \eta_b$, which corresponds to the second term in square brackets in eq. (4.19). Matter perturbations can contribute to the angular momentum for some time after η_b, when the two PBHs forming the binary start falling towards each other. Here we have not included this contribution, which in principle can have a more complicated mass dependence. However, by order of magnitude, this effect is comparable to the contribution up to the time η_b. This characterization suffices in order to check whether perturbations in radiation are dominant or not. The numerical coefficient $\psi(p)$ is represented in figure 7, where we can see that $\psi > 0.44$ for all values of p, and that it diverges near both ends of the interval $0 < p < 2$. Such divergences correspond to the infrared and ultraviolet logarithmic divergences in the integral (3.16), respectively. In practice, these are cut-off by the finite range where the power spectrum has the specified behaviour, as we discussed for the case $p = 0$. Here, we shall simply consider a generic $p \sim 1$, which is not too close to 0 or 2, so that $\psi \sim 1$. In this case, we obtain

$$\sigma_{cp}^{2\,(p)} \approx 0.97 \cdot 10^3 \, \frac{\psi(p)}{0.44} \left[1 + 3.7\lambda \left(\frac{2\bar{m}}{M}\right)\right]^2 (m\lambda)^{-p/3} \left(\frac{10^6 k_{\rm eq}}{2k_B}\right)^p B_\Phi. \quad (p \sim 1) \tag{4.20}$$

In order to estimate the merger rates, let us first start by neglecting matter perturbations in (4.20). Using (2.14), we have

$$\frac{j_0^2}{\sigma^2} \approx \left(\frac{\lambda}{\lambda_B^{(p)}}\right)^{\frac{7p-32}{21}}, \tag{4.21}$$

with

$$\lambda_B^{(p)} = \left[\frac{2.7 \cdot 10^{-9}}{B_\Phi} \left(\frac{0.44}{\psi(p)}\right) \left(\frac{M}{2\bar{m}}\right)^2 \left(\frac{4m_1 m_2}{M^2}\right)^{2/7}\right]^{\frac{21}{32-7p}} m^{\frac{10+7p}{32-7p}}, \tag{4.22}$$

where we have set $k_B = 5 \cdot 10^5 k_{\rm eq}$. For $B_\Phi \gtrsim 10^6$ and $m \lesssim 100$, we find that $\lambda_B^{(p)} \ll 1$. This is consistent with the assumption that perturbations in radiation dominate over perturbations in matter, since the peak of the differential rate $W(\lambda)$, given by (4.5), occurs at $\lambda \sim \lambda_B^{(p)} \ll 1$.

For $0 \lesssim p \lesssim 1$, the integral in (2.21) quickly converges for $\lambda \gg \lambda_B^{(p)}$ and the upper limit of integration becomes irrelevant. In this case we have

$$\Gamma_M(t_0) \approx \frac{\rho_m}{M_\odot t_0} \frac{f^2}{14m} \left(\frac{21}{32-7p}\right) \Gamma\left(\frac{11-7p}{32-7p}\right) \lambda_B^{(p)} e^{-Y_{\rm min}}. \quad (0 \lesssim p \lesssim 1)\,. \tag{4.23}$$

JCAP09(2019)043

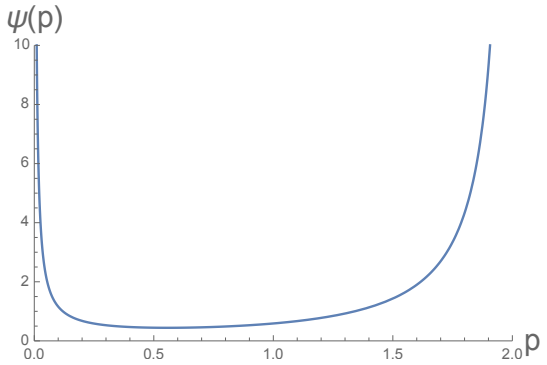

Figure 7. The coefficient $\psi(p)$, introduced in eq. (4.18), is represented as a function of the spectral index p. The behaviour near the edges of the interval are due to the logarithmically divergent behaviour of the momentum integral in (4.18), both for $p = 0$ and $p = 2$. These divergences are regulated by the finite range of wavelenghts contributing to the integral. Near $p = 0$, the divergence is infrared and has been taken into consideration in eq. (4.9), where a few orders of magnitude in k contribute to the integral. Consequently, the logarithm is of order ~ 10. Similarly, near $p \approx 2$, the behaviour of $\psi(p)$ should be regulated at $\psi(p) \lesssim 10$, since no more than a few orders of magnitude in k will contribute to the corresponding ultraviolet logarighmic divergence, from the scale k_0 to the scale $k_{\rm max}$ where the power spectrum reaches its maximum value.

As p approaches the value 11/7, the ratio given in (4.21) approaches the behaviour $(j_0^2/\sigma^2) \propto \lambda^{-1}$, and the integral (2.21) becomes logarithmically divergent at large λ. This is regulated by the finite range of λ. Indeed, for $1 \lesssim p \lesssim 2$, the integral (2.21) is dominated by the interval $\lambda_B^{(p)} \lesssim \lambda < \lambda_m$. Here, $\lambda_m \sim 0.3$ is the value for which matter perturbations start becoming important. At that point, the behaviour of the integrand switches to $(j_0^2/\sigma^2) \propto \lambda^{-3+\frac{7p-11}{21}}$, which rapidly converges. Hence, in that case we can approximate

$$\Gamma_M(t_0) \approx \frac{\rho_m}{M_\odot t_0}\frac{f^2}{14m}\ln\left[\lambda_m/\lambda_B^{(p)}\right]\lambda_B^{(p)}e^{-Y_{\rm min}}, \quad (1 \lesssim p \lesssim 2)\,. \tag{4.24}$$

Let us now consider the "universality" coefficient α, defined in eq. (2.48). From (4.23) or (4.24), we immediately obtain

$$\alpha \approx -M^2\partial^2_{m_1,m_2}\ln[\lambda_B^{(p)}] \approx \frac{30}{32-7p}, \quad (0 \lesssim p \lesssim 2) \tag{4.25}$$

where in the case (4.24) we have ignored the subleading logarithmic dependence on M (we will comment on this subleading correction below).

Factoring out the f^2 and $Y_{\rm min}$ dependence in Γ_M, as

$$\Gamma_M \approx \tilde{\Gamma}(p) f^2 e^{-Y_{\rm min}}\,{\rm Gpc}^{-3}\,{\rm Yr}^{-1}, \tag{4.26}$$

we have represented the approximations (4.23) and (4.24) in figure 8 as dashed lines (for the case $m = 1$). For comparison, we numerically calculate the rate which is obtained when we include, in addition to the effect of perturbations in radiation, the torque exerted by non-relativistic matter perturbations up to the time $\eta \approx \eta_b$ when the binary decouples from the Hubble flow. The latter torque corresponds to the second term in square brackets in eq. (4.19). The numerical result for $m = 1$ and $m = 30$ is depicted in thick lines in figure 8.

JCAP09(2019)043

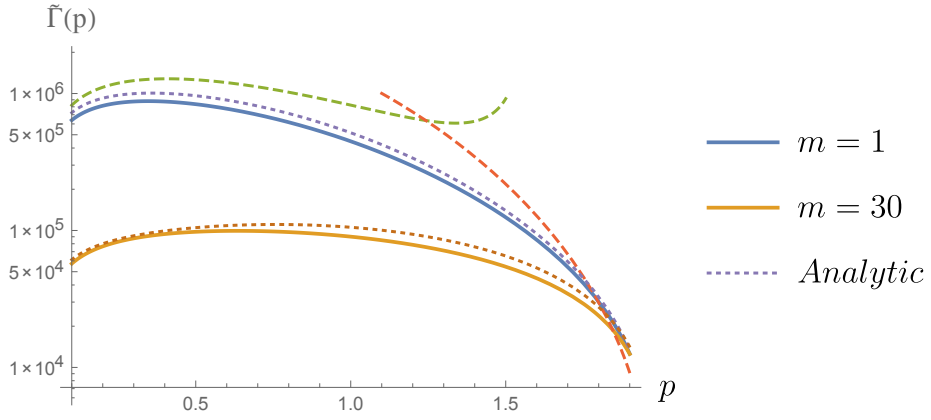

Figure 8. The merger rate $\tilde{\Gamma}(p)$ with the f and $Y_{\rm min}$ dependence factored out, as in eq. (4.26), for $B_\Phi = 10^{-5}$. The dashed lines represent the approximations (4.23) and (4.24), where the torque from non-relativistic matter perturbations is neglected. Here, we use the value $m = 1$. The thick lines correspond to the numerical evaluation of the rate, for $m = 1$ and $m = 30$, including the torque of matter perturbations up to the time $\eta = \eta_b$ when the binary decouples from the Hubble flow. The dotted lines correspond to the analytic estimate given in eq. (4.28), which is a very accurate approximation. All curves are for a monochromatic mass distribution.

Note that the approximations (4.23) and (4.24) can be imprecise, by up to a factor of 2 or so in the region $p \sim 1$, due to the fact that we have neglected the effect of matter perturbations, which can affect the merger rates by a sizable fraction even if they are subdominant.

A much better analytic approximation to the numerical result can be obtained by keeping the effect of matter perturbations in σ^2_{cp}. Using $\lambda_B^{(p)} \ll 1$, we may approximate

$$\int_0^{\frac{2M}{\bar{m}}} W d\lambda \approx 2 \int_{\lambda_B^{(p)}}^{\infty} \left(\frac{\lambda}{\lambda_B^{(p)}}\right)^{\frac{7p-32}{21}} \left[1 + 3.7\lambda \left(\frac{2\bar{m}}{M}\right)\right]^{-2} d\lambda. \tag{4.27}$$

Here, we have neglected the integrand for $\lambda \lesssim \lambda_B^{(p)}$, since this is a small interval where W is suppressed relative to its peak value at $\lambda \sim \lambda_B^{(p)}$, and we have also neglected the exponential factor in W for $\lambda \gtrsim \lambda_B^{(p)}$, since the exponent is small in this range. The integral in the right hand side can be calculated in terms of the incomplete Euler's β function. Expanding this function for small $\lambda_B^{(p)}$ we find

$$\tilde{\Gamma}(p) \approx \frac{\rho_m}{M_\odot t_0} \frac{\lambda_B^{(p)}}{14m} \left(\frac{21}{11-7p} + \left[3.7 \left(\frac{2\bar{m}}{M}\right) \lambda_B^{(p)}\right]^{\frac{11-7p}{21}} \frac{\pi \frac{32-7p}{21}}{\sin\left(\pi \frac{32-7p}{21}\right)} \right). \tag{4.28}$$

The analytic approximation (4.26) with (4.28) is plotted in figure 8 in dotted lines for $m = 1$ and $m = 30$. We find that it reproduces the full numerical result plotted in thick lines, with very good accuracy in the full range of p. The term in round brackets contains additional dependence on m_1 and m_2 which is not present in (4.23), and this will contribute a correction $\Delta\alpha$ to the expression (4.25), given by

$$\Delta\alpha = -M^2 \partial^2_{m_1,m_2} \ln \left| \left[3.7 \left(\frac{2\bar{m}}{M}\right) \lambda_B^{(p)}\right]^{\frac{11-7p}{21}} \frac{(32-7p)}{21\ \mathrm{sinc}\left(\pi \frac{11-7p}{21}\right)} - 1 \right|. \tag{4.29}$$

JCAP09(2019)043

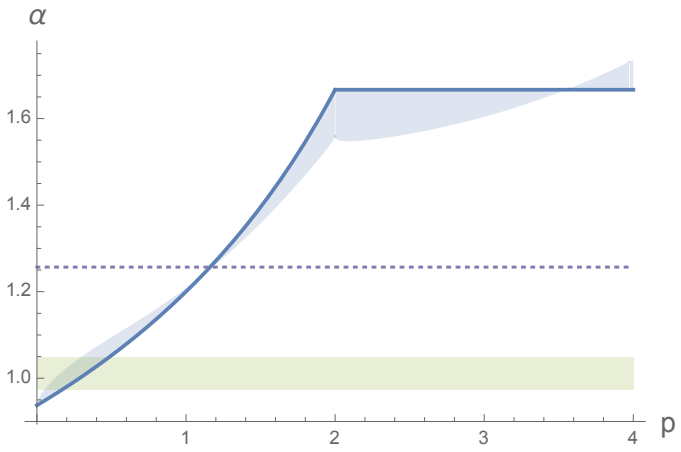

Figure 9. The "universality" coefficient α, defined in (2.48), is plotted as a thick line for an enhanced power spectrum with spectral index p and amplitude $B_\Phi \gtrsim 10^{-6}$ at scales comparable to the co-moving size of the binaries. This coefficient is given by eq. (4.25) in the range $0 \lesssim p \lesssim 2$. For comparison, the case where cosmological perturbations are neglected and the torque of binaries is entirely due to neighboring PBHs corresponds to the horizontal shaded interval, given in eq. (2.51), or to the horizontal dotted line when binaries for which the nearest PBH has $Y < Y_{\rm min} \sim 2$ are excluded from the count. The latter are likely to be severely affected by infalls, as discussed around eq. (2.58). The shade around the thick line corresponds to the correction $\Delta\alpha$ given in eq. (4.29), where we have taken $\bar{m} = 20$ and $m_1 \sim m_2 \sim 20$. For $2 \lesssim p \lesssim 4$, and $\lambda_C \ll 1$ we have $\alpha \approx 5/3$ [see the discussion around eq. (4.41)]. The shade around the horizontal line $\alpha \approx 5/3$ corresponds to $\Delta\alpha$ taken from the analytic estimate (4.39), with $C_\Phi \approx 10^{-3}$ and $k_C = 10^7 k_{\rm eq}$.

This correction turns out to be rather small, and typically $\Delta\alpha \lesssim 0.05 - 0.1$, unless the mass ratio is hierarchical. The reason can be understood as follows. The mass dependence comes from the term in square brackets in (4.29),

$$\left[\left(\frac{2\bar{m}}{M}\right)\lambda_B^{(p)}\right]^{\frac{11-7p}{21}} \propto M^\beta (m_1 m_2)^\gamma. \tag{4.30}$$

The exponents β and γ happen to be very small $\beta, \gamma \lesssim 0.1$ in the range of interest. Then, unless one of the two masses is hierarchically smaller than the total mass M, we have $\Delta\alpha \propto \beta + O(\beta^2, \beta\gamma, \gamma^2) \sim \beta$. The correction $\Delta\alpha$ is plotted in figure 10 for $p = 1.8$, $\bar{m} = 10 M_\odot$, and a range of values of m_1 and m_2. Note that $|\Delta\alpha| \lesssim 0.08$, unless we consider the region where $m_1 \ll m_2$. We have checked that for the case of similar masses $m \lesssim 30$, we have $|\Delta\alpha| \lesssim 0.08$ in the full range $0.2 \lesssim p \lesssim 1.8$

We conclude that, in the range $0 \lesssim p \lesssim 2$ the spectral index p determines the parameter α, which may range from $15/16 \approx .93$ up to $5/3 \approx 1.66$. This is represented in figure 9. A measurement of α may therefore provide valuable information on the primordial perturbation power spectrum at intermediate scales. Note that the value of α is independent of the amplitude of perturbations, as long as this amplitude is sufficiently large[14] $B_\Phi \gtrsim 10^{-6}$.

[14] At low amplitudes, $B \lesssim 10^{-7}$ the torque from matter perturbations becomes as important as that from radiation perturbations. In general, in this case, the dependence of Γ_M on M does not necessarily factor out as a power of M. Still, if we make the assumption that the torque from matter perturbations is dominated by the contribution from times up to η_b, then using (4.19) and neglecting the first term in square brackets (which is due to radiation perturbations), we find $\alpha = 72/(74 - 7p)$, which is larger than $36/37 \approx 0.97$ and smaller than $6/5 = 1.2$. This is a narrower range than allowed by perturbations in radiation.

JCAP09(2019)043

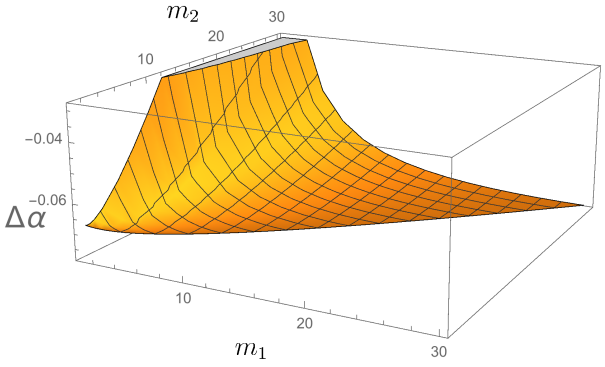

Figure 10. The correction $\Delta\alpha$ in eq. (4.29), for $p = 1.8$, and $\bar{m} = 10M_\odot$, as a function of m_1 and $m_2 > m_1$ (expressed in solar masses). The correction is small unless the mass ratio is hierarchical ($m_1 \ll m_2$), corresponding to the region near the left boundary of the plot.

It should also be pointed out that the bound on f from the observed merger rates can be considerably relaxed by the enhanced power spectrum at intermediate scales. For instance, if we take $m = 30$ and $B_\Phi = 10^{-5}$, then from figure 8 we have $\tilde{\Gamma}(p) \lesssim 10^5$. Consequently, for a monochromatic PBH mass function, the bound

$$\Gamma(t_0) \approx \tilde{\Gamma}(p) f^2 e^{-Y_{\rm min}}\,{\rm Gpc}^{-1}\,{\rm Yr}^{-1} \lesssim 10^2\,{\rm Gpc}^{-1}\,{\rm Yr}^{-1}, \tag{4.31}$$

with $Y_{\rm min} \approx 2$ is satisfied for $f \lesssim 0.1$.[15]

4.3 Case C: steep spectrum at very small scales

Consider a power spectrum with spectral index $p \gtrsim 2$ up to some high scale k_C. In this case, the contribution of perturbations to the angular momentum of binaries will be dominated by $k \sim k_C$, rather than $k \sim k_0$, and it is convenient to parametrize by using k_C as the pivot scale:

$$P_\Phi(k) = C_\Phi \left(\frac{k}{k_C}\right)^p. \quad (p > 2, \quad k \lesssim k_C) \tag{4.32}$$

From the constraints in figure 3, and assuming $k_C \geq 10^7 k_{\rm eq}$, we require

$$C_\Phi \equiv P_\Phi(k_C) \lesssim 10^{-2}\text{–}10^{-3}. \tag{4.33}$$

The case with $p < 2$ was discussed in the previous subsection, with the correspondence

$$C_\Phi = B_\Phi \left(\frac{k_C}{k_B}\right)^p, \tag{4.34}$$

between the prefactors in (4.8) and (4.32). Here we concentrate in the case $p > 2$. The specific form of $P_\Phi(k)$ for $k \gtrsim k_C$ will not be important, as long as it grows slower than k^2, or that it decays for $k > k_C$.

From (3.16), the contribution of radiation perturbations to the variance of j is dominated by wavelengths shorter than the binary size x_0, and is given by

$$\sigma^2_{cp(rad)} \approx 2.2 \cdot 10^3 \int_{k_0}^{k_C} \frac{dk}{k} P_\Phi(k) \frac{1}{(k^2 x_0^2)} \approx \frac{2.2}{p-2} \left(\frac{C_\Phi}{10^{-3}}\right) \left(\frac{k_0}{k_C}\right)^2. \tag{4.35}$$

[15] For smaller values of the power spectrum, in the range $10^{-7} < B_\Phi < 10^{-5}$, the merger rate scales approximately in proportion to $\lambda_B^{(p)} \propto B_\Phi^{-21/(32-7p)}$. This translates into the bound $f \lesssim 0.1 (B_\phi/10^{-5})^{21/(64-14p)}$.

JCAP09(2019)043

In the last step we have neglected the contribution from the lower limit of integration, assuming that p is not too close to 2. As we discussed in the previous subsection, we can easily incorporate the torque of matter perturbations up to the time $\eta = \eta_b$, which gives a combined total of

$$\sigma_{cp}^2 \approx \frac{2.2}{p-2}\left(\frac{C_\Phi}{10^{-3}}\right)\left(\frac{k_B}{k_C}\right)^2 (m\lambda)^{-2/3}\left[1+3.7\lambda\left(\frac{2\bar{m}}{M}\right)\right]^2. \tag{4.36}$$

Here we have used $k_0/k_B = (m\lambda)^{-1/3}$, with $k_B = 5\cdot 10^5 k_{\rm eq}$.

Given that C_ϕ is bounded above by (4.33), the factor $(k_B/k_C)^2$ will considerably suppress the effect of cosmological perturbations unless k_C is not too far from the intermediate scale k_B. Eq. (4.36) can be compared with de contribution of neighboring PBH to the torque, given in (4.4)

$$\sigma_{nb}^2 \approx \frac{K}{4Y_{\rm min}} f^2\lambda^2\left(\frac{2\bar{m}}{M}\right)^2 \sim 10^{-1}\lambda^2 f^2, \tag{4.37}$$

where in the last step we use the fiducial values $K\sim 1$, $M\sim 2\bar{m}$ and $Y_{\rm min}\approx 2$. For p not too close to 2, and $m\sim 30$, the effect of cosmological perturbations can only be dominant for a narrow range of k_C:[16]

$$10^7 k_{\rm eq} \leq k_C \lesssim 2\cdot 10^7 f^{-1}(p-2)^{-1/2} m^{-1/3} k_{\rm eq}. \tag{4.38}$$

Hence, the existence of a window for k_C where $\sigma_{nb} \ll \sigma_{cp}$ requires $f \ll 1$.

Following similar steps as in subsection 4.2, we find that the expected merger rate of binaries will be given by (4.26), with

$$\tilde{\Gamma}(p) \approx \frac{\rho_m}{M_\odot t_0}\frac{\lambda_C}{14m}\left(\left[3.7\left(\frac{2\bar{m}}{M}\right)\lambda_C\right]^{-1/7}\frac{6\pi/7}{\sin(6\pi/7)} - 7\right). \quad (\lambda_C \ll 1) \tag{4.39}$$

Here,

$$\lambda_C \equiv \left[1.2(p-2)10^{-6}\left(\frac{k_C}{k_B}\right)^2\left(\frac{10^{-3}}{C_\Phi}\right)\right]^{7/6}\left(\frac{M}{2\bar{m}}\right)^{7/3}\left(\frac{4m_1m_2}{M^2}\right)^{1/3} m^{4/3}. \tag{4.40}$$

This leads to a value of the universality coefficient which is given by (4.25) with $p=2$. That is

$$\alpha \approx \frac{5}{3}. \quad (\lambda_C \ll 1) \tag{4.41}$$

Eq. (4.41) corresponds to the thick horizontal line in the range $p>2$ in figure 9. Note, however, that the approximation (4.39) requires $\lambda_C \ll 1$ (since it is obtained by Taylor expanding an incomplete Euler beta function in small λ_C). The merger rates for $k_C = 10^7 k_{\rm eq}$ are plotted in figure 11, where it can be seen that the approximation (4.39) plotted as dashed lines, agrees very well with the numerical result plotted in thick lines, for $m \lesssim 30$. For higher values of k_C or higher values of m, we are outside the regime $\lambda_C \ll 1$, and the approximation is not valid. Nonetheless, the behaviour of the merger rates from the numerical result is similar for all masses up to $m \lesssim 100$. In particular, we find that f should be less than a few percent in the whole range $m = 1$–100. This is in contrast with the results for Case B ($p<2$), where values of f as large as 10% can be consistent with the observed merger rates. In spite of the high amplitude of the power spectrum, the effect in Case C is not as significant as in case B, since perturbations are now on scales smaller than the binary size.

[16] In the case of cosmological perturbations, the merger rate for $p>2$ is dominated by the values of λ where the behaviour of the variance (4.36) changes from $\sigma_{cp}^2 \propto \lambda^{-2/3}$ to $\sigma_{cp}^2 \propto \lambda^{4/3}$. This happens at $\lambda \sim 1/3$, and we use this in the relation $\sigma_{cp} \gtrsim \sigma_{nb}$ in order to estimate the upper limit of the range (4.38).

JCAP09(2019)043

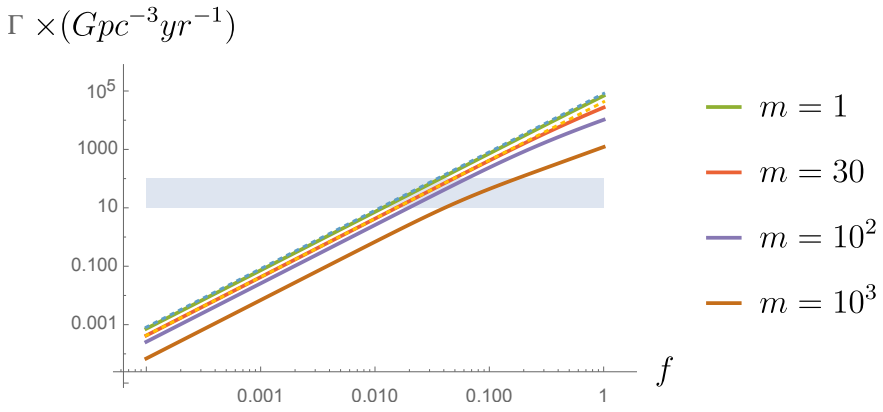

Figure 11. The merger rates for Case C, with power spectrum amplitude $C_\Phi = 10^{-3}$ at $k_C = 10^7 k_{\rm eq}$, and with $p = 4$. The thick lines correspond to the numerical evaluation of the rates for different values of the mass, while the dashed lines correspond to the analytic estimate (4.39), which is a very good approximation for $m \lesssim 30$. Note that the rate has only a very mild dependence on the mass, at least up to $m \lesssim 10^2$. Despite a large amplitude of primordial perturbations, the effect on the merger rate is not as significant as in Case B, since now the perturbations are on scales smaller than the binary size.

4.4 Effect of a peak at the PBH scale

The mechanism of PBH formation from adiabatic perturbations relies on a prominent enhancement in P_ϕ, with a maximum at some co-moving scale $k_{\rm PBH}$ with amplitude

$$P_\Phi(k_{\rm PBH}) \sim 10^{-3}\text{–}10^{-2}. \tag{4.42}$$

This is enough to produce PBHs in significant abundance, in regions where high peaks in the Gaussian random field of cosmological perturbations reach non-linear values above a certain threshold. As discussed in refs. [35, 36], PBH formation does not occur when $k_{\rm PBH}$ crosses the horizon, but slightly later, when the scale

$$r_m \sim 3\ k_{\rm PBH}^{-1} \tag{4.43}$$

crosses the horizon.[17] The mass of the black hole is typically equal to the mass within the horizon at that time, so that $2GM = H_{r_m}^{-1}$, and we have

$$k_{\rm PBH} \approx 3 \cdot 10^9 m^{-1/2} k_{\rm eq}. \tag{4.44}$$

Comparing with eq. (4.1) this corresponds to lengthscales which are shorter than the co-moving size of the binary, by three orders of magnitude or so, corresponding to the present co-moving wave-number of order

$$\bar{k}_{\rm PBH} \sim 3 \cdot 10^7 m^{-1/2}\,{\rm Mpc}^{-1}. \tag{4.45}$$

On a logarithmic scale, this is not too far from the intermediate scales discussed in subsection 4.2, and hence it is natural to ask about the consequences of this peak on the merger rates, in the light of our earlier results.

[17] The scale r_m corresponds to the maximum of the so-called compaction function $\mathcal{C}(r)$, which characterizes the averaged overdensity as a function of the distance to its center. The approximate factor of 3 in (4.43) depends somewhat on the shape of the overdensity profile, which for amplitudes well above the standard deviation is in turn determined by the form of $P_\Phi(k)$. For instance, for a monochromatic power spectrum, $P_\Phi(k) \propto \delta(k - k_{\rm PBH})$, we have $r_m \approx 2.7\ k_{\rm PBH}^{-1}$. On the other hand, the strong overdensity causes a non-linear distortion of the spatial metric which affects the relation between co-moving and physical distance. Generically, the combination of these non-linear effects gives a mass of the black hole which is ~ 10 times bigger than the mass within the unperturbed horizon at the time when $k_{\rm PBH}$ crosses it. Hence the factor of 3 in (4.44).

JCAP09(2019)043

For illustration, in figure 3 we include an example extracted from [41], where the enhancement of the power spectrum is obtained from a period where the inflaton goes from slow roll to ultra-slow roll and back to slow roll, through a discrete set of values of the second slow roll parameter η. This model may be somewhat artificial, but it will be useful for illustrative purposes since it includes several features which may be present in more general cases. The curve includes a steep growth with $P_\Phi \propto k^p$ from the cosmological plateau up to a very high value $P_\Phi \sim 10^{-3}$, at $k \sim k_C$, as in Case C. This is followed by a less steep part up to some maximum value $k_{\rm PBH}$, corresponding to the scale of PBH formation. Finally, the spectrum decays for $k > k_{\rm PBH}$.

It has been argued that $p = 4$ corresponds to the theoretical upper bound for the spectral index for a wide class of inflationary one field models [41]. Values in the range $3 \lesssim p \lesssim 4$ are easily obtained in the case where the enhancement is due to a short period of ultra-slow roll and constant roll inflation. The upper bound can be saturated in relatively simple models where the constant roll phase has a sufficiently negative value of the slow roll parameter η (see e.g. [44]). For $p \gtrsim 2$, the regime where cosmological perturbations dominate over the effect of neighboring PBHs is given by eq. (4.38), which requires

$$f \lesssim 6.7 \cdot 10^{-3} \frac{m^{1/6}}{\sqrt{p-2}} \left(\frac{k_{\rm PBH}}{k_C} \right) . \quad (p \gtrsim 2) \tag{4.46}$$

Here we have used (4.44). For a sizable value of the fraction of dark matter in the form of PBHs, say $f \gtrsim 10^{-2}$, cosmological perturbations will only play a role if the peak of the power spectrum is rather *broad*, with $k_{\rm PBH} \gtrsim 10\, k_C$. Conversely, for a *narrow* peak with $k_{\rm PBH} \sim k_C$ and sizable $f \gtrsim 10^{-2}$, the eccentricity of binaries is determined by the tidal forces from neighboring PBHs. Broad peaks in the power spectrum are not necessarily generic, but as shown by the example in figure 3, they can in principle be obtained in phenomenological models.

The merger rate of binaries is plotted in the left pannel of figure 12 for different values of the mass, for the case of a broad peak which raises steeply with $p = 4$ up to the scale $k_C \approx 10^8 k_{\rm eq}$, and then proceeds with moderate slope to the maximum at $k_{\rm PBH} = 10 k_C \approx 10^9 k_{\rm eq}$. In this case the analytic approximation (4.39) does not apply, since $\lambda_C \gtrsim 1$ in the relevant range of f. The effect of cosmological perturbations is only significant for low masses $m \lesssim 1$. For the case of a narrow peak with $p = 4$, which raises from low values with a steep spectral index to all the way to the PBH scale $k_{\rm PBH} = k_C \approx 10^9 k_{\rm eq}$, the merger rate is plotted in the right pannel of figure 12, where we see that the effect of the narrow peak is completely insignificant.

For less steep spectral index $0 < p \lesssim 2$, the growing part of the spectrum corresponds to Case B. The condition that cosmological perturbations provide the dominant source of torque on binaries can be derived along similar lines, and is given by

$$f \lesssim 2^{1-p}\ 10^{1-\frac{3p}{2}}\, m^{p/12} \left(\frac{k_{\rm PBH}}{k_C} \right)^{p/2} . \quad (0 \lesssim p \lesssim 2) \tag{4.47}$$

This is much less restrictive on f than (4.46). Indeed, for $p \lesssim 1$, the condition does not significantly restrict the fraction f, even for the case where $k_C \approx k_{\rm PBH}$.[18] The effect of such a feature in the power spectrum is described in subsection 4.2.

[18] Note, however, that in order to interpolate between the cosmological value $P_\Phi \sim 10^{-9}$ and the peak value $P_\Phi \sim 10^{-3}$ in the span of wavelengths which goes from $10\,{\rm Mpc}^{-1}$ to $10^7\,{\rm Mpc}^{-1}$, we need $p \gtrsim 1$. Incidentally, for $p = 1$ the value of the "universality" parameter α which is obtained when cosmological perturbations provide the dominant torque (see figure 9) is quite similar to the value 1.26 which corresponds to a dominant torque from neighboring PBHs (at a distance larger than the infall radius $Y_{\rm min}$), so for this particular value of p it seems harder to distinguish one mechanism from the other.

JCAP09(2019)043

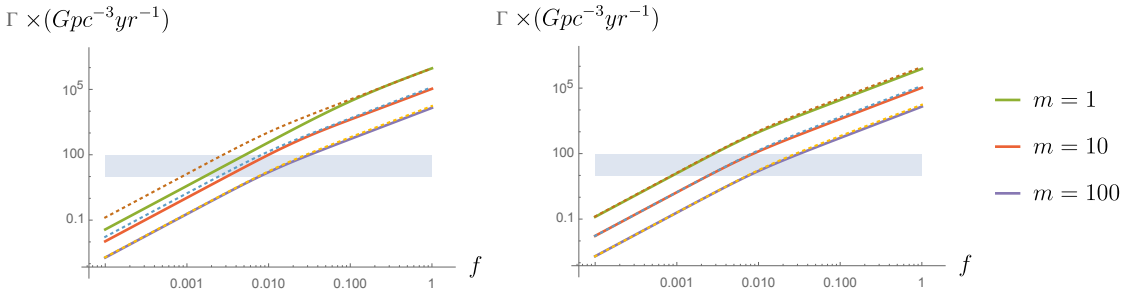

Figure 12. The thick lines in the left pannel represent the merger rates for a steep power spectrum of cosmological perturbations with $p = 4$, and a broad peak spanning from $k_c \approx 10^8 k_{\rm eq}$ to $k_{\rm PBH} \approx 10^9 k_{\rm eq}$, with amplitude $C_\Phi \approx 10^{-3}$ and different values of the mass. Since the peak only affects very small scales and has no power at intermediate scales, we have added a cosmological plateau with normalization $P_\phi \approx 10^{-9}$, representing a minimal contribution we may expect for $k < 10^7 k_{\rm eq}$. For reference, the dashed lines represent the case where only the flat plateau with cosmological normalization is taken into consideration, as in Case A. The effect of the steep bump can be significant for low mass PBHs $m \sim 1$, but not for higher masses. In the right pannel, we consider the case with $k_C = k_{\rm PBH} = 10^9 k_{\rm eq}$, corresponding to a sharp peak at the PBH scale. The effect of the steep bump is completely negligible in this case.

5 Summary and conclusions

We have studied the effect of cosmological perturbations on the merger rate of PBHs in the stellar mass range. The effect can be quite significant depending on the amplitude of the power spectrum at different scales.

For a scale invariant spectrum with amplitude $P_\Phi \approx 10^{-9}$ (Case A), matter perturbations have a dominant effect on the eccentricity of binaries for $f \lesssim 10^{-2}$, while for larger f the distribution of j is actually dominated by tidal torques from PBHs in the vicinity. In this case, the merger rates would be greater than the current LIGO/Virgo bounds unless the fraction of dark matter in the form of PBH is rather small, of the order $f \lesssim 10^{-2}$ for PBHs with $m \sim 30$.

On the other hand, P_Φ could be much larger at scales 10–$10^5\,{\rm Mpc}^{-1}$ (Case B). For instance, we find that a nearly flat spectrum with amplitude $P_\Phi \gtrsim 10^{-7}$ within such scales leads to a dimensionless angular momentum with mean squared value

$$\langle j_{cp}^2 \rangle \sim 10^3 P_\Phi, \tag{5.1}$$

which is mostly due to perturbations in the radiation fluid. For a nearly flat P_Φ, the variance of j is almost independent of the mass of the PBH and the size of the binaries. There is only a mild subleading logarithmic dependence on such parameters, which accounts for the range of scales contributing to the effect, from the co-moving size of the binary to the co-moving size of the horizon at the time when the binary forms. The situation is different when we have a tilted spectrum, of the form $P_\Phi \propto k^p$, ($p \lesssim 2$), in which case the variance of j depends on binary size and masses. In this case the effect is determined by the amplitude of P_Φ near the co-moving scale of the binaries $k \sim k_0$, which is in the intermediate range 10^3–$10^5\,{\rm Mpc}^{-1}$. The bound from spectral distorsions in the CMB caused by dissipation of acoustic modes requires $P_\Phi \lesssim 10^{-5}$ at such scales [45]. In the situation where this bound is saturated, the torque can be large enough to significantly suppress the merger rate to a level consistent with LIGO/Virgo observations even for $f \sim 10\%$.

JCAP09(2019)043

An even stronger enhancement of the power spectrum may occur at scales beyond $10^5\,\mathrm{Mpc}^{-1}$. These are smaller than the co-moving size of the binaries, but they can contribute to the peculiar velocities of the PBHs and hence to the initial orbital angular momentum. For a steep power spectrum (Case C), with spectral index $p \gtrsim 2$ up to some short wavelength $k_C \gtrsim 10^7 k_{\rm eq}$, the contribution to $\langle j^2 \rangle$ is dominated by the shortest scales $k \sim k_C$, rather than $k \sim k_0$. The observational upper bound $P_\Phi(k_C) \lesssim 10^{-3}$–$10^{-2}$ is comparable to the amplitude which is necessary to produce PBH in significant abundances by the collapse of adiabatic perturbations. For generality, we may assume that beyond k_C, the power spectrum can still grow slightly (say, with a much lower spectral index $p' \lesssim 2$), by a factor of a few, up to a maximum value at the scale which we may call $k_{\rm PBH}$, corresponding to the scale which dominates PBH formation (see figure 3). In this case, and assuming $P_\Phi(k_C) \sim 10^{-3}$, the effect on the orbital parameter of binaries is of order $\langle j^2 \rangle \sim (k_0/k_C)^2$, and becomes irrelevant unless $k_C \lesssim 10^3 k_0$. Since $k_0 < 10^5 k_{\rm eq}$ while $k_{\rm PBH} \sim 10^9 k_{\rm eq}$ for PBH in the stellar mass range, the effect of the steeply rising power spectrum on the eccentricity of binaries will only be important if this is crowned by a *broad* peak with a maximum at $k_{\rm PBH} \gtrsim 10 k_C$. The corresponding effect on the merger rates is somewhat intricate in general, but it is only significant at low masses. For $m \lesssim 100$, the bound on the fraction of dark matter can relaxed to $f \lesssim 2 \cdot 10^{-2}$ due to this effect, for sufficiently low $k_C \sim 10^7 k_{\rm eq}$. Interestingly, in this regime the merger rate becomes almost independent of m (see figure 11). This is in contrast with the standard situation where the angular momentum is supplied by a neighboring PBH, where we have $\Gamma \propto m^{-32/37}$.

We have also investigated the dependence of merger rates on the constituent masses, with particular attention to the universality coefficient α [1]. This is rather insensitive to the unknown initial PBH mass distribution function, and can be determined observationally with some precision (of order 15% given a sufficiently large number of PBH merger events $\sim 10^3$ [1, 38]). It seems therefore of great empirical relevance for PBH scenarios. Our results for α are summarized in figure 9. In the case where cosmological perturbations are subdominant relative to the torque from neighboring PBH, it was argued in [1] that $\alpha \approx 1 \pm 0.05$ (this is displayed as a horizontal shading in figure 9). We point out, however, that this narrow range shifts to $\alpha \approx 1.26$ once the effect of PBH infall onto binaries is taken into consideration, by excluding disturbed binaries from the merger count (after the infall these binaries are likely to have a much larger lifetime than the present age of the universe).[19] On the other hand, in the case where cosmological perturbations dominate the variance of j, the coefficient α ranges from 15/16 to 5/3 depending on the value of the spectral index p [see figure 9]. In this case, the value of α is unaffected by infalls. We conclude that, as a matter of principle, an accurate measurement of merger rates of PBH might carry some information on the circumstances surrounding PBH binary formation, including the amplitude and spectral index of primordial perturbations on very short wavelengths or the effect of PBH infalls.

In turn, any information on the primordial power spectrum which may be obtained through a measument of α would constrain the underlying inflationary dynamics, from the scale of binaries down to the scale of PBH. This might complement other possible probes

[19] The shift of α in the case where cosmological perturbations are subdominant is due to the factor $Y_{\rm min}^{21/74}$ in eq. (2.56). Note that the merger rates have an additional exponential dependence on the infall radius $Y_{\rm min}$. Such dependence drops out from the universality coefficient α due to the linearity of $Y_{\rm min}$ in the total mass M [see eq. (2.52)]. The assumption of linear behaviour seems very reasonable [12, 19], but may require further validation from numerical simulations, since any departures from it may have a significant effect on α. This study is outside the scope of the present work and is left for further research.

JCAP09(2019)043

on the amplitude of P_Φ at small scales, such as upcoming searches for spectral distortions in the CMB, or pulsar timing array constraints [40, 41, 43].

There are several directions in which our study could be extended. It was recently pointed out in [18] that for $f \ll 1$ a dark matter dress may develop around PBH before they form binaries, and that this would affect the semi-major axis and the eccentricity of binaries after the first few oscilations which shake off most of the dark matter cloud. It was also shown that the effect on the merger rates is nonetheless small. In the present context, the effect may be even smaller, since in the presence of enhanced cosmological perturbations the merger rate is dominated by much smaller binaries forming deeper in the radiation era, when the halo around each PBH has had less time to accrete. Nonetheless, it might be interesting to be more quantitative about this effect, taking also into consideration the case of constituent masses which differ by a sizable factor, in order to assess the possible impact on α. Finally, it was pointed out in [19] that for $f \gtrsim 0.1$ binaries can be disrupted by collision with compact N-body systems, which may substantially deplete the population of pristine binaries. Investigation of these issues seems to require further simulations, and remains an interesting direction of research.

Acknowledgments

We thank V. Atal, N. Bellomo, J. Bernal, C. Byrnes, J. Miralda, M. Sasaki and T. Tanaka for useful discussions. This work has been partically supported by FPA2016-76005-C2-2-P, MDM-2014-0369 of ICCUB (Unidad de Excelencia Maria de Maeztu), and AGAUR2017-SGR-754. N.T. is supported by an INPhINIT grant from "la Caixa" Foundation (ID 100010434) code LCF/BQ/IN17/11620034. This project has also received funding from the European Union's Horizon 2020 research and innovation programme under the Marie Sklodowska-Curie grant agreement No. 713673. We have used the publicly available WebPlotDigitizer [46] to digitise plots.

References

[1] B. Kocsis, T. Suyama, T. Tanaka and S. Yokoyama, *Hidden universality in the merger rate distribution in the primordial black hole scenario*, *Astrophys. J.* **854** (2018) 41 [arXiv:1709.09007] [INSPIRE].

[2] B. Carr, M. Raidal, T. Tenkanen, V. Vaskonen and H. Veermäe, *Primordial black hole constraints for extended mass functions*, *Phys. Rev.* **D 96** (2017) 023514 [arXiv:1705.05567] [INSPIRE].

[3] S. Bird et al., *Did LIGO detect dark matter?*, *Phys. Rev. Lett.* **116** (2016) 201301 [arXiv:1603.00464] [INSPIRE].

[4] M. Sasaki, T. Suyama, T. Tanaka and S. Yokoyama, *Primordial Black Hole Scenario for the Gravitational-Wave Event GW150914*, *Phys. Rev. Lett.* **117** (2016) 061101 [arXiv:1603.08338] [INSPIRE].

[5] LIGO Scientific and VIRGO collaborations, *GW170104: Observation of a 50-Solar-Mass Binary Black Hole Coalescence at Redshift 0.2*, *Phys. Rev. Lett.* **118** (2017) 221101 [*Erratum ibid.* **121** (2018) 129901] [arXiv:1706.01812] [INSPIRE].

[6] LIGO Scientific and Virgo collaborations, *Observation of Gravitational Waves from a Binary Black Hole Merger*, *Phys. Rev. Lett.* **116** (2016) 061102 [arXiv:1602.03837] [INSPIRE].

JCAP09(2019)043

[7] LIGO Scientific and Virgo collaborations, *GW151226: Observation of Gravitational Waves from a 22-Solar-Mass Binary Black Hole Coalescence*, *Phys. Rev. Lett.* **116** (2016) 241103 [arXiv:1606.04855] [INSPIRE].

[8] LIGO Scientific and Virgo collaborations, *Binary Black Hole Mergers in the first Advanced LIGO Observing Run*, *Phys. Rev.* **X 6** (2016) 041015 [arXiv:1606.04856] [INSPIRE].

[9] Y. Ali-Haïmoud, E.D. Kovetz and M. Kamionkowski, *Merger rate of primordial black-hole binaries*, *Phys. Rev.* **D 96** (2017) 123523 [arXiv:1709.06576] [INSPIRE].

[10] Y.N. Eroshenko, *Gravitational waves from primordial black holes collisions in binary systems*, *J. Phys. Conf. Ser.* **1051** (2018) 012010 [arXiv:1604.04932] [INSPIRE].

[11] T. Nakamura, M. Sasaki, T. Tanaka and K.S. Thorne, *Gravitational waves from coalescing black hole MACHO binaries*, *Astrophys. J.* **487** (1997) L139 [astro-ph/9708060] [INSPIRE].

[12] K. Ioka, T. Chiba, T. Tanaka and T. Nakamura, *Black hole binary formation in the expanding universe: Three body problem approximation*, *Phys. Rev.* **D 58** (1998) 063003 [astro-ph/9807018] [INSPIRE].

[13] M. Raidal, V. Vaskonen and H. Veermäe, *Gravitational Waves from Primordial Black Hole Mergers*, *JCAP* **09** (2017) 037 [arXiv:1707.01480] [INSPIRE].

[14] G. Ballesteros, P.D. Serpico and M. Taoso, *On the merger rate of primordial black holes: effects of nearest neighbours distribution and clustering*, *JCAP* **10** (2018) 043 [arXiv:1807.02084] [INSPIRE].

[15] V. Desjacques and A. Riotto, *Spatial clustering of primordial black holes*, *Phys. Rev.* **D 98** (2018) 123533 [arXiv:1806.10414] [INSPIRE].

[16] T. Bringmann, P.F. Depta, V. Domcke and K. Schmidt-Hoberg, *Towards closing the window of primordial black holes as dark matter: The case of large clustering*, *Phys. Rev.* **D 99** (2019) 063532 [arXiv:1808.05910] [INSPIRE].

[17] Z.-C. Chen and Q.-G. Huang, *Merger Rate Distribution of Primordial-Black-Hole Binaries*, *Astrophys. J.* **864** (2018) 61 [arXiv:1801.10327] [INSPIRE].

[18] B.J. Kavanagh, D. Gaggero and G. Bertone, *Merger rate of a subdominant population of primordial black holes*, *Phys. Rev.* **D 98** (2018) 023536 [arXiv:1805.09034] [INSPIRE].

[19] M. Raidal, C. Spethmann, V. Vaskonen and H. Veermäe, *Formation and Evolution of Primordial Black Hole Binaries in the Early Universe*, *JCAP* **02** (2019) 018 [arXiv:1812.01930] [INSPIRE].

[20] J. García-Bellido and E. Ruiz Morales, *Primordial black holes from single field models of inflation*, *Phys. Dark Univ.* **18** (2017) 47 [arXiv:1702.03901] [INSPIRE].

[21] J.M. Ezquiaga, J. García-Bellido and E. Ruiz Morales, *Primordial Black Hole production in Critical Higgs Inflation*, *Phys. Lett.* **B 776** (2018) 345 [arXiv:1705.04861] [INSPIRE].

[22] C. Germani and T. Prokopec, *On primordial black holes from an inflection point*, *Phys. Dark Univ.* **18** (2017) 6 [arXiv:1706.04226] [INSPIRE].

[23] H. Motohashi and W. Hu, *Primordial Black Holes and Slow-Roll Violation*, *Phys. Rev.* **D 96** (2017) 063503 [arXiv:1706.06784] [INSPIRE].

[24] V. Atal and C. Germani, *The role of non-Gaussianities in Primordial Black Hole formation*, *Phys. Dark Univ.* **24** (2019) 100275 [arXiv:1811.07857] [INSPIRE].

[25] S. Passaglia, W. Hu and H. Motohashi, *Primordial black holes and local non-Gaussianity in canonical inflation*, *Phys. Rev.* **D 99** (2019) 043536 [arXiv:1812.08243] [INSPIRE].

[26] G. Ballesteros and M. Taoso, *Primordial black hole dark matter from single field inflation*, *Phys. Rev.* **D 97** (2018) 023501 [arXiv:1709.05565] [INSPIRE].

JCAP09(2019)043

[27] G. Ballesteros, J. Beltran Jimenez and M. Pieroni, *Black hole formation from a general quadratic action for inflationary primordial fluctuations*, *JCAP* **06** (2019) 016 [arXiv:1811.03065] [INSPIRE].

[28] J. Garriga, A. Vilenkin and J. Zhang, *Black holes and the multiverse*, *JCAP* **02** (2016) 064 [arXiv:1512.01819] [INSPIRE].

[29] H. Deng, J. Garriga and A. Vilenkin, *Primordial black hole and wormhole formation by domain walls*, *JCAP* **04** (2017) 050 [arXiv:1612.03753] [INSPIRE].

[30] H. Deng, A. Vilenkin and M. Yamada, *CMB spectral distortions from black holes formed by vacuum bubbles*, *JCAP* **07** (2018) 059 [arXiv:1804.10059] [INSPIRE].

[31] R.V. Konoplich, S.G. Rubin, A.S. Sakharov and M. Yu. Khlopov, *Formation of black holes in first-order phase transitions as a cosmological test of symmetry-breaking mechanisms*, *Phys. Atom. Nucl.* **62** (1999) 1593 [INSPIRE].

[32] M. Yu. Khlopov, R.V. Konoplich, S.G. Rubin and A.S. Sakharov, *First-order phase transitions as a source of black holes in the early universe*, *Grav. Cosmol.* **6** (2000) 153 [INSPIRE].

[33] S.G. Rubin, M. Yu. Khlopov and A.S. Sakharov, *Primordial black holes from nonequilibrium second order phase transition*, *Grav. Cosmol.* **6** (2000) 51 [hep-ph/0005271] [INSPIRE].

[34] F. Ferrer, E. Masso, G. Panico, O. Pujolàs and F. Rompineve, *Primordial Black Holes from the QCD axion*, *Phys. Rev. Lett.* **122** (2019) 101301 [arXiv:1807.01707] [INSPIRE].

[35] C.-M. Yoo, T. Harada, J. Garriga and K. Kohri, *Primordial black hole abundance from random Gaussian curvature perturbations and a local density threshold*, *PTEP* **2018** (2018) 123E01 [arXiv:1805.03946] [INSPIRE].

[36] C. Germani and I. Musco, *Abundance of Primordial Black Holes Depends on the Shape of the Inflationary Power Spectrum*, *Phys. Rev. Lett.* **122** (2019) 141302 [arXiv:1805.04087] [INSPIRE].

[37] P.C. Peters, *Gravitational Radiation and the Motion of Two Point Masses*, *Phys. Rev.* **136** (1964) B1224 [INSPIRE].

[38] M. Sasaki, T. Suyama, T. Tanaka and S. Yokoyama, *Primordial black holes — perspectives in gravitational wave astronomy*, *Class. Quant. Grav.* **35** (2018) 063001 [arXiv:1801.05235] [INSPIRE].

[39] V. Mukhanov, *Physical Foundations of Cosmology*, Cambridge University Press (2005).

[40] K. Inomata and T. Nakama, *Gravitational waves induced by scalar perturbations as probes of the small-scale primordial spectrum*, *Phys. Rev.* **D 99** (2019) 043511 [arXiv:1812.00674] [INSPIRE].

[41] C.T. Byrnes, P.S. Cole and S.P. Patil, *Steepest growth of the power spectrum and primordial black holes*, *JCAP* **06** (2019) 028 [arXiv:1811.11158] [INSPIRE].

[42] PLANCK collaboration, *Planck 2018 results. X. Constraints on inflation*, arXiv:1807.06211 [INSPIRE].

[43] A. Kogut et al., *The Primordial Inflation Explorer (PIXIE): A Nulling Polarimeter for Cosmic Microwave Background Observations*, *JCAP* **07** (2011) 025 [arXiv:1105.2044] [INSPIRE].

[44] V. Atal, J. Garriga and A. Marcos-Caballero, *Primordial black hole formation with non-Gaussian curvature perturbations*, arXiv:1905.13202 [INSPIRE].

[45] J. Chluba, R. Khatri and R.A. Sunyaev, *CMB at 2x2 order: The dissipation of primordial acoustic waves and the observable part of the associated energy release*, *Mon. Not. Roy. Astron. Soc.* **425** (2012) 1129 [arXiv:1202.0057] [INSPIRE].

[46] A. Rohatgi, *Webplotdigitizer*, https://automeris.io/WebPlotDigitizer (2018).

JCAP09(2019)043

2.2 Clustering of primordial black holes and non-Gaussianities

Journal of Cosmology and Astroparticle Physics
An IOP and SISSA journal

LIGO/Virgo black holes and dark matter: the effect of spatial clustering

Vicente Atal, Albert Sanglas and Nikolaos Triantafyllou

Departament de Física Quàntica i Astrofísica i Institut de Ciències del Cosmos,
Universitat de Barcelona,
Martí i Franquès 1, 08028 Barcelona, Spain

E-mail: vicente.atal@icc.ub.edu, asanglas@icc.ub.edu, nitriant@icc.ub.edu

Received August 4, 2020
Accepted September 25, 2020
Published November 19, 2020

Abstract. We discuss the effect of clustering for the determination of the merger rate of binary black holes in the LIGO/Virgo mass range. While for a Poissonian initial distribution, and assuming isolated binaries, the allowed fraction of Primordial Black Holes (PBHs) to dark matter (DM) is a few percent, we show that this bound can be relaxed if PBHs are clustered. More precisely we show that for large clustering the merger rate can drop with increasing fraction of PBHs, introducing a degeneracy in the parameters of the theory consistent with a given present merger rate, and allowing all the DM to be in the form of stellar mass PBHs. This degeneracy can however be broken by looking at the evolution of the merger rate with redshift. For a simple clustering model that we consider, we show that the LIGO/Virgo projected sensitivity can disentangle, through the observation of a stochastic background of gravitational waves, different clustered distributions having the same present merger rate.

Keywords: dark matter theory, gravitational waves / sources, physics of the early universe, primordial black holes

ArXiv ePrint: 2007.07212

https://doi.org/10.1088/1475-7516/2020/11/036

JCAP11(2020)036

Contents

JCAP11(2020)036

1 Introduction

The merger rate of binary black holes observed by LIGO provides one of the strongest constraints for the presence of Primordial Black Holes (PBH) of masses $\mathcal{O}(1-100)$ $M_\odot$ [1–4]. Assuming that PBHs follow an initial Poissonian spatial distribution — and that binaries are isolated objects (see [5–7] for caveats) — it has been found that PBH binaries merging today are mainly formed in the radiation dominated Universe [3, 8], and that they can account for a small fraction of the dark matter (DM) in this range of masses, of the order of a few percent [3, 9].[1] A related constraint, although weaker in this mass range, comes from the non-observation of a stochastic background of gravitational waves (GWs), generated from past binary mergers [13, 14].

Poissonian spatial distributions for PBHs arise if the density field is a Gaussian random field with a spiky power spectrum [15–17] (for earlier discussions, see [18]). On the contrary, if PBH arise from non-Gaussian perturbations, then their distribution will not be Poissonian. In particular, a coupling between small and long wavelengths of the density perturbations, or the modulation of the density field by a secondary field, can result in a clustered spatial distribution [19–23]. Its effect on the merger rate of late and early time binaries has been estimated in [4, 17, 24–27], and on the stochastic background of gravitational waves in [28]. Other effects can alter the merger rate, such as enhanced large scales perturbations [9, 29, 30], three-body [6, 7] and many-body interactions [5] and PBH mass accretion [31]

In this paper we re-examine the question of how an initial clustering of PBH can affect the bounds on their abundance coming from present and past merger rate of binaries. Clustering enhances the local density of PBHs and so it has been usually found that the allowed fraction of PBH to DM, $f_{\rm PBH}$, is smaller than that of a Poissonian initial distribution (see e.g. [28]). As we will show, this is only the case in the limit in which $f_{\rm PBH}$ is very low. For larger abundances, the present merger rate drops, and larger values of $f_{\rm PBH}$ are allowed with

[1] PBHs of masses around $10^{-16}-10^{-11}$ $M_\odot$ can still form all of the dark matter under these assumptions [10] (see [11, 12] for recent reviews on the constraints for the presence of PBHs in all the mass ranges).

respect to the Poissonian case. This degeneracy, i.e. the fact that the same merger rate can be achieved with different values of $f_{\rm PBH}$, can be disentangled either by directly measuring the merger rate as a function of redshift (possible with future experiments like Cosmic Explorer [32] or Einstein Telescope [33]), or by measuring the stochastic GW background created by past mergers (possible with current experiments like LIGO/Virgo [1]).

We will show explicitly how this works in a specific model for the clustering, in which the reduced local threshold for gravitational collapse, $\nu(x)$, is a local parameter linearly related to a secondary field $\psi(x)$. This simple model will allow us to analytically compute the correlation function $\xi(r)$ encoding the properties of the clustering. In particular, we will show how a comparison between the present merger rate and the stochastic GW background can help us disentangle the initial distribution of PBHs.

We will begin in section 2 by calculating the PBH abundance and correlation function for a simple model of non-Gaussianity, inducing clustering. We will then compute in section 3 its effect on the present and past merger rates, and show in section 4 how LIGO/Virgo capabilities in measuring the stochastic background of gravitational waves can determine the initial distribution of PBHs. Throughout this paper we use natural units, $G = c = 1$.

2 The PBH abundance and correlation function

Clustering appears if the local properties of the overdensity field $\delta(x)$ are space dependent. The probability of forming a PBH can then be modeled as depending on a "secondary" field $\psi(x)$. This effect might either come from an actual field different from the overdensity field, or from a long wavelength modulation of the overdensity field itself, resulting from a self-coupling of long and short scales as happens e.g. in local models of non-Gaussianity [34]. In both cases, the field $\psi(x)$ acts as a long wavelength modulation of the small scale perturbations $\delta(x)$, inducing a local change on the variance $\sigma_\delta(x) \equiv \sigma_\delta(\psi(x))$, and/or on the threshold for collapse into a BH, $\delta_c(x) \equiv \delta_c(\psi(x)))$. Assuming that both fields are independent and that $\delta(x)$ is locally Gaussian, then the probability for forming a BH depends on the local reduced threshold $\nu(x) \equiv \delta_c(x)/\sigma_\delta(x)$ in the following way[2]

$$P_1^{\rm local} = \frac{1}{2}{\rm erfc}\left(\frac{\nu(x)}{\sqrt{2}}\right) . \tag{2.1}$$

This means that local changes in δ_c or σ_δ are in practice indistinguishable. The total probability for a given region to form a BH, that we denote P_1, is obtained by integrating over the configurations of the field $\psi(x)$, that we assume to be a Gaussian random field. Similarly we can define $P_2^{\rm local}(r)$, the joint probability of having two black holes at a distance r, given that the local reduced thresholds at x_1 and x_2 are given by $\nu(x_1)$ and $\nu(x_2)$. This is given by [38]

$$\begin{aligned} P_2^{\rm local}(r) = {} & \frac{1}{4}{\rm erfc}\left(\frac{\nu_1}{\sqrt{2}}\right) + \frac{1}{4}{\rm erfc}\left(\frac{\nu_2}{\sqrt{2}}\right) + \frac{{\rm sgn}\left(\nu_1\right){\rm sgn}\left(\nu_2\right) - 1}{4} \\ & - T\left(\nu_1, \frac{\nu_2 - \omega_\delta(r)\nu_1}{\nu_1\sqrt{1-\omega_\delta^2(r)}}\right) - T\left(\nu_2, \frac{\nu_1 - \omega_\delta(r)\nu_2}{\nu_2\sqrt{1-\omega_\delta^2(r)}}\right) , \end{aligned} \tag{2.2}$$

[2]For simplicity we compute the abundance of PBHs and the correlation function that encodes the clustering using the Press-Schechter formalism. More accurate criteria for the formation of PBH can be obtained from the statistics of peaks [35], although we do not expect qualitatively differences with the results obtained here. The statistics of peaks has been recently revisited to count for peaks in the so-called compaction function [36], which is the object that controls the critical collapse for the formation of a BH [37].

JCAP11(2020)036

where $\omega_\delta(r) = \langle\delta(x_1)\delta(x_2)\rangle/\langle\delta(0)^2\rangle$ is the reduced correlation function of $\delta(x)$, $\nu_i = \nu(x_i)$ and $T(z,a)$ is the Owen T-function [39]

$$T(z,a) \equiv \frac{1}{2\pi}\int_0^a \mathrm{d}t \frac{e^{-\frac{(1+t^2)z^2}{2}}}{1+t^2}\,. \tag{2.3}$$

The total $P_2(r)$ can be found by integrating this expression over the fields $\psi_1 \equiv \psi(x_1)$ and $\psi_2 \equiv \psi(x_2)$ inducing the spatial dependence on $\nu_i(x)$.

The clustering of PBHs can be encoded in the N-point correlation functions $\xi^{(N)}(r)$, that measure the excess probability, relative to an uncorrelated distribution, of finding $N-1$ black holes at distances $r_1,\ldots,r_{N-1}$ from a BH at $r=0$. This is then given by

$$\xi^{(N)}(r_1,\ldots,r_{N-1}) = \frac{P_N(r_1,\ldots,r_{N-1})}{P_1^N} - 1\,. \tag{2.4}$$

As we will see, the merger rate of BHs depends on all the N-point correlation functions (as shown in (B.15) of appendix B). However in some cases all that information is contained in the 2-point correlation function $\xi^{(2)}(r) \equiv \xi(r)$. Whenever this is not possible, we will show that the use of $\xi(r)$ can nevertheless provide useful insights into the qualitative behaviour of the mergers.

In the following we briefly discuss the Gaussian case.

2.1 Gaussian case

The Gaussian case is recovered if we turn-off the field $\psi(x)$. In this case $\nu_1 = \nu_2 = \nu_g$, where $\nu_g \equiv \delta_{c,g}/\sigma_\delta$ is space independent (and $\delta_{c,g}$ is the threshold for collapse in the Gaussian case). Then we get

$$P_1 = \frac{1}{2}\mathrm{erfc}\left(\frac{\nu_g}{\sqrt{2}}\right) \quad \text{and} \quad P_2(r) = \frac{1}{2}\mathrm{erfc}\left(\frac{\nu_g}{\sqrt{2}}\right) - 2T\left(\nu_g, \sqrt{\frac{1-\omega_\delta(r)}{1+\omega_\delta(r)}}\right)\,, \tag{2.5}$$

and the 2-point correlation function $\xi(r)$ is given by[3]

$$\xi(r) = 2\frac{T\left(\nu_g,1\right) - T\left(\nu_g, \sqrt{\frac{1-\omega_\delta(r)}{1+\omega_\delta(r)}}\right)}{P_1^2}\,. \tag{2.6}$$

This expression is exact, valid for any ν_g and ω_δ. Simpler expressions can be obtained in the regime for which ν is large or small [15, 40]. For example, for large ν, which is the relevant limit for PBH formation, we can make use of the expansion

$$T(\nu,a) \sim \frac{1}{4}\mathrm{erfc}\left(\frac{\nu}{\sqrt{2}}\right) - \frac{1}{2\pi}\frac{e^{(-1+a^2)\nu^2/2}}{\nu^2 a(1+a^2)} + \mathcal{O}\left(\frac{e^{-\nu^2}}{\nu^4}\right)\,, \tag{2.7}$$

and then $\xi(r)$ is given by [15]

$$1+\xi(r) \sim \frac{(1+\omega_\delta(r))^{\frac{3}{2}}}{(1-\omega_\delta(r))^{\frac{1}{2}}}\exp\left(\nu_g^2\frac{\omega_\delta(r)}{1+\omega_\delta(r)}\right)\,. \tag{2.8}$$

In the following we will present a simple model for which the correlation function in the non-Gaussian case can be computed.

[3] Some properties of Owen T-functions can be found in [38].

JCAP11(2020)036

2.2 A simple model for clustering

Here we consider a simple model of clustering were the parameter $\nu(x)$ is linearly related to the secondary field $\psi(x)$ as[4]

$$\nu(x) = \nu_g \left(1 + \beta\psi(x)\right) , \tag{2.9}$$

where β denotes the strength of the coupling between $\psi(x)$ and $\delta(x)$. With this simple model we can solve for P_1 and $P_2(r)$ exactly, getting (see appendix A)

$$P_1 = \frac{1}{2}\text{erfc}\left[\frac{\nu_g}{\sqrt{2}}\frac{1}{\sqrt{1+\alpha^2}}\right] , \tag{2.10}$$

$$P_2(r) = \frac{1}{2}\text{erfc}\left(\frac{\nu_g}{\sqrt{2}}\frac{1}{\sqrt{1+\alpha^2}}\right) - 2T\left(\frac{\nu_g}{\sqrt{2}}\frac{1}{\sqrt{1+\alpha^2}}, \sqrt{\frac{1-\bar{\omega}}{1+\bar{\omega}}}\right) . \tag{2.11}$$

Here

$$\alpha \equiv \delta_{c,g}\beta\left(\frac{\sigma_\psi}{\sigma_\delta}\right) \quad \text{and} \quad \bar{\omega}(r) = \frac{\omega_\delta(r) + \alpha^2\omega_\psi(r)}{1+\alpha^2} , \tag{2.12}$$

where σ_ψ and σ_δ stands for the variance of the long and short wavelength perturbations respectively. Let us notice that the effective coupling is determined by α, which not only takes into account the coupling between both fields (given by β), but is also sensitive to the relative amplitude of the variances. By comparing (2.10) and (2.11) with the expressions found for the Gaussian case (2.5), we see that this model is equivalent to a Gaussian model with the replacements

$$\nu_g \to \bar{\nu} = \frac{\nu_g}{\sqrt{1+\alpha^2}} \quad \text{and} \quad \omega_g \to \bar{\omega} . \tag{2.13}$$

This is actually true for all N-point probabilities, as shown in the appendix A. In particular, this implies that in this model the total abundance is amplified with respect to the Gaussian case. For concreteness let us choose a two-point correlation function for ω_δ and ω_ψ as given from a peaked power spectrum at both scales. In particular we choose[5]

$$\mathcal{P}_i(k) = \sigma_i^2 k_i \delta(k - k_i) \tag{2.14}$$

where $i = (\delta, \psi)$. Here the short mode k_δ contributes to the formation of the PBHs and the long mode k_ψ modulates the amplitude of the short one. As both $\psi(x)$ and $\delta(x)$ are Gaussian random fields, their two-point correlation function $\xi_i(r)$ is given by [35]

$$\xi_i(r) = \int d\ln k\, \mathcal{P}_i(k)\frac{\sin(k_i r)}{k_i r} . \tag{2.15}$$

We then have that

$$\omega_i(r) = \frac{\sin\left(k_i r\right)}{k_i r} . \tag{2.16}$$

In figure 1 we show how $\xi(r)$ varies as a function of the strength of the coupling α (left panel), the relative scales between the short and long wavelengths, $\gamma \equiv k_\psi/k_\delta$, and the

[4]This relation can be seen as the first order term of a Taylor expansion in the field $\psi(x)$ around $\psi = 0$. Let us note that if $\psi = 0$ corresponds to an extremum of $\nu(\psi)$, then the expansion would start at second order in $\psi(x)$. It might then be interesting to study generalizations of this model, even if in principle we would expect similar qualitative effects on the merger rate. We thank Jaume Garriga for pointing this out.

[5]This is the power spectrum for the density fluctuation evaluated at the time when the small scales perturbations δ enters the horizon.

JCAP11(2020)036

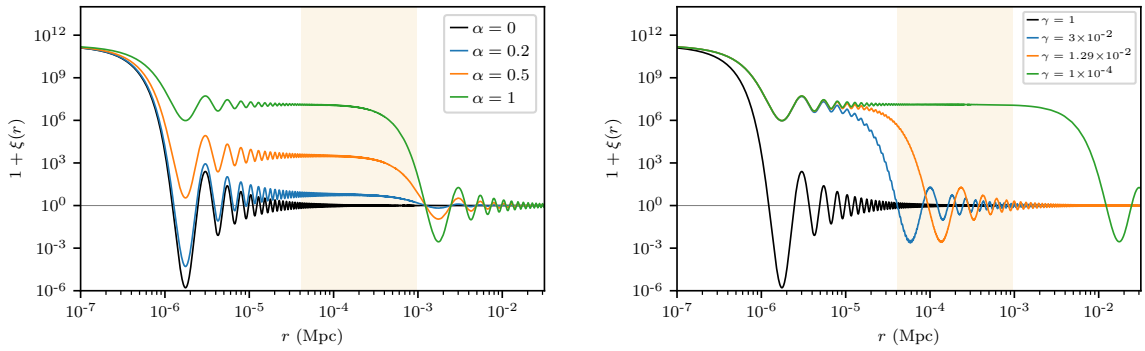

Figure 1. The two-point correlation function $\xi(r)$ for the linear model (2.9) and for power spectra given by the delta functions (2.14). *Left*) The correlation function $\xi(r)$ as we vary the strength of the coupling α between $\delta(x)$ and $\psi(x)$. For $\alpha \ll 1$, the Gaussian case is recovered. Here we fix $\gamma = 10^{-3}$. *Right*) The correlation function $\xi(r)$ as we vary the hierarchy between the short and large wavelengths, given by $\gamma \equiv k_\psi/k_\delta$. We fix $\alpha = 1$. In both left and right panels we choose $\bar{\nu} = 6.8$ and $k_\delta \simeq 2.5{\times}10^6$ Mpc^{-1}, which corresponds to a present PBH abundance of $f_{\rm PBH} = 10^{-3}$ for BHs of masses $M = 30{\rm M}_\odot$. The orange region $(x_{\rm min}, x_{\rm max})$ indicates the scale of binaries that merge today ($t \sim 14$Gyr). The first drop in the correlation function corresponds to the size of the BH, $R_{\rm BH} \sim k_\delta^{-1}$, so the region below this point reflects the autocorrelation of $\delta(r)$. The second drop corresponds to the typical scale of the secondary field $R_{\rm cl} \sim k_\psi^{-1}$ and it defines the clustering length of the PBHs. Beyond $R_{\rm cl}$ the correlation is effectively zero so the distribution becomes Poissonian.

fraction of DM in form of PBHs, $f_{\rm PBH} \equiv \Omega_{\rm DM}/\Omega_{\rm PBH}$. Let us note that for the Gaussian case, corresponding to $\alpha = 0$ or $\gamma = 1$, all the N-point correlation functions are zero for $r > R_{\rm BH}$, meaning that the distribution of BHs is Poissonian [15, 17]. On the other hand as can be seen in figure 1, in the non-Gaussian regime there is a region for $r > R_{\rm BH}$ where the 2-point correlation is constant and possibly large. This plateau is a consequence of the nearly constant correlation function $\bar{\omega}$ induced by the long wavelength perturbation. For N BHs within this region, it is possible to calculate their N-point correlation function for large thresholds. These are given by [41]

$$1 + \xi^{(N)}(\bar{\omega}, \bar{\nu}) \sim \frac{(1 + (N-1)\bar{\omega})^{N-\frac{1}{2}}}{(1-\bar{\omega})^{\frac{N-1}{2}}} \exp\left(\frac{N\bar{\nu}^2}{2}\frac{(N-1)\bar{\omega}}{(1+(N-1)\bar{\omega})}\right), \tag{2.17}$$

which is valid when $\bar{\omega} \in (-1/(N-1), 1)$. For $N = 2$ we have

$$1 + \xi^{(2)}(\bar{\omega}, \bar{\nu}) \sim \frac{(1+\bar{\omega})^{\frac{3}{2}}}{(1-\bar{\omega})^{\frac{1}{2}}} \exp\left(\bar{\nu}^2 \frac{\bar{\omega}}{(1+\bar{\omega})}\right). \tag{2.18}$$

In general not all the BHs determining the properties of the binary will necessarily be within this region, since the N-point correlation eventually vanishes for $r > 1/k_\psi$. This estimate provides then an upper bound for the amplitude of their correlation.

3 Merger rate

Now we consider the effect of the clustering on the merger rate of binaries. When the torque of the binary (preventing a head-on collision) is provided by a third BH, we need to consider

JCAP11(2020)036

the probability density function to find the nearest BH at distance x and the next-to-nearest BH at distance y from a reference BH at $r = 0$. We call this distribution $Q(x, y)$ and in general it takes the following form (see appendix B)

$$Q(x,y) = 16\pi^2 n^2 x^2 y^2 G_0(x) G_1(y) \exp\left[-4\pi n \left(\int_0^x G_0(z) z^2 \mathrm{d}z + \int_x^y G_1(z) z^2 \mathrm{d}z\right)\right] \Theta(y-x)\,, \tag{3.1}$$

with n the comoving number density of BHs and where $G_m(r)$, the m-particle conditional pair correlation function, refers to the conditional probability of finding a BH at radius r given that there is one at $r = 0$ and m additional BHs in the interior of the region of radius r [42]. The functions $G_m(r)$ depend on all the N-point correlation functions and so in general they are hard to determine. However in some cases they take simple forms. For a Poissonian distribution, the presence of a BH at any given position is independent on the absence or presence of BHs at any other position implying $G_m = 1$. Then, for a Poissonian distribution $Q(x, y)$ takes the following form (see e.g. [8])

$$Q(x,y) = 16\pi^2 x^2 y^2 n^2 \exp\left[-4\pi \int_{R_{\rm BH}}^y n z^2 \mathrm{d}z\right] \Theta(y-x)\,. \tag{3.2}$$

Here $R_{\rm BH}$ is the radius of the BH at[6] $r = 0$. Under certain conditions, a non-Poissonian distribution can also be written as in (3.2), provided that the comoving number density is promoted to a local density

$$n \to n(r) = n\, g_2(r) \quad \text{with} \quad g_2(r) \equiv 1 + \xi(r)\,. \tag{3.3}$$

In particular, if the N-point correlation functions $\xi^{(N)}$ satisfy

$$1 + \xi^{(N)}(r_1, \ldots, r_{N-1}) = \prod_{i=1}^{N-1} (1 + \xi(r_i))\,, \tag{3.4}$$

then $G_m(r) = g_2(r)$ for all m and $Q(x, y)$ takes the form [17] (see also appendix B)

$$Q(x,y) = 16\pi^2 x^2 y^2 n(x) n(y) \exp\left[-4\pi \int_{R_{\rm BH}}^y n(z) z^2 \mathrm{d}z\right] \Theta(y-x)\,. \tag{3.5}$$

This is for example the case for biased Gaussian distributions, as our model, with a constant and small correlation function $\xi^{(N)}$ [43]. In the case in which the correlation functions $\xi^{(N)}$ are larger than expected from the separability condition (3.4) we expect to have

$$G_n(r) \geq g_2(r)\,. \tag{3.6}$$

For some distributions this inequality can be shown to hold explicitly [44–46]. Using the bounds found in e.g. [45, 47], it can be shown that for small radius $G_0(r) \simeq g_2(r)$. For larger radius, and because the probability of finding a void decreases, we expect G_0 to be an increasing function of r. This would then imply that $G_0(r) \geq g_2(r)$ at all relevant scales (we also expect the same to happen for $G_1(r)$). Then the expression (3.5) becomes either an upper or a lower bound, depending on whether the linear or the exponential term in (3.1) dominates. In the rest of the paper, we test whether (3.4) holds using the N-correlation

[6] As shown in figure 1, for $r < R_{\rm BH}$, the function $\xi(r)$ measures the autocorrelation of $\delta(r)$.

JCAP11(2020)036

function as given by (2.17), for N up to the expected number of BHs in the volume where the correlation is non-vanishing.

In the following we will compute the merger rate as given by the simple expression (3.5), taking into consideration that this expression will be an upper or lower bound for the true merger rate for large correlations, as explained above.

In order to find the merger rate at a given time t, we need to integrate $Q(x, y)$ over the positions (x, y). Binaries that merge today were initially separated by a comoving distance x in the interval $(x_{\rm min},\ x_{\rm max})$. The distance $x_{\rm max}$ is the maximum distance such that a pair of BHs can form a binary system, and can be found by imposing that the mass of the binary system is larger than the background mass within a volume whose radius is the initial separation of the binary [3, 5]. This radius is maximised at matter-radiation equality and then $x_{\rm max}$ is given by[7]

$$x_{\rm max} \simeq \left(\frac{M}{\rho_{eq}}\right)^{1/3}, \tag{3.7}$$

where $M = m_1 + m_2$ is the total mass of the binary, ρ_{eq} is the background energy density at matter-radiation equality. The distance $x_{\rm min}$ is the distance below which a binary with any orbital parameter would have already merged. The time t for an orbit to collapse with dimensionless angular momentum[8] is given by [48]

$$t = \frac{3}{85}\frac{r_x^4}{\eta M^3} j^7 \quad \text{with} \quad j = (x/y)^3\,, \tag{3.8}$$

where r_x is the semi-major axis of the binary and $\eta \equiv m_1 m_2/M^2$ is the symmetric mass ratio. Then, for a given semi-major axis, the longest possible time for a binary to merge is if they have initially a circular orbit ($j = 1$). The semi-major axis r_x is proportional to the physical distance at the time the binary decouples from the Hubble flow. We then need to find the scale factor $a_{\rm dec}$ at which the condition

$$M = \rho(a) r^3 \tag{3.9}$$

is satisfied, where $\rho(a)$ is the total energy density at radiation domination. Using $a_{\rm eq} = 1$, we find

$$r_x = \left(\frac{x}{x_{\rm max}}\right)^3 x\,, \tag{3.10}$$

and so

$$x_{\rm min} = \left(\frac{85\,\eta\,M^3\,t}{3\,x_{\rm max}^4}\right)^{1/16} x_{\rm max}\,. \tag{3.11}$$

For each position x within $(x_{\rm min},\ x_{\rm max})$ there is a corresponding y such that the merging time is t, as given by eq. (3.8). For $t = t_0$ the present age of the Universe, and $m_1 = m_2 = 30\,{\rm M}_\odot$, $x_{\rm min} \simeq 4 \times 10^{-5}$ Mpc and $x_{\rm max} \simeq 9.6 \times 10^{-4}$ Mpc. By integrating $Q(x, y)$ over this interval we find the total merger rate per unit time at a given time t. In order to find the merger rate per unit time and volume element, we multiply by the total density of PBHs, $\bar{n}$. This is found by integrating $n(r)$ in (3.3) over a Hubble patch and dividing by the total volume. As the radius of the Hubble patch under consideration is much bigger than $R_{\rm cl} \sim k_\psi^{-1}$, the

[7] Slightly different estimates for $x_{\rm max}$ are obtained depending on whether the volume is defined in cartesian or spherical coordinates.

[8] More precisely $j = c\,(x/y)^3$, where c is a factor $\mathcal{O}(1)$. We choose $c = 1$.

JCAP11(2020)036

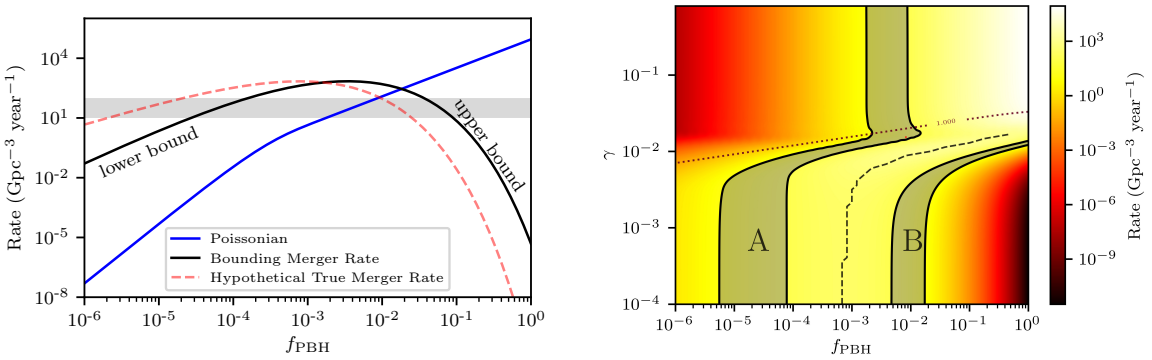

Figure 2. *Left*) For large clustering, $\gamma \ll 1$, the merger rate in eq. (3.5) (in black) becomes either an upper bound or lower bound of the unknown true merger rate (depicted here in red), depending on whether the linear or the exponential term in (3.1) dominates. For the Poissonian case (blue), the linear term always dominates. *Right*) Present merger rate from (3.5) for a monochromatic mass spectrum with $m = 30\,\mathrm{M}_\odot$, as a function of $f_{\rm PBH}$ and γ for $\alpha = 1$. In the grey band we show the present rate of binary mergers as determined by LIGO/Virgo observations. We distinguish two branches, branch A which is linked to the Poissonian case ($\gamma = 1$), and branch B that appears as a result of the drop in the merger rate for large $f_{\rm PBH}$ and small γ. Above the dotted line the condition (3.4) holds, and the true merger rate is accurately described by (3.5). Below that line, the merger rate depicted here is either an upper or lower bound of the true merger rate, depending on whether this rate is an increasing or decreasing function of $f_{\rm PBH}$ (as seen in the left panel). This limit is shown as a dashed line, where we show the position of the maximum of the merger rate. From here we deduce that the positions of branch A and B below the dotted line should be displaced towards smaller values of $f_{\rm PBH}$. This implies that, for a given γ, the merger rate consistent with LIGO/Virgo will happen for smaller $f_{\rm PBH}$ than shown here.

contribution of $\xi(r)$ to the average number density of PBH is negligible, and so $\bar{n} \simeq n$. By using (3.7) the number density is related to $f_{\rm PBH}$ by

$$\bar{n} = \frac{f_{\rm PBH}}{{x_{\rm max}}^3}\,. \tag{3.12}$$

Then, the merger rate at a given time t is

$$\frac{\mathrm{d}R}{\mathrm{d}t} = \frac{\bar{n}}{2}\int_{x_{\rm min}}^{x_{\rm max}} Q(x, y(x,t))\left|\frac{\mathrm{d}y}{\mathrm{d}t}(t,x)\right| dx\,, \tag{3.13}$$

where the factor 1/2 avoids overcounting the binaries. In figure 2 we show the merger rates for the linear model (2.9), with the power spectra given by (2.14). We fix $\alpha = 1$ and show the merger rate as a function of $f_{\rm PBH}$ and $\gamma \equiv k_\psi/k_\delta$. The Poissonian case corresponds to $\gamma = 1$ (in such case there is no long wavelength modulation). From figure 2 we see that while for the Poissonian case the merger rate increases monotonically with $f_{\rm PBH}$, for the clustered distribution ($\gamma \ll 1$) the rate increases with increasing $f_{\rm PBH}$ only until a certain value of $f_{\rm PBH}$. For $f_{\rm PBH} \gtrsim 10^{-3}$ and $\gamma \lesssim 10^{-2}$, the merger rate decreases with increasing $f_{\rm PBH}$. The drop is due to the fact that the exponential term in (3.5) dominates, which is never the case in the Poissonian case (if we would consider an unphysical $f_{\rm PBH} > 1$ we would eventually also notice the exponential drop in this case).

To understand the reason behind the drop in the merger rate, we recall that binaries merging today were initially separated by a distance x inside the interval $(x_{\rm min},\, x_{\rm max})$, as

JCAP11(2020)036

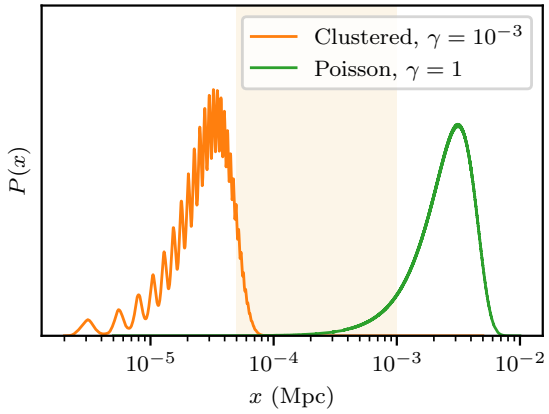

Figure 3. Distribution of the comoving distance of the nearest BH in a Poissonian and in a clustered distribution of BHs, for parameters giving the same present rate ($(\gamma = 1, f_{\rm PBH} = 4.6 \times 10^{-3})$ in the Poissonian case and $(\gamma = 10^{-3}, f_{\rm PBH} = 2.2 \times 10^{-5})$ for the clustered distribution). The distributions are normalized so that they can be easily compared in the same figure. For a Poissonian distribution, most of BHs are separated by a distance $x > x_{\rm max}$. For a clustered distribution, most of BHs are separated by a distance $x < x_{\rm min}$. BHs at a distance in the interval $(x_{\rm min},\ x_{\rm max})$, shown in grey, can merge by today (provided the third BH provides the right amount of torque).

depicted in figure 3. In the Poissonian case, BHs have a mean separation $\bar{x}$ much larger than $x_{\rm max}$. Few of them would have a separation $x \lesssim x_{\rm max} \ll \bar{x}$, then forming a binary. These binaries merge today if their orbits were initially very eccentric (otherwise, their merging time is too large). As $f_{\rm PBH}$ increases, the typical distance between two BHs diminishes and then it is more likely for them to have a separation $x \lesssim x_{\rm max}$. Then the merger rate increases. The picture changes for the clustered distribution. For small γ, the typical distance to the nearest BH is smaller than $x_{\rm min}$. That is, binaries merging today are, contrary to the Poissonian case, rare binaries separated by a distance $x \gtrsim x_{\rm min} \gg \bar{x}$. These will merge today if their initial orbits are circular (otherwise their merging time is too short). As $f_{\rm PBH}$ increases, the typical distance between two BHs becomes even smaller, and so it is more rare to have binaries separated by a distance larger than $x_{\rm min}$. This explains the drop of the merger rate for $f > 10^{-3}$ in the small γ region.[9] In figure 3 we show the typical distance of two BHs in the Poissonian and in the clustered regimes. In an intermediate regime there are two local maxima of the distribution. That behaviour is better seen by looking at the angular momentum of the binaries, that we show in figure 4.

The fact that the merger rate can drop as we increase $f_{\rm PBH}$ for clustered distributions means that the rate observed by LIGO/Virgo is, for small and constant γ, consistent with two different values of $f_{\rm PBH}$.[10] This is the origin of the two branches of parameter space consistent with LIGO/Virgo that we see in figure 2. One is connected to the Poissonian case ($\gamma = 1$), and we call it branch A. We call branch B the one resulting from the decrease in the

[9] As we have already said, this drop in the merger rate would also be visible in the Poissonian case if we would allow $f_{\rm PBH}$ to be much larger that unity. In that hypothetical case, the typical distance of a binaries goes from being much larger than $x_{\rm max}$, to be much smaller than $x_{\rm min}$.

[10] For very small $f_{\rm PBH}$ and γ, the rate still increases with $f_{\rm PBH}$, since, while the area under the curve in figure 3 is more or less constant with $f_{\rm PBH}$, there is a prefactor proportional to the total abundance of PBHs in eq. (3.13) that dominates the estimation of the total rate.

JCAP11(2020)036

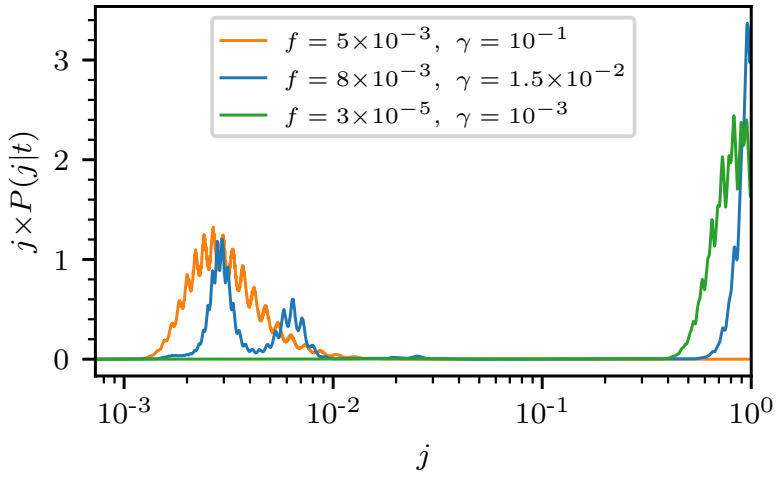

Figure 4. Distribution of initial angular momenta for binaries merging today. Here we see three cases in branch A in which most binaries are eccentric (corresponding to a Poissonian distribution, in orange), circular (corresponding to a fully clustered distribution, in green) and mixed (corresponding to the intermediate case, in blue).

rate at large clustering ($\gamma < 10^{-2}$) and large $f_{\rm PBH}$. In branch A and in the Poissonian case ($\gamma = 1$), as we previously explained, most binaries merging today were initially very eccentric. As γ decreases, and the probability to form a BH increases at small radii, a new population of BH appears with mean distance smaller than $x_{\rm min}$. At some point as we move in branch A these two populations of binaries coexist, and we have a mixed population of binaries. In order to assess the relative abundances of both excentric and circular orbit populations we need to determine the probability distribution of j for binaries merging at time t, $P(j|t)$, which can be related to $Q(x, y)$ as

$$P(j|t) = S(t)^{-1} Q(x(j,t), y(j,t)) \left| \frac{\partial(x,y)}{\partial(j,t)} \right|, \tag{3.14}$$

where $x(j,t)$ and $y(j,t)$ can be found from eq. (3.8) and $S(t)$ is a normalization factor. Notice that for a given merging time, the allowed separation of binaries ($x_{\rm min},\ x_{\rm max}$) translates into possible values for j in the interval $(j_{\rm min}, 1)$ with $j_{\rm min} = (x_{\rm min}/x_{\rm max})^{16/7}$. In figure 4 we show the distribution of angular momenta for three cases having the same present merger rate ($R \simeq 50$ Gpc^{-3} yr^{-1}). These three cases follow a mostly Poissonian, clustered or mixed distribution of BHs. In the mixed case, there are two populations of circular and eccentric binaries contributing equally to the present merger rate. The degeneracy between branch A and B is broken if we consider the merging history. In figure 5 we show the merger rate as a function of redshift, for four different parameters for which the present merger rate is the same (two of them belong to branch A — solid lines — and two belong to branch B — dashed lines). While the merging history can then help us disentangle whether binaries come from branch A or B, the differences within each branch are less noticeable, in particular for the case of branch A. In principle there is a range of parameters for which the present merger rate can be explained with $f_{\rm PBH} = 1$, around $\gamma \simeq 0.01$ in figure 2. We should however be cautious since at large $f_{\rm PBH}$ most of the binaries are disrupted under the influence of others

JCAP11(2020)036

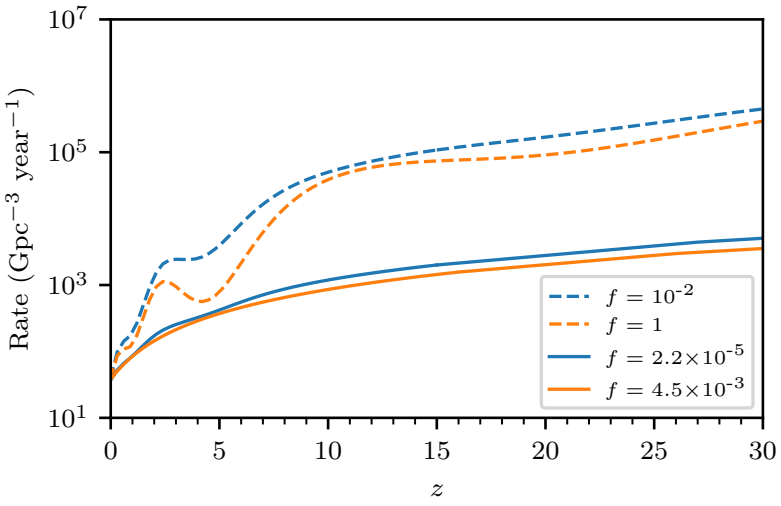

Figure 5. Merger rate as a function of redshift z for two different families of parameters. All of them have the same present merger rate, consistent with LIGO/Virgo, but different values for $f_{\rm PBH}$. Solid lines corresponds to parameters in the branch A (($f = 2.2 \times 10^{-5}$, $\gamma = 10^{-3}$) and ($f = 4.5 \times 10^{-3}$, $\gamma = 10^{-1}$)), and dashed lines corresponds to parameters in branch B (($f = 1, \gamma = 1.3\times10^{-2}$) and ($f = 10^{-2}, \gamma = 10^{-3}$)). Note that, as we explained in the previous section, because we expect branch A and B to be displaced towards smaller $f_{\rm PBH}$ below the dotted line in figure 2 these curves should correspond to larger values of γ than the ones quoted here. For example for $f_{\rm PBH} = 1$, we expect $\gamma > 1.3 \times 10^{-2}$.

PBHs [5], thus yielding smaller present merger rates.[11] A quantitative estimation on how this effect changes the rate is however only possible by the use of numerical simulations.

A direct detection of the merger rate as a function of redshift will of course first contribute in determining whether these binaries are of primordial origin or not. For astrophysical binaries, the merger rate drops for $z > 2$ and then dies off. These different histories might be directly disentagled with more events in the LIGO/Virgo channel [49] and with future experiments like the Cosmic Explorer [32] or Einstein Telescope [33] (see e.g. [50]). At last, let us note that the merger rate in branch B is several orders of magnitude larger that of branch A. For such large rates, the gravitational waves created by the binaries would be strongly lensed by other PBHs, leading to signatures that might explain some features of the LIGO/Virgo events [51, 52].

The integrated effect of the merging history can also be deduced by looking at the stochastic background of gravitational waves, which we discuss in more detail in the following section. As we will show, when LIGO/Virgo acquires full capability, a detection of the stochastic background will make it possible to distinguish between these different merging histories.

4 The stochastic background of binary mergers

The energy released by binaries that have already merged contribute to a stochastic background of gravitational waves. The energy density of the stochastic background $\Omega_{\rm GW}$ can be

[11] Let us note however that for slightly larger γ, a merger rate larger by many orders of magnitude can be achieved. Thus it is possible that there is a $\gamma > 0.01$ for which the merger rate is consistent with $f_{\rm PBH} = 1$, even if most of the mergers are disrupted at early times.

JCAP11(2020)036

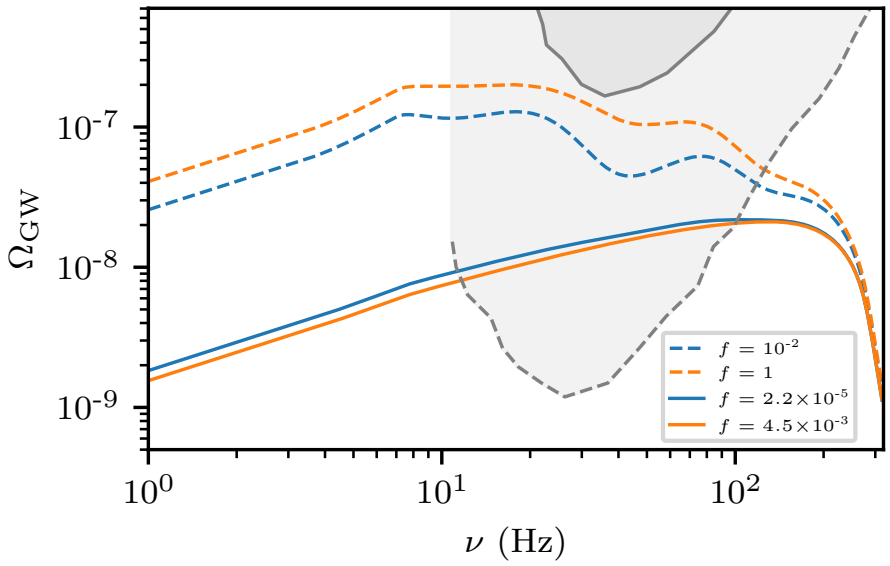

Figure 6. Stochastic background of gravitational waves. We choose the same parameters as in figure 5, having the same present merger rate. The solid grey indicates the current LIGO/Virgo bounds whereas the dashed line indicates the projected final sensitivity [63].

expressed in terms of the critical density ρ_c as

$$\Omega_{\rm GW} \equiv \frac{1}{\rho_c}\frac{d\rho_{\rm GW}}{d\log\nu} \tag{4.1}$$

where $\rho_{\rm GW}$ is the energy density at a given frequency ν. The contribution coming from early formed binaries can then be expressed as (see e.g. [14])

$$\Omega_{\rm GW} = \frac{\nu}{\rho_c H_0}\int_0^{z_*}\frac{R_{\rm PBH}(z)}{(1+z)E(z)}\frac{dE_{\rm GW}}{d\nu_s}(\nu_s)dz \tag{4.2}$$

where $dE_{\rm GW}/d\nu_s$ is the GW energy spectrum of the merger and ν_s is the frequency in the source frame, related to the observed frequency as $\nu_s = (1+z)\nu$. The function $E(z) \equiv H(z)/H_0 = [\Omega_r(1+z)^4 + \Omega_m(1+z)^3 + \Omega_\Lambda]^{1/2}$. Black holes of $m \sim 10^2\,{\rm M}_\odot$ were formed at $z_* \sim 10^{10}$, and so this is the maximum redshift at to which we possibly integrate the relation above (even though the integrand stops contributing much earlier).

As can be seen from figure 6, under the hypothesis that all mergers are of primordial origin, LIGO/Virgo will be able to disentangle the initial orbits of the binaries.

The energy released as GWs can be deduced from its waveform. This has been modeled for the inspiral, merger, and ringdown phases of BHs binary mergers, and fitted through numerical simulations [53, 54]. For non-precessing binaries, as it is the case for solar mass PBHs [55–57], it takes the following form (see also [58, 59])

$$\frac{dE_{\rm GW}}{d\nu_s}(\nu_s) = \frac{\pi^{2/3}M_c^{5/3}}{3}\begin{cases}\nu_s^{-1/3} & \text{for } \nu_s < \nu_1\\ \omega_1\nu_s^{2/3} & \text{for } \nu_1 \le \nu_s < \nu_2\\ \omega_2\frac{\sigma^4\nu_s^2}{\left(\sigma^2+4(\nu_s-\nu_2)^2\right)^2} & \text{for } \nu_2 \le \nu_s < \nu_3\\ 0 & \text{for } \nu_3 \le \nu_s\end{cases} \tag{4.3}$$

JCAP11(2020)036

where $\nu_i \equiv (\nu_1, \nu_2, \sigma, \nu_3) = (a_i\eta^2 + b_i\eta + c_i)/(\pi M)$, $M = m_1 + m_2$ is the total mass, M_c is the chirp mass ($M_c^{5/3} = m_1 m_2 M^{-1/3}$), and $\eta = m_1 m_2 M^{-2}$ is the symmetric mass ratio. The parameters a_i, b_i and c_i can be found in [53], and (ω_1, ω_2) are chosen such that the spectrum is continuous. In the template (4.3) the three regimes corresponds, towards larger frequencies, to the inspiral, merging and ringdown phases, and for $30\,\mathrm{M}_\odot$ they correspond to $\nu_i = (135, 271, 79, 387)$ Hz.

In figure 6 we show the stochastic background of gravitational waves for a set of parameters producing the same present merger rate. We take $(\Omega_r, \Omega_\Lambda, \Omega_m)$ as determined by the Planck satellite [60]. On the one hand, let us note that the shape of the stochastic background of gravitational waves coming from astrophysical binaries is qualitatively very similar to the one coming from branch A and from a Poissonian distribution of PBHs [61, 62], and thus a very careful comparison should be done in order to discriminate between the two. On the other hand, the signal from branch B features oscillations — residuals of the oscillations in the merger rate — that might act as a smoking gun for this type of distribution.

5 Discussion and conclusions

We have presented a model for initial clustering of PBHs and computed the merger rates of binary black holes. We have shown that because of the clustering the merger rate can decrease as the fraction of black holes increases, inducing a degeneracy in the value of f_{PBH} for which a certain merger rate is obtained and opening the possibility that all DM is in the form of PBHs of stellar mass. We have showed that the detection of the stochastic background (within the projected sensitivity of LIGO/Virgo) should be able to break this degeneracy, determining the initial distribution of PBHs.

While in this paper we have discussed the constraints coming from the present and past merger rates, there are other constraints that put bounds on the abundance of PBHs at these scales. Depending on the mass function of the PBHs, more observables related to binary mergers can be used to confront with LIGO/Virgo data, such as the mass ratios, total mass and chirp mass [64]. Additionally, other observables not related to binaries can be used, such as distortions in the Cosmic Microwave Background (CMB) [65, 66], gravitational lensing of Type IA Supernova [67], pulsar timings [68], and the survival of star clusters [69]. In general we expect these constraints to be alleviated by the presence of clustered distributions (see e.g. [4, 70, 71]), however a quantitative analysis taking into account the full space of parameters that we have considered here is still lacking.

Our analysis is based on binary orbits induced by a third BH. For large values of f_{PBH}, as well as highly clustered distributions, this assumption might not hold. We thus expect some changes in the quantitative results for some of the parameters of the theory, when N-body effects are considered. Moreover, we used an estimate for the merger rate that assumes the separability condition eq. (3.4), and we identified the regions of parameter space where this estimate is accurate, or provides a lower or upper bound of the true merger rate. This is sufficient for having a qualitative understanding of the possible merger histories at large clustering. A quantitative estimate can be obtained by calculating explicitly the probability of finding nearest neighbours at a given position, by applying e.g. the analytic techniques of [42, 45, 47]. These issues can also be tackled by using numerical simulations to determine the initial distribution of BHs and by looking at their time evolution (see e.g. [78] for recent considerations on these problems). These lines of research will be further pursued in future

JCAP11(2020)036

work. Let us note that both of these effects make the merger rate drop for larger abundances, and thus both contribute in opening the window for having all the DM as stellar PBHs.

Acknowledgments

We thank Jaume Garriga for enlightening discussions and Salvatore Torquato for a stimulating correspondence. We also thank Jose M. Diego for comments on the manuscript. This work has been partially supported by FPA2016-76005-C2-2-P, MDM-2014-0369 of ICCUB (Unidad de Excelencia Maria de Maeztu), and AGAUR2017SGR-754. A.S is supported by an APIF grant from Universitat de Barcelona. N.T. is supported by an INPhINIT grant from la Caixa Foundation (ID 100010434) code LCF/BQ/IN17/11620034. This project has also received funding from the European Unions Horizon 2020 research and innovation programme under the Marie Sklodowska-Curie grant agreement No. 713673.

A N-th point distribution of PBHs

In this appendix we compute the probability of having N primordial black holes at the points $x_1, \ldots, x_N$ for the case where the local critical threshold for collapse follows a linear relation with the secondary field ψ

$$\nu(x_i) = \nu_g \left(1 + \beta\psi(x_i)\right) = \nu_g + \alpha\mu(x_i)\,, \tag{A.1}$$

where we have defined $\alpha \equiv \nu_g \beta \sigma_\psi$ and $\mu(x_i) = \psi(x_i)/\sigma_\psi$. We denote by $P_N^{\rm local}(\boldsymbol{x})$ the probability of having N primordial black holes at points $x_1, \ldots, x_N$ given that the local threshold for collapse has a value $\nu(x_1), \ldots, \nu(x_N)$. We denote this probability by $P_N^{\rm local}(x_1, \ldots, x_N)$. By using threshold statistics[12] we write this probability as

$$P_N^{\rm local}(x_1, \ldots, x_N) = \int_{\nu(x_N)}^{\infty} \mathrm{d}\eta_N \cdots \int_{\nu(x_1)}^{\infty} \mathrm{d}\eta_1 P^{(N)}\left(\eta, \Omega_\delta\right)\,. \tag{A.2}$$

Here we introduced the quantity $P^{(N)}(\eta, \Omega_\delta)$, the joint probability density of the δ-field with correlation matrix $\Omega_\delta^{ij} = \omega_\delta(r_{ij})$ if $i \neq j$ and 1 if $i = j$. Here $r_{ij} = |x_i - x_j|$. We also defined the vector $\eta = (\eta_1, \ldots, \eta_N)$, $\eta_i = \delta(x_i)/\sigma_\delta$. The explicit form for $P^{(N)}(\eta, \Omega_\delta)$ is

$$P^{(N)}\left(\eta, \Omega_\delta\right) = \frac{1}{(2\pi)^{N/2}\left(\det \Omega_\delta\right)^{1/2}} \exp\left(-\frac{1}{2}\eta^T \Omega_\delta^{-1} \eta\right)\,. \tag{A.3}$$

The quantity $P_N^{\rm local}(x_1, \ldots, x_N)$ is a conditional probability. To obtain the total probability of finding PBH at the points $x_1, \ldots, x_N$ we need to integrate over the configurations of the secondary field $\psi(x)$. Therefore, we have

$$P_N(x_1, \ldots, x_N) = \int_{-\infty}^{\infty} \mathrm{d}\mu_N \cdots \int_{-\infty}^{\infty} \mathrm{d}\mu_1 P^{(N)}\left(\mu, \Omega_\psi\right) P_N^{\rm local}(x_1, \ldots, x_N)\,, \tag{A.4}$$

where μ and Ω_ψ are analogous to η and Ω_δ for the secondary field ψ. By using the change of variables

$$\tilde{\eta} = \frac{\eta - \alpha\mu}{\sqrt{1+\alpha^2}}\,, \quad \tilde{\nu} = \frac{\alpha\mu}{\sqrt{1+\alpha^2}} \tag{A.5}$$

[12] The main result of this appendix also applies to peak theory.

JCAP11(2020)036

and defining the new covariance matrices $\tilde{\Omega}_\delta = (1+\alpha^2)^{-1}\Omega_\delta$ and $\tilde{\Omega}_\psi = \alpha^2(1+\alpha^2)^{-1}\Omega_\psi$ we can write eq. (A.4) as

$$P_N(x_1,\ldots,x_N) = \int_{-\infty}^{\infty} \frac{\mathrm{d}^N\tilde{\mu}}{\sqrt{(2\pi)^N \det\tilde{\Omega}_\psi}} \int_{\bar{\nu}}^{\infty} \frac{\mathrm{d}^N\tilde{\eta}}{\sqrt{(2\pi)^N \det\tilde{\Omega}_\delta}} e^{-\frac{1}{2}(\tilde{\eta}+\tilde{\mu})^T\tilde{\Omega}_\delta^{-1}(\tilde{\eta}+\tilde{\mu})-\frac{1}{2}\tilde{\mu}^T\tilde{\Omega}_\psi^{-1}\tilde{\mu}} \tag{A.6}$$

where we used the notation $\mathrm{d}^N z = \mathrm{d}z_N\cdots\mathrm{d}z_1$ and we have defined $\bar{\nu} = \nu_g/\sqrt{1+\alpha^2}$. By using the following known result for gaussian integrals

$$\frac{1}{(2\pi)^N}\int_{-\infty}^{\infty}\mathrm{d}^N z e^{-iy^Tz-\frac{1}{2}z^TMz} = \frac{1}{\sqrt{(2\pi)^N\det M}} e^{-\frac{1}{2}y^TM^{-1}y}\,, \tag{A.7}$$

we can write

$$P_N(x_1,\ldots,x_N) = \int_{-\infty}^{\infty}\mathrm{d}^N\tilde{\mu}\int_{\bar{\nu}}^{\infty}\mathrm{d}^N\tilde{\eta}\int_{-\infty}^{\infty}\frac{\mathrm{d}^N\eta'}{(2\pi)^N}\int_{-\infty}^{\infty}\frac{\mathrm{d}^N\mu'}{(2\pi)^N} e^{-i\tilde{\mu}^T\mu'-i(\tilde{\eta}+\tilde{\mu})^T\eta'-\frac{1}{2}\mu'^T\tilde{\Omega}_\psi\mu-\frac{1}{2}\eta'^T\tilde{\Omega}_\delta\eta} \tag{A.8}$$

We can first integrate over $\tilde{\mu}$ giving us a factor of $(2\pi)^N\delta^N(\mu'+\eta')$ allowing us to perform automatically the integral on μ'. Then, we are left with

$$P_N(x_1,\ldots,x_N) = \int_{\bar{\nu}}^{\infty}\mathrm{d}^N\tilde{\eta}\int_{\infty}^{\infty}\frac{\mathrm{d}^N\eta'}{(2\pi)^N} e^{-i\tilde{\eta}^T\eta'-\frac{1}{2}\eta'(\tilde{\Omega}_\delta+\tilde{\Omega}_\psi)\eta}\,. \tag{A.9}$$

By defining

$$\bar{\Omega} \equiv \tilde{\Omega}_\delta + \tilde{\Omega}_\psi = \frac{\Omega_\delta + \alpha^2\Omega_\psi}{1+\alpha^2} \tag{A.10}$$

and using again the identity (A.7) we end up with

$$P_N(x_1,\ldots,x_N) = \int_{\bar{\nu}}^{\infty}\mathrm{d}\tilde{\eta}_N\cdots\int_{\bar{\nu}}^{\infty}\mathrm{d}\tilde{\eta}_1 P^{(N)}\left(\tilde{\eta},\bar{\Omega}\right)\,. \tag{A.11}$$

But this is just the probability of finding N primordial black holes at the points $x_1,\ldots,x_N$ if the overdensity field was a *single* gaussian field with correlation matrix $\bar{\Omega}$ and the threshold for the collapse was $\bar{\nu}$. There exist "closed forms" for the some values of N.

For $P_1(x_1)$ we have

$$P_1(x_1) = \frac{1}{2}\mathrm{erfc}\left(\frac{\bar{\nu}}{\sqrt{2}}\right)\,, \tag{A.12}$$

and for $P_2(x_1,x_2)$ we have [39]

$$P_2(x_1,x_2) = \frac{1}{2}\mathrm{erfc}\left(\frac{\bar{\nu}}{\sqrt{2}}\right) - 2T\left(\bar{\nu},\sqrt{\frac{1-\bar{\omega}(r)}{1+\bar{\omega}(r)}}\right)\,,\quad \bar{\omega}(r) = \frac{\omega_\delta(r)+\alpha^2\omega_\psi(r)}{1+\alpha^2}\,, \tag{A.13}$$

where $r = |x_1-x_2|$ and $T(z,a)$ is the T-Owen function defined as [39]

$$T(z,a) \equiv \frac{1}{2\pi}\int_0^a \mathrm{d}t\frac{e^{-\frac{(1+t^2)z^2}{2}}}{1+t^2}\,. \tag{A.14}$$

For $a=1$, a simpler form can be found [38]

$$T(z,1) = \frac{1}{8}\mathrm{erfc}\left(-\frac{z}{\sqrt{2}}\right)\mathrm{erfc}\left(\frac{z}{\sqrt{2}}\right)\,. \tag{A.15}$$

JCAP11(2020)036

B Nearest neighbours distance distributions

Here we follow the notation and approach of refs. [42, 45, 47]. For a homogeneous distribution, the N-point density is given by

$$\rho_N(x_1, \ldots, x_N) = \rho^N g_N(x_1, \ldots, x_N) \tag{B.1}$$

where $g_N(x_1, \ldots, x_N)$ is the N-point correlation function. For the homogeneous system $\rho_1(x_1) = \rho = \text{constant}$.

We are interested in the following probability

> $Q(x, y)\mathrm{d}x\mathrm{d}y \equiv$ given that there is a PBH at some position (could be the origin), the probability that the nearest PBH lies at a distance between x and $x + \mathrm{d}x$ and the second nearest PBH lies at a distance between y and $y + \mathrm{d}y$.

To compute it, we need to define some quantities.

> $H_n(r)\mathrm{d}r \equiv$ given that there is a PBH at the origin, the probability that the n-th nearest PBH lies at a distance between r and $r + \mathrm{d}r$

for $n \geq 1$. Clearly, from the above definition we have

$$H_2(y) = \int_0^y Q(x, y)\mathrm{d}x \,. \tag{B.2}$$

So, if we manage to express $H_2(y)$ as eq. (B.2) we can obtain an expression for $Q(x, y)$.

We define the following regions:

> $\Omega(r) \equiv$ the volume of a sphere of radius r encompasing the reference PBH.
>
> $s(r)\mathrm{d}r \equiv$ the volume of the spherical shell of a sphere of radius r.

Let us now introduce more quantities

> $E_n(r) \equiv$ given that there is a PBH at some position (the origin), the probability that the region $\Omega(r)$, encompassing the central PBH, contains n additional PBHs.
>
> $\rho s(r) G_n(r)\mathrm{d}r \equiv$ given that there are n PBHs in the region $\Omega(r)$ (in addition to the central PBH), the probability that PBHs are contained in the shell $s(r)\mathrm{d}r$ surrounding the central PBH.

The function $G_n(r)$ is a conditional pair correlation function. Note that if all the correlation function can be expressed as products of the 2-point, then $G_n(r) = g_2(r)$, with $g_2(r)$ the pair correlation function (denoted by $G(r)$ in ref. [17]). By the above definitions, we can write then

$$H_n(r)\mathrm{d}r = \rho s(r) G_{n-1}(r) E_{n-1}(r)\mathrm{d}r \,. \tag{B.3}$$

Moreover, $H_n(r)\mathrm{d}r$ and $E_n(r)$ are related by

$$H_n(r)\mathrm{d}r = -\sum_{i=0}^{n-1} \frac{\partial E_i(r)}{\partial r}\mathrm{d}r \;, \text{ or } \sum_{i=0}^{n-1} E_i(r) = 1 - \int_0^r H_n(r')\mathrm{d}r' \,. \tag{B.4}$$

Let us first find an expression for $H_1(x)$. By using eq. (B.2) we can write eq. (B.3) as

$$-\frac{\partial E_0(x)}{\partial x} = \rho s(x) G_0(x) E_0(x) \implies E_0(x) = \exp\left(-\int_0^x \rho s(x') G_0(x')\mathrm{d}x'\right) . \tag{B.5}$$

The lower bound acually should be $R_{\rm BH}$, but we can set it later. The lower limit is set by imposing the condition that $E(0)$ (or $E(R_{\rm BH})$) is one, since for sure there will be no PBHs (apart from the central one). Then we can write $H_1(x)$ as

$$H_1(x)\mathrm{d}x = \rho s(x) G_0(x) \exp\left(-\int_0^x \rho s(x') G_0(x') \mathrm{d}x'\right) \mathrm{d}x \tag{B.6}$$

This is normalized, no matter the lower bound. Indeed if we consider the variables $X = \int_0^x \rho s(x') G_0(x') \mathrm{d}x'$ then

$$H_1(X)\mathrm{d}X = \exp(-X)\mathrm{d}X\,, \;\; X \in (0,\infty) \tag{B.7}$$

Let us now compute $H_2(y)$ in a similar way. Note that

$$H_2(y) = H_1(y) - \frac{\partial E_1(y)}{\partial y} \tag{B.8}$$

Then we can write eq. (B.3) as

$$\frac{\partial E_1(y)}{\partial y} + \rho s(y) G_1(y) E_1(y) = H_1(y) \tag{B.9}$$

This is a first order ODE for $E_1(y)$ and can be solved by the use of the integrating factor. Consider the integrating factor

$$I(y) = \exp\left(\int_0^y \rho s(z) G_1(z) \mathrm{d}z\right) \tag{B.10}$$

and multiply eq. (B.9) by $I(y)$. Then we can write it as

$$\frac{\partial I(y) E_1(y)}{\partial y} = I(y) H_1(y) \tag{B.11}$$

So

$$E_1(y) = \exp\left(-\int_0^y \rho s(z) G_1(z) \mathrm{d}z\right) \left(\int_0^y H_1(x) \exp\left(\int_0^x \rho s(z) G_1(z) \mathrm{d}z\right) \mathrm{d}x + C\right) \tag{B.12}$$

where C is a constant to be determined. Observe that now we have that $E_1(0) = 0$ (or $E_1(R_{\rm BH}) = 0$) since the probability of having one PBH inside the volume $\Omega(0)$ (or $\Omega(R_{\rm BH})$) is zero. Then we require $C = 0$. Hence we can write eq. (B.3) as

$$H_2(y) = \int_0^y \rho^2 s(x) s(y) G_0(x) G_1(y) \exp\left[-\left(\int_0^x \rho s(z) G_0(z) \mathrm{d}z + \int_x^y \rho s(z) G_1(z) \mathrm{d}z\right)\right] \mathrm{d}x \tag{B.13}$$

where we used eq. (B.6), we put the $\rho s(y) G_1(y) e^{-\int^y \rho s(y) G_1}$ factor inside the x integral and used the fact that $x < y$. Therefore we can write $Q(x,y)$ as

$$Q(x,y) = \rho^2 s(x) s(y) G_0(x) G_1(y) \exp\left[-\left(\int_0^x \rho s(z) G_0(z) \mathrm{d}z + \int_x^y \rho s(z) G_1(z) \mathrm{d}z\right)\right] \Theta(y-x)\,. \tag{B.14}$$

JCAP11(2020)036

G_n will depend on all the N-point correlation functions g_N. Indeed we can write E_n as [42]

$$E_n(r) = \frac{1}{n!}\left[\left(\frac{\partial}{\partial t}\right)^n \left(1 + \sum_{i=1}^{N-1} \frac{t^i}{i!}\rho^i \int g_{i+1}\left(\mathbf{r}_{12}, \ldots, \mathbf{r}_{1i}\right) \prod_{k=2}^{i+1} \Theta\left(r - |\mathbf{r}_{1k}|\right) \mathrm{d}\mathbf{r}_{1k}\right)\right]_{t=-1} , \tag{B.15}$$

where $\mathbf{r}_{1i} = \mathbf{r}_1 - \mathbf{r}_i$. If the separability condition (3.4) holds, then

$$E_0(r) = \exp\left(-\int \rho s(z) g_2(z) \mathrm{d}z\right) , \tag{B.16}$$

$$E_1(r) = \left[\int \rho s(z) g_2(z)\right] \exp\left(-\int \rho s(z) g_2(z) \mathrm{d}z\right) , \tag{B.17}$$

which combined with eqs. (B.5), (B.6) and (B.12) give

$$G_0(r) = G_1(r) = g_2(r) . \tag{B.18}$$

References

[1] LIGO Scientific and Virgo collaboration, *GW*170104*: observation of a* 50*-solar-mass binary black hole coalescence at redshift* 0.2, *Phys. Rev. Lett.* **118** (2017) 221101 [*Erratum ibid.* **121** (2018) 129901] [arXiv:1706.01812] [INSPIRE].

[2] S. Bird et al., *Did LIGO detect dark matter?*, *Phys. Rev. Lett.* **116** (2016) 201301 [arXiv:1603.00464] [INSPIRE].

[3] M. Sasaki, T. Suyama, T. Tanaka and S. Yokoyama, *Primordial black hole scenario for the gravitational-wave event GW*150914, *Phys. Rev. Lett.* **117** (2016) 061101 [*Erratum ibid.* **121** (2018) 059901] [arXiv:1603.08338] [INSPIRE].

[4] S. Clesse and J. García-Bellido, *The clustering of massive primordial black holes as dark matter: measuring their mass distribution with advanced LIGO*, *Phys. Dark Univ.* **15** (2017) 142 [arXiv:1603.05234] [INSPIRE].

[5] M. Raidal, C. Spethmann, V. Vaskonen and H. Veermäe, *Formation and evolution of primordial black hole binaries in the early universe*, *JCAP* **02** (2019) 018 [arXiv:1812.01930] [INSPIRE].

[6] K. Jedamzik, *Primordial black hole dark matter and the LIGO/Virgo observations*, *JCAP* **09** (2020) 022 [arXiv:2006.11172] [INSPIRE].

[7] K. Jedamzik, *Evidence for primordial black hole dark matter from LIGO/Virgo merger rates*, arXiv:2007.03565 [INSPIRE].

[8] T. Nakamura, M. Sasaki, T. Tanaka and K.S. Thorne, *Gravitational waves from coalescing black hole MACHO binaries*, *Astrophys. J. Lett.* **487** (1997) L139 [astro-ph/9708060] [INSPIRE].

[9] Y. Ali-Haïmoud, E.D. Kovetz and M. Kamionkowski, *Merger rate of primordial black-hole binaries*, *Phys. Rev. D* **96** (2017) 123523 [arXiv:1709.06576] [INSPIRE].

[10] A. Katz, J. Kopp, S. Sibiryakov and W. Xue, *Femtolensing by dark matter revisited*, *JCAP* **12** (2018) 005 [arXiv:1807.11495] [INSPIRE].

[11] B. Carr, K. Kohri, Y. Sendouda and J. Yokoyama, *Constraints on primordial black holes*, arXiv:2002.12778 [INSPIRE].

[12] A.M. Green and B.J. Kavanagh, *Primordial black holes as a dark matter candidate*, arXiv:2007.10722 [INSPIRE].

[13] LIGO Scientific and Virgo collaborations, *GW*150914*: implications for the stochastic gravitational wave background from binary black holes*, *Phys. Rev. Lett.* **116** (2016) 131102 [arXiv:1602.03847] [INSPIRE].

JCAP11(2020)036

[14] S. Wang, Y.-F. Wang, Q.-G. Huang and T.G.F. Li, *Constraints on the primordial black hole abundance from the first advanced LIGO observation run using the stochastic gravitational-wave background*, *Phys. Rev. Lett.* **120** (2018) 191102 [arXiv:1610.08725] [INSPIRE].

[15] Y. Ali-Haïmoud, *Correlation function of high-threshold regions and application to the initial small-scale clustering of primordial black holes*, *Phys. Rev. Lett.* **121** (2018) 081304 [arXiv:1805.05912] [INSPIRE].

[16] V. Desjacques and A. Riotto, *Spatial clustering of primordial black holes*, *Phys. Rev. D* **98** (2018) 123533 [arXiv:1806.10414] [INSPIRE].

[17] G. Ballesteros, P.D. Serpico and M. Taoso, *On the merger rate of primordial black holes: effects of nearest neighbours distribution and clustering*, *JCAP* **10** (2018) 043 [arXiv:1807.02084] [INSPIRE].

[18] J.R. Chisholm, *Clustering of primordial black holes: basic results*, *Phys. Rev. D* **73** (2006) 083504 [astro-ph/0509141] [INSPIRE].

[19] K.M. Belotsky et al., *Clusters of primordial black holes*, *Eur. Phys. J. C* **79** (2019) 246 [arXiv:1807.06590] [INSPIRE].

[20] Y. Tada and S. Yokoyama, *Primordial black holes as biased tracers*, *Phys. Rev. D* **91** (2015) 123534 [arXiv:1502.01124] [INSPIRE].

[21] S. Young and C.T. Byrnes, *Signatures of non-Gaussianity in the isocurvature modes of primordial black hole dark matter*, *JCAP* **04** (2015) 034 [arXiv:1503.01505] [INSPIRE].

[22] T. Suyama and S. Yokoyama, *Clustering of primordial black holes with non-Gaussian initial fluctuations*, *PTEP* **2019** (2019) 103E02 [arXiv:1906.04958] [INSPIRE].

[23] S. Young and C.T. Byrnes, *Initial clustering and the primordial black hole merger rate*, *JCAP* **03** (2020) 004 [arXiv:1910.06077] [INSPIRE].

[24] S. Clesse and J. García-Bellido, *Seven hints for primordial black hole dark matter*, *Phys. Dark Univ.* **22** (2018) 137 [arXiv:1711.10458] [INSPIRE].

[25] M. Raidal, V. Vaskonen and H. Veermäe, *Gravitational waves from primordial black hole mergers*, *JCAP* **09** (2017) 037 [arXiv:1707.01480] [INSPIRE].

[26] V. Vaskonen and H. Veermäe, *Lower bound on the primordial black hole merger rate*, *Phys. Rev. D* **101** (2020) 043015 [arXiv:1908.09752] [INSPIRE].

[27] Q. Ding, T. Nakama, J. Silk and Y. Wang, *Detectability of gravitational waves from the coalescence of massive primordial black holes with initial clustering*, *Phys. Rev. D* **100** (2019) 103003 [arXiv:1903.07337] [INSPIRE].

[28] T. Bringmann, P.F. Depta, V. Domcke and K. Schmidt-Hoberg, *Towards closing the window of primordial black holes as dark matter: the case of large clustering*, *Phys. Rev. D* **99** (2019) 063532 [arXiv:1808.05910] [INSPIRE].

[29] Y.N. Eroshenko, *Gravitational waves from primordial black holes collisions in binary systems*, *J. Phys. Conf. Ser.* **1051** (2018) 012010 [arXiv:1604.04932] [INSPIRE].

[30] J. Garriga and N. Triantafyllou, *Enhanced cosmological perturbations and the merger rate of PBH binaries*, *JCAP* **09** (2019) 043 [arXiv:1907.01455] [INSPIRE].

[31] V. De Luca, G. Franciolini, P. Pani and A. Riotto, *Primordial black holes confront LIGO/Virgo data: current situation*, *JCAP* **06** (2020) 044 [arXiv:2005.05641] [INSPIRE].

[32] LIGO Scientific collaboration, *Exploring the sensitivity of next generation gravitational wave detectors*, *Class. Quant. Grav.* **34** (2017) 044001 [arXiv:1607.08697] [INSPIRE].

[33] M. Punturo et al., *The Einstein telescope: a third-generation gravitational wave observatory*, *Class. Quant. Grav.* **27** (2010) 194002 [INSPIRE].

JCAP11(2020)036

[34] E. Komatsu and D.N. Spergel, *Acoustic signatures in the primary microwave background bispectrum*, *Phys. Rev. D* **63** (2001) 063002 [astro-ph/0005036] [INSPIRE].

[35] J.M. Bardeen, J.R. Bond, N. Kaiser and A.S. Szalay, *The statistics of peaks of Gaussian random fields*, *Astrophys. J.* **304** (1986) 15 [INSPIRE].

[36] C. Germani and R.K. Sheth, *Nonlinear statistics of primordial black holes from Gaussian curvature perturbations*, *Phys. Rev. D* **101** (2020) 063520 [arXiv:1912.07072] [INSPIRE].

[37] M. Shibata and M. Sasaki, *Black hole formation in the Friedmann universe: formulation and computation in numerical relativity*, *Phys. Rev. D* **60** (1999) 084002 [gr-qc/9905064] [INSPIRE].

[38] Y.A. Brychkov and N.V. Savischenko, *Some properties of the Owen T-function*, *Integral Transforms Special Funct.* **27** (2015) 163.

[39] D.B. Owen, *Tables for computing bivariate normal probabilities*, *Annals Math. Statist.* **27** (1956) 1075.

[40] N. Kaiser, *On the spatial correlations of Abell clusters*, *Astrophys. J. Lett.* **284** (1984) L9 [INSPIRE].

[41] H. Ruben, *An asymptotic expansion for the multivariate normal distribution and Mills' ratio*, *J. Res. Nat. Bureau Standards B* **68** (1964) 3.

[42] T.M. Truskett, S. Torquato and P.G. Debenedetti, *Density fluctuations in many-body systems*, *Phys. Rev. E* **58** (1998) 7369.

[43] L.G. Jensen and A.S. Szalay, *Density peaks and large scale velocities*, *Acta Phys. Hung.* **62** (1987) 263.

[44] S. Torquato, A. Scardicchio and C.E. Zachary, *Point processes in arbitrary dimension from fermionic gases, random matrix theory, and number theory*, *J. Stat. Mech.* **2008** (2008) P11019 [arXiv:0809.0449].

[45] S. Torquato, B. Lu and J. Rubinstein, *Nearest-neighbor distribution functions in many-body systems*, *Phys. Rev. A* **41** (1990) 2059.

[46] S. Torquato, G. Zhang and F. Stillinger, *Ensemble theory for stealthy hyperuniform disordered ground states*, *Phys. Rev. X* **5** (2015) 021020.

[47] S. Torquato, *Microstructure characterization and bulk properties of disordered two-phase media*, *J. Statist. Phys.* **45** (1986) 843.

[48] P.C. Peters, *Gravitational radiation and the motion of two point masses*, *Phys. Rev.* **136** (1964) B1224 [INSPIRE].

[49] M. Fishbach, D.E. Holz and W.M. Farr, *Does the black hole merger rate evolve with redshift?*, *Astrophys. J. Lett.* **863** (2018) L41 [arXiv:1805.10270] [INSPIRE].

[50] Z.-C. Chen and Q.-G. Huang, *Distinguishing primordial black holes from astrophysical black holes by Einstein telescope and cosmic explorer*, *JCAP* **08** (2020) 039 [arXiv:1904.02396] [INSPIRE].

[51] T. Broadhurst, J.M. Diego and G. Smoot, *Reinterpreting low frequency LIGO/Virgo events as magnified stellar-mass black holes at cosmological distances*, arXiv:1802.05273 [INSPIRE].

[52] J.M. Diego, *Constraining the abundance of primordial black holes with gravitational lensing of gravitational waves at LIGO frequencies*, *Phys. Rev. D* **101** (2020) 123512 [arXiv:1911.05736] [INSPIRE].

[53] P. Ajith et al., *A template bank for gravitational waveforms from coalescing binary black holes. I. Non-spinning binaries*, *Phys. Rev. D* **77** (2008) 104017 [*Erratum ibid.* **79** (2009) 129901] [arXiv:0710.2335] [INSPIRE].

JCAP11(2020)036

[54] P. Ajith et al., *Inspiral-merger-ringdown waveforms for black-hole binaries with non-precessing spins*, *Phys. Rev. Lett.* **106** (2011) 241101 [arXiv:0909.2867] [INSPIRE].

[55] M. Mirbabayi, A. Gruzinov and J. Noreña, *Spin of primordial black holes*, *JCAP* **03** (2020) 017 [arXiv:1901.05963] [INSPIRE].

[56] V. De Luca, V. Desjacques, G. Franciolini, A. Malhotra and A. Riotto, *The initial spin probability distribution of primordial black holes*, *JCAP* **05** (2019) 018 [arXiv:1903.01179] [INSPIRE].

[57] V. De Luca, G. Franciolini, P. Pani and A. Riotto, *The evolution of primordial black holes and their final observable spins*, *JCAP* **04** (2020) 052 [arXiv:2003.02778] [INSPIRE].

[58] S. Wang, T. Terada and K. Kohri, *Prospective constraints on the primordial black hole abundance from the stochastic gravitational-wave backgrounds produced by coalescing events and curvature perturbations*, *Phys. Rev. D* **99** (2019) 103531 [*Erratum ibid.* **101** (2020) 069901] [arXiv:1903.05924] [INSPIRE].

[59] X.-J. Zhu, E. Howell, T. Regimbau, D. Blair and Z.-H. Zhu, *Stochastic gravitational wave background from coalescing binary black holes*, *Astrophys. J.* **739** (2011) 86 [arXiv:1104.3565] [INSPIRE].

[60] PLANCK collaboration, *Planck* 2015 *results. XIII. Cosmological parameters*, *Astron. Astrophys.* **594** (2016) A13 [arXiv:1502.01589] [INSPIRE].

[61] Z.-C. Chen, F. Huang and Q.-G. Huang, *Stochastic gravitational-wave background from binary black holes and binary neutron stars and implications for LISA*, *Astrophys. J.* **871** (2019) 97 [arXiv:1809.10360] [INSPIRE].

[62] M. Safarzadeh, S. Biscoveanu and A. Loeb, *Constraining the delay time distribution of compact binary objects from the stochastic gravitational wave background searches*, *Astrophys. J.* **901** (2020) 137 [arXiv:2004.12999] [INSPIRE].

[63] LIGO SCIENTIFIC and VIRGO collaborations, *Upper limits on the stochastic gravitational-wave background from advanced LIGO's first observing run*, *Phys. Rev. Lett.* **118** (2017) 121101 [*Erratum ibid.* **119** (2017) 029901] [arXiv:1612.02029] [INSPIRE].

[64] A.D. Gow, C.T. Byrnes, A. Hall and J.A. Peacock, *Primordial black hole merger rates: distributions for multiple LIGO observables*, *JCAP* **01** (2020) 031 [arXiv:1911.12685] [INSPIRE].

[65] Y. Ali-Haïmoud and M. Kamionkowski, *Cosmic microwave background limits on accreting primordial black holes*, *Phys. Rev. D* **95** (2017) 043534 [arXiv:1612.05644] [INSPIRE].

[66] V. Poulin, P.D. Serpico, F. Calore, S. Clesse and K. Kohri, *CMB bounds on disk-accreting massive primordial black holes*, *Phys. Rev. D* **96** (2017) 083524 [arXiv:1707.04206] [INSPIRE].

[67] M. Zumalacarregui and U. Seljak, *Limits on stellar-mass compact objects as dark matter from gravitational lensing of type-IA supernovae*, *Phys. Rev. Lett.* **121** (2018) 141101 [arXiv:1712.02240] [INSPIRE].

[68] K. Schutz and A. Liu, *Pulsar timing can constrain primordial black holes in the LIGO mass window*, *Phys. Rev. D* **95** (2017) 023002 [arXiv:1610.04234] [INSPIRE].

[69] T.D. Brandt, *Constraints on MACHO dark matter from compact stellar systems in ultra-faint dwarf galaxies*, *Astrophys. J. Lett.* **824** (2016) L31 [arXiv:1605.03665] [INSPIRE].

[70] J. García-Bellido, *Massive primordial black holes as dark matter and their detection with gravitational waves*, *J. Phys. Conf. Ser.* **840** (2017) 012032 [arXiv:1702.08275] [INSPIRE].

[71] S. Clesse and J. García-Bellido, *GW*190425 *and GW*190814*: two candidate mergers of primordial black holes from the QCD epoch*, arXiv:2007.06481 [INSPIRE].

JCAP11(2020)036

[72] S. Hawking, *Gravitationally collapsed objects of very low mass*, *Mon. Not. Roy. Astron. Soc.* **152** (1971) 75 [INSPIRE].

[73] B.J. Carr and S.W. Hawking, *Black holes in the early universe*, *Mon. Not. Roy. Astron. Soc.* **168** (1974) 399 [INSPIRE].

[74] V. Atal and C. Germani, *The role of non-Gaussianities in primordial black hole formation*, *Phys. Dark Univ.* **24** (2019) 100275 [arXiv:1811.07857] [INSPIRE].

[75] V. Atal, J. Garriga and A. Marcos-Caballero, *Primordial black hole formation with non-Gaussian curvature perturbations*, *JCAP* **09** (2019) 073 [arXiv:1905.13202] [INSPIRE].

[76] J. Garriga, A. Vilenkin and J. Zhang, *Black holes and the multiverse*, *JCAP* **02** (2016) 064 [arXiv:1512.01819] [INSPIRE].

[77] H. Deng, J. Garriga and A. Vilenkin, *Primordial black hole and wormhole formation by domain walls*, *JCAP* **04** (2017) 050 [arXiv:1612.03753] [INSPIRE].

[78] M. Trashorras, J. García-Bellido and S. Nesseris, *The clustering dynamics of primordial black boles in N-body simulations*, arXiv:2006.15018 [INSPIRE].

JCAP11(2020)036

3 *Nanongrav and supermassive PBHs*

Besides being a favorable candidate for DM as well as a possible explanation for a considerable fraction of the *LIGO/VIRGO* merger events (see [113, 155, 68] for a list of cosmological and astrophysical conundra that could be potentially resolved by PBHs), PBHs have been also proposed to form or provide the seeds for the supermassive black holes that have been observed in galactic nuclei at very high shifts, $z \sim 7$ having masses of order $M \sim 10^9$ $M_\odot$ [156, 157]. Currently, there are two main astrophysical pathways that can provide the seed mass of order $10 - 10^5$ $M_\odot$; the intermediate mass *Population III* stars at $z \sim 15 - 20$ that grow by accreting at the *super-Eddington* limit or by hierarchical binary mergers and the direct gravitational collapse of massive gas clouds, $M \sim 10^6$ $M_\odot$ around the same redshifts [158]. These models fail, though, to provide a convincing solution to the mysterious origin of such supermassive black holes. Firstly, the number of quasars that accrete at the *super-Eddington* limit at high z have been constrained by observations [159], while the spatial distribution of black holes originating from the direct collapse of gas clouds seems incompatible with the one of the massive black holes at large redshifts. PBHs, on the other hand, could pose as a viable candidate for these supermassive compact objects in the galactic centers, or act as an intermediate-mass primordial seed that can reach such sizes, $M \gtrsim 10^9$ $M_\odot$ via accretion. The former scenario, where PBHs could form with such high masses, a non-Gaussian distribution of enhanced perturbations needs to be considered in order for the constraints, coming from the CMB temperature anisotropies and spectral distortions, to be evaded [160, 161, 162, 121]. In the latter case, PBHs originating from a Gaussian distribution with masses around $M_{PBH} \lesssim 10^4$ $M_\odot$, could form the seeds

of the supermassive black holes and grow close to 12 e-folds, eventually migrating to the center of galaxies [157, 163].

In this Chapter, I present a model that predicts the existence of a population of stupendounsly massive PBHs, with $M \sim 10^{12}\ \mathrm{M}_{\odot}$, namely a locally non-Gaussian model with a spike feature in the primordial power spectrum that evades the constraints set by the non-detection of CMB spectral distortions by *COBE/FIRAS*. The recently detected signal by NANOGrav, which points towards a stochastic background of gravitational waves, is used in order to constrain the abundance of such a population.

Journal of Cosmology and Astroparticle Physics
An IOP and SISSA journal

NANOGrav signal as mergers of Stupendously Large Primordial Black Holes

Vicente Atal,[a,b] **Albert Sanglas**[a] **and Nikolaos Triantafyllou**[a]

[a]Departament de Física Quàntica i Astrofísica i Institut de Ciències del Cosmos, Universitat de Barcelona,
Martí i Franquès 1, 08028 Barcelona, Spain
[b]Department of Physics, University of the Basque Country, UPV/EHU,
Bilbao, Spain

E-mail: vicente.atal@icc.ub.edu, asanglas@icc.ub.edu, nitriant@icc.ub.edu

Received April 19, 2021
Accepted May 28, 2021
Published June 11, 2021

Abstract. We give an explanation for the signal detected by NANOGrav as the stochastic gravitational wave background from binary mergers of primordial "Stupendously Large Black Holes"(SLABs) of mass $M \sim (10^{11} - 10^{12})M_\odot$, and corresponding to roughly 0.1% of the dark matter. We show that the stringent bounds coming from μ distortions of the CMB can be surpassed if the perturbations resulting in these BHs arise from the non-Gaussian distribution of fluctuations expected in single field models of inflation generating a spike in the power spectrum. While the tail of the stochastic background coming from binaries with $M \lesssim 10^{11}M_\odot$ could both fit NANOGrav and respect μ distortions limits, they become excluded from large scale structure constraints.

Keywords: gravitational waves / theory, primordial black holes, non-gaussianity

ArXiv ePrint: 2012.14721

https://doi.org/10.1088/1475-7516/2021/06/022

JCAP06(2021)022

Contents

JCAP06(2021)022

1 Introduction

The NANOGrav collaboration has recently reported evidence for a signal consistent with a gravitational wave background of frequency $\nu \in (2.5\times10^{-9},\, 1.2\times10^{-8})$ Hz and amplitude at 1-σ confidence level $\Omega_{\rm GW} \in (3\times10^{-10},\, 2\times10^{-9})$. If the signal is modelled as $\Omega_{\rm GW} \propto (\nu/\nu_\star)^\xi$, the tilt $\xi \in (-1.5,\, 0.5)$ at $\nu_\star = 5.5$ nHZ and at 1-σ confidence level [1].

The nature of the signal has still to be confirmed with further observations and analysis (e.g. whether it is really a gravitational wave (GW) and whether it is of stochastic origin or not), but since a potential GW detection might have tremendous consequences for our understanding of the Universe, it is important to investigate the potential implications of such discovery. A suggestion of particular interest entails the signal being related to a population of primordial black holes (PBHs) [2], which might be an important constituent of our Universe (for recent reviews, see e.g [3, 4]). In this line, several possible interpretations of the NANOGrav signal being the gravitational background induced by large scalar perturbations responsible for PBH formation has been proposed [5–12].[1] In these works it has been shown that the signal could be accommodated by a population of sublunar, solar, or slightly supersolar PBHs.

A quite different possibility, although historically one of the first to be conceived for explaining a signal at such frequencies [16], is that it corresponds to the stochastic background resulting from the past mergers of large black holes, with masses $M > 10^6 M_\odot$. This possibility was studied in [1, 18] where the distributions of the binaries was inspired from astrophysical models.

Here we show that BH-inspirals accounting for NANOGrav could be of primordial origin. For this to happen, their mass should be $\sim 10^{11} - 10^{12} M_\odot$, and so they enter in the class of so-called "Stupendously Large Black Holes" (SLABs) [19]. Their abundance with respect to dark matter, $f \equiv \Omega_{\rm PBH}/\Omega_{\rm DM}$, should be at the $\mathcal{O}(0.1\%)$ level in order to explain the observed amplitude.

While primordial SLABs are heavily constrained by spectral distortions, we will show that a proper account of the non-Gaussianities (NG) arising in single-field inflation models leading to PBH production can easily relax these constraints. For these abundances, the lower limit on the mass, $M > 10^{11} M_\odot$, is obtained from dynamical constraints of large scale structure (LSS) (for a recent review on this topic, see [19]).

[1] For general considerations on the link between PBHs and the stochastic background from binary mergers, see e.g. [13–15].

2 Mergers of SuperMassive Black Holes and their Stochastic Gravitational Wave Signal

The energy released by BH binaries contribute to a stochastic background of gravitational waves, whose energy density $\Omega_{\rm GW}$ is given by (we use $c = G = 1$) [17, 20]

$$\begin{aligned}\Omega_{\rm GW} &\equiv \frac{1}{\rho_c}\frac{d\rho_{\rm GW}}{d\log\nu} \\ &= \frac{\nu}{\rho_c H_0}\int_0^{z_*}\frac{R_{\rm BH}(z)}{(1+z)E(z)}\frac{dE_{\rm GW}}{d\nu_s}(\nu_s)dz\end{aligned} \tag{2.1}$$

where $\rho_{\rm GW}$ is the energy density at a given frequency ν, ρ_c is the critical density, $\mathrm{d}E_{\rm GW}/\mathrm{d}\nu_s$ is the GW energy spectrum of the merger, $R_{\rm BH}$ is their merger rate at redshift z and ν_s is the frequency in the source frame, related to the observed frequency as $\nu_s = (1+z)\nu$. The function $E(z) \equiv H(z)/H_0 = [\Omega_r(1+z)^4 + \Omega_m(1+z)^3 + \Omega_\Lambda]^{1/2}$, and the GW energy spectrum of the merger is [21]

$$\frac{dE_{\rm GW}}{d\nu_s}(\nu_s) = \frac{\pi^{\frac{2}{3}}M_c^{\frac{5}{3}}}{3}\begin{cases}\nu_s^{-1/3} & \nu_s < \nu_1 \\ \omega_1\nu_s^{2/3} & \nu_1 \le \nu_s < \nu_2 \\ \frac{\omega_2\sigma^4\nu_s^2}{\left(\sigma^2+4(\nu_s-\nu_2)^2\right)^2} & \nu_2 \le \nu_s < \nu_3 \\ 0 & \nu_3 \le \nu_s\end{cases} \tag{2.2}$$

where $\nu_i \equiv (\nu_1, \nu_2, \sigma, \nu_3) = (a_i\eta^2 + b_i\eta + c_i)/(\pi M_t)$, $M_t = m_1 + m_2$ is the total mass of binary system, M_c is the chirp mass ($M_c^{5/3} = m_1 m_2 M_t^{-1/3}$), and $\eta = m_1 m_2 M_t^{-2}$ is the symmetric mass ratio. The parameters a_i, b_i and c_i can be found in [21], and (ω_1, ω_2) are chosen such that the spectrum is continuous. Note that eq. (2.2) describes all the stages of the merger. All these stages are relevant for describing the peak and decay of the stochastic background, which will be important for the fits that we present in the following section.[2] In the following we use a monochromatic population for the PBH binaries.

The merger rate $R_{\rm BH}(z)$ depends on the formation channel of the binary system. If these are formed from primordial fluctuations, then it will further depend on the their initial distribution, which might be Poissonian (if perturbations are Gaussian [22–24]), or clustered (if departures from Gaussianities are large [25–30]).

While we will deal with non-Gaussian primordial fluctuations, the effect on their merger rate is going to be negligible since in the minimal model of inflation that we will consider here there is no large variance at large scales that can source a spatial modulation in the number density of PBHs. We consider thus a merger rate as coming from a Poissonian distribution of PBHs and a monochromatic mass function ($M \equiv m_1 = m_2$), that is [31][3]

$$R_{\rm BH}(t) = 8\pi^2\bar{n}^3\int_{x_{\rm min}}^{x_{\rm max}} x^2 y^2 \left|\frac{\mathrm{d}y}{\mathrm{d}t}(t,x)\right| dx\,, \tag{2.3}$$

[2] On the other hand, if we are interested in describing only the IR tail of the stochastic background, it is enough to consider the circular inspiraling phase described by frequencies $\nu < \nu_1$, as done e.g. in [18].

[3] In eq. (2.3) we have neglected an exponential factor that is irrelevant in this case but can be very important when large scale correlations are present [30].

JCAP06(2021)022

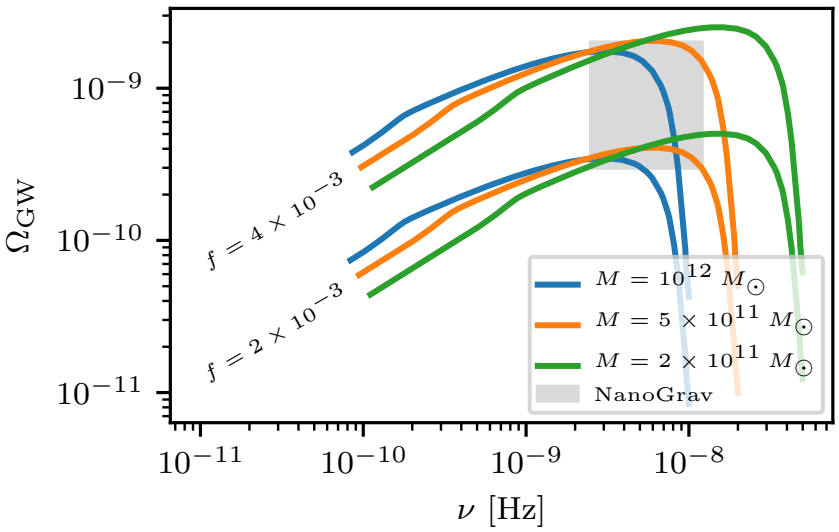

Figure 1. The stochastic background of binary mergers. In grey we show the 1-σ region consistent with NANOGrav signal.

where $\bar{n}$ is the comoving number density of BHs, $y = x\,(x/x_{\rm min})^{\frac{16}{21}}$, where $x_{\rm min}$ and $x_{\rm max}$ are the minimum and maximum distances of the binaries such that they merge at time t [32],

$$x_{\rm max} \simeq \left(\frac{M_t}{\rho_{eq}}\right)^{\frac{1}{3}} \quad \text{and} \quad x_{\rm min} = \left(\frac{85\,\eta\,M_t^3\,t}{3\,x_{\rm max}^4}\right)^{\frac{1}{16}} x_{\rm max}\,, \tag{2.4}$$

with ρ_{eq} the background energy density at matter-radiation equality.[4] In figure 1 we show how the NANOGrav signal can be fitted with the stochastic GW signal given by eq. (2.1). It can be attributed to the peak of the signal if PBHs are of masses $M \sim (5\times10^{11} - 10^{12})M_\odot$ and make a fraction $f \sim (2-4)\times10^{-3}$ of the total DM. The infrared tail of the stochastic background has a spectral index $\xi = 2/3$, and is thus within the 2-σ interval determined by observations. Thus BHs of $M < 5\times10^{11}M_\odot$ and $f > 2\times10^{-3}$ could also provide a good fit. However, as we will see in the next section, these become in conflict with LSS constraints. In figure 1 we show the smallest mass that provides a fit to NANOGrav that is not in tension with LSS constraints. The combination of both constraints imply $M \sim (2\times10^{11} - 10^{12})M_\odot$ and $f \sim (2-4)\times10^{-3}$.

While such large BHs have yet to be observed in nature (the largest reported BH has a mass $7\times10^{10}M_\odot$ [35]), the presence of more massive BHs is not ruled out.[5] In the following we discuss limits on the fraction of PBHs of this range of masses, most notably the spectral distortion and large scale structure bounds.

[4] Recently BHs described by the so-called Thakurta metric have been studied [33]. In that description, and due to a constant energy flow towards the BHs, their masses are time dependent, which alters their merger rate. Since in the cosmological setup that we are interested there is no fluid sustaining this mass grow, these BHs are not the ones that we are interested in (see also [34]).

[5] For astrophysical considerations on their presence, see [36].

JCAP06(2021)022

3 Spectral distortions, non-Gaussianities and LSS

Spectral distortions provide the most stringent bound for the presence of PBHs in the mass range $M = (10^4 - 10^{12})M_\odot$. The large fluctuations necessary for the production of PBHs dissipate through Silk damping and might leave a large imprint in the CMB as departures from a black-body spectrum.[6] In particular, these primordial inhomogeneities are constrained by a non-detection of μ distortions, which from COBE/FIRAS is bounded to be smaller than 9×10^{-5} [39].

The amplitude of the μ distortions depends on both the scale and the variance of the power spectrum of the scalar perturbations [40]. Both of these are related to the abundance of PBHs, and so constraints on μ distortions can be used to constraint the presence of PBHs. From here it has been deduced that PBHs in the mass range $(6 \times 10^4 - 5 \times 10^{13})M_\odot$ are excluded [41] (for earlier application of this idea, see [42, 43]).

These constraints can be relaxed if NG are considered [44, 45]. The abundance of PBH is most sensitive to the ratio $\nu \equiv \zeta_c/\sigma$, and NG might change both σ, the variance of the perturbations, and ζ_c, the critical threshold for collapse. In general the role that NG plays in determining the threshold for collapse has been neglected, and only the effect coming from changes in the PDF has been considered [12, 44, 45]. However, the threshold for collapse depends on the shape of the overdensity [46–52], and non-Gaussianities modify its shape [53–56].

For example, if we consider local models of NG, for which the curvature perturbations ζ are related to a Gaussian variable ζ_G with a local function $\zeta = F(\zeta_G)$, the profile of an overdensity is simply $F(\zeta_G(r))$, where $\zeta_G(r)$ is its shape as given by a Gaussian random field [57]. Then the treshold for collapse can be simply determined numerically (with public codes [51]) and/or analytically [52].

Note that since local models of NG can be written in terms of an underlying Gaussian field, it is not necessary to find how the PDF changes by the local transformation for computing the abundances. It is actually sufficient to count the regions for which the image of the underlying Gaussian field is above the threshold of collapse. That is, if ζ^c_{NG} is the critical value for collapse of the NG profile, we can define its counterpart in the underlying Gaussian field, μ_c, given by $\mu_c \equiv F^{-1}(\zeta^c_{NG})$. Then, if the PBH abundance for a Gaussian field is $\beta_G \sim e^{-\left(\zeta^c_G\right)^2/\sigma^2_G}$ with ζ^c_G the treshold for the Gaussian field, then the abundance of PBHs in the local NG theory is simply given by $\beta_{NG} \sim e^{-\mu_c^2/\sigma^2_G}$.

It is thus fortunate that in the case of single-field inflationary models producing a spike in the power spectrum (necessary for a controled production of PBHs), the NGs are of the local type. Its precise shape and amplitude were established in [53], and are given by

$$\zeta = -\mu_* \log\left(1 - \frac{\zeta_g}{\mu_*}\right) \tag{3.1}$$

where μ_* is related to the curvature of the local maxima that the inflaton field traverses, as [53, 58]

$$\mu_* = -3 + \sqrt{9 - \eta_V|_{\max}} \tag{3.2}$$

where $\eta_V \equiv V''/V$, with $V(\phi)$ the inflaton potential, and where $'$ denotes derivatives with respect to inflaton field ϕ. The parameter η_V in eq. (3.2) is to be evaluated at the local maxima of the potential. As the field overcomes the local maxima it enters a stage of

[6] A natural exception are models in which the PBHs are not associated to an enhancement of the power spectrum (like [37, 38]). These models are thus essentially unconstrained by spectral distortions measurements.

JCAP06(2021)022

constant-roll, perturbations are largely amplified and the abundance of PBHs increases. The local transformation eq. (3.1) is a non-perturative completion of the well known perturbative version $F(\zeta_G) = \zeta_G + (3/5) f_{\rm NL} \zeta_{\rm G}^2$ [56]. Thus, we can relate the parameter μ_* to $f_{\rm NL}$, as

$$\mu_* = \frac{5}{6 f_{\rm NL}} \ . \tag{3.3}$$

The local transformation eq. (3.1) induces a change in the shape of the overdensity field with respect to a Gaussian field. In [56] it was determined how the threshold for collapse changes as the parameter μ_* (or equivalently $f_{\rm NL}$) varies. For a peaked power spectrum growing as k^4, as expected in single-field inflationary models [59], we find[7]

$$\mu_{\rm c} = \begin{cases} 0.663 - 0.183 f_{\rm NL} + 0.0169 f_{\rm NL}^2 & f_{\rm NL} < 5 \\ 5/(6 f_{\rm NL}) & f_{\rm NL} > 5 \end{cases} \tag{3.4}$$

Thus, as the amplitude of the NG is increased (which in terms of the potential means that the hill that the inflaton must traverse is more and more spiky), the threshold for collapse diminishes. Note that in the non-perturbative template described here the change in the threshold is more important than in its perturbative version $F(\zeta_G) = \zeta_G + (3/5) f_{\rm NL} \zeta_{\rm G}^2$ [56]. Also, since the threshold is found here in terms of ζ, we avoid complications related to additional NGs from the non-linear relation between curvature and density perturbation.

For determining the spectral distortions it is necessary to calculate the variance of the non-Gaussian field.[8] This is given by

$$\sigma^2 = \frac{1}{\sqrt{2\pi\sigma_0^2}} \int_{-\infty}^{\mu_*} \log\left(1 - \frac{\zeta_g}{\mu_*}\right)^2 e^{-\frac{\zeta_g^2}{2\sigma_0^2}} d\zeta_g - \langle\zeta\rangle^2 \ . \tag{3.5}$$

The amplitude of the μ distortion is related to the amplitude and scale of a perturbation as [40]

$$\mu \simeq 2.2\sigma^2 \left[\exp\left(-\frac{k_\star}{5400}\right) - \exp\left(-\left(\frac{k_\star}{31.6}\right)^2\right)\right] \ . \tag{3.6}$$

Here the wavenumber $k_\star$ is in $M_{\rm pc}^{-1}$. Assuming a monochromatic mass function -a good approximation for peaked power spectra- $k_\star$ is related to the mass of the PBH as [60]

$$k_\star \simeq 7.5 \times 10^5 \gamma^{\frac{1}{2}} \left(\frac{g}{10.75}\right)^{-\frac{1}{12}} \left(\frac{M}{30 M_\odot}\right)^{-\frac{1}{2}} \ . \tag{3.7}$$

Here γ is the ratio between the mass of the BH and the mass enclosed within the horizon $H = a k^{-1}$, and g is the number of relativistic species (we fix $g = 10.75$). For simplicity we take $\gamma = 1$, knowing that we expect some departures from unity from the fact that the BH collapse is a critical phenomena [61], and because the size of the overdensity undergoing the collapse is typically some factors larger than $a k^{-1}$ [48, 49].

The fraction of PBH to DM, f, is related to their primordial abundance as [60]

$$\beta \simeq 10^{-8} \gamma^{-\frac{1}{2}} \left(\frac{g}{10.75}\right)^{\frac{1}{4}} \left(\frac{\Omega_{\rm DM}}{0.27}\right)^{-1} \left(\frac{M}{30 M_\odot}\right)^{\frac{1}{2}} f \ . \tag{3.8}$$

[7] Actually there are no large differences at the level of the threshold if we had considered a power spectrum given by a δ function. For details, see [56].

[8] This turns out to be very close to the Gaussian variance, since the logarithm in eq. (3.1) only affects profiles close to μ_*, which are very rare with respect to the typical profiles of ζ.

JCAP06(2021)022

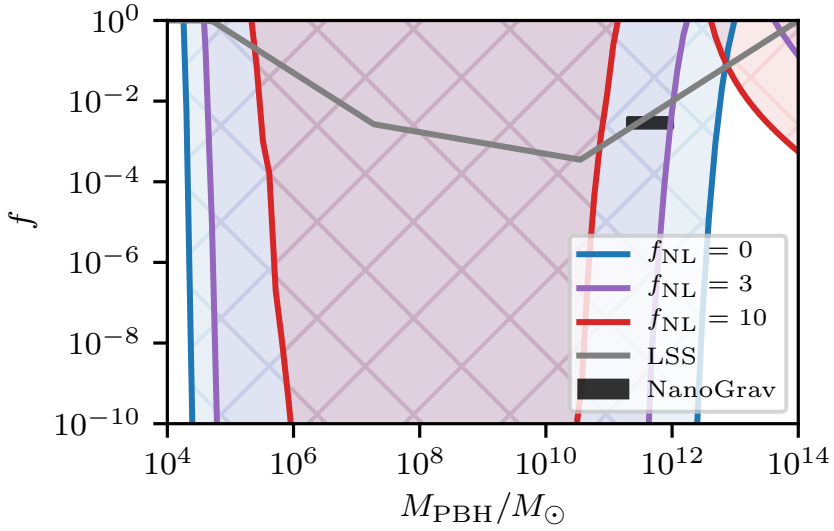

Figure 2. Limits on the abundance of PBHs coming from the non observations of μ distortions in the CMB and from large scale structure considerations. We can see that for $f_{\rm NL} \gtrsim 3$, PBHs with the mass and abundance appropiate to fit NANOGrav are not constrained by μ distortions. However, for these abundances, the formation of clusters imposes $M > 2 \times 10^{11} M_\odot$. The region in black corresponds to the fits shown in figure 1.

The abundance can be calculated using the standard peak theory [57], since we mention previously that we can always refer to the underlying Gaussian field.[9] For the case of a monochromatic power spectrum, it is simply given by [48, 49]

$$\beta \simeq \frac{\mu_c^3}{\sigma_0^4} \exp\left(-\frac{\mu_c^2}{2\sigma_0^2}\right) . \tag{3.9}$$

Here μ_c is the threshold of the underlying Gaussian field, and σ_0 its variance. In figure 2 we show the constrains from the FIRAS limit on μ, and how they vary with increasing non-Gaussianity parameter $f_{\rm NL}$. For $f_{\rm NL} > 3$ these constraints can be avoided. Interestingly, $f_{\rm NL} > 3$ sets the limit above which most PBHs are baby Universes, resulting from trapped regions in the false vacuum of the potential [56]. Let us note that by considering a power spectrum growing as k^4, we should also worry about the constraints at scales larger than the peak of the power spectrum, since those are also constrained by the bounds on μ distortion. In this respect, we should note that by virtue of a duality between the background before and after the peak in the power spectrum, the amplitude of the non-Gaussianity remains constant during the transition [58, 63]. Thus, the most critical test concerning μ distortions is at the scale of the peak, $k_\star$, irrespective of the steepness of the power spectrum. Note also that in similar inflationary scenarios than the one we describe here, there might be an additional source of μ distortions, coming from shock waves of an expanding bubble of false vacuum in the thermalized fluid [64]. In our case, when the BH corresponds to regions in the false vacuum ($f_{\rm NL} > 3$), the energy of the false vacuum is larger than the background energy

[9] It has been shown that computing the abundances using the compaction function gives a similar result for peaked power spectra [62].

JCAP06(2021)022

density and so the bubble does not expand from the point of view of an outside observer and thus there are no such shock waves.

Limits from μ distortions are not the only ones constraining PBHs of these masses. The effects of gas accretion in the thermal history of the Universe might also be important. For this range of masses, their effect was studied in [65]. In the simplified model considered there, for an efficiency $\epsilon < 0.03$, $f \sim 10^{-3}$ is allowed. We note that these constraints should be updated considering more recent studies, that however mostly focused in $M < 10^4 M_\odot$ (see e.g. [66, 67]).

We can also consider dynamical constraints. Massive PBHs could destroy galaxies in clusters [68] and/or trigger an undesirably early formation of cosmic structure [69]. In figure 2 we show the limits coming from the formation of dwarf galaxies up to clusters of galaxies. For example, in the mass range $M \sim (3 \times 10^{10} - 10^{14}) M_\odot$, the strongest limit comes from the formation of clusters of galaxies, and reads [69]

$$f < \frac{M}{10^{14} M_\odot} \quad \text{for} \quad 3 \times 10^{10} M_\odot < M < 10^{14} M_\odot \, . \tag{3.10}$$

These constraints are fully consistent with fitting NANOGrav with the peak of the stochastic background, but put limits on the fits coming from its tail, fixing $M > 2 \times 10^{11} M_\odot$. All in all, these constraints imply that the NANOGrav signal can be explained if $M \sim (2 \times 10^{11} - 10^{12}) M_\odot$, $f \sim (2 - 4) \times 10^{-3}$ and $f_{\rm NL} > 3$. Note that for these parameters the signal is no longer well described by a power law in the relevant range of frequencies, and thus motivates an extension of the templates used in [1, 18] to assess the significance of the fits. We also expect some spectral differences in the stochastic background coming from binaries of astrophysical versus primordial origin due to their different merger history. As shown in [71] for the specific case of larger frequencies, these differences might be disentangled with future experiments like SKA for the nHz range.

4 Conclusions

We have provided an explanation of the NANOGrav signal as coming from the binary mergers of Stupendously Large Black Holes, of masses in the range $M \sim (2 \times 10^{11} - 10^{12}) M_\odot$. For a mild non-Gaussianity resulting from the dynamics of single field inflation, the spectral distortions constraints can be avoided. For the abundance needed to explain NANOGrav, $f \sim 10^{-3}$, the dynamical constraints fix their mass to be $M > 2 \times 10^{11} M_\odot$.

These results provide yet another motivation for studying the presence of SLABs, and illustrate the importance of non-Gaussianities and their connection to the formation mechanism of PBHs for determining bounds on their presence.

Finally, we should indicate that in this work we have neglected the mass evolution of the PBHs. Since most of the signal from the stochastic background comes from late mergers, the mass evolution could be important (see e.g. [70]). Then it would be necessary to invoke PBHs of smaller masses for having a late time signal at the frequencies of NANOGrav. While large values of $f_{\rm NL}$ can easily be obtained to surpass the μ distortion limits [53], bounds on LSS are more difficult to overcome. Considering that at the moment bounds from LSS and gas accretion are only order of magnitude constraints for such masses, a deeper examination of them should be pursued for a more robust model selection.

JCAP06(2021)022

Acknowledgments

We thank Jaume Garriga for comments on the manuscript. This work has been partially supported by FPA2016-76005-C2-2-P, MDM-2014-0369 of ICCUB (Unidad de Excelencia Maria de Maeztu), and AGAUR2017SGR-754 (V.A), by an APIF grant from Universitat de Barcelona (A.S), and by an INPhINIT grant from laCaixa Foundation (ID 100010434) code LCF/BQ/IN17/11620034 (N.T). This project has also received funding from the European Unions Horizon 2020 research and innovation programme under the Marie Sklodowska-Curie grant agreement No. 713673.

References

[1] NANOGrav collaboration, *The NANOGrav 12.5 yr data set: search for an isotropic stochastic gravitational-wave background*, *Astrophys. J. Lett.* **905** (2020) L34 [arXiv:2009.04496] [INSPIRE].

[2] S. Hawking, *Gravitationally collapsed objects of very low mass*, *Mon. Not. Roy. Astron. Soc.* **152** (1971) 75 [INSPIRE].

[3] M. Sasaki, T. Suyama, T. Tanaka and S. Yokoyama, *Primordial black holes — perspectives in gravitational wave astronomy*, *Class. Quant. Grav.* **35** (2018) 063001 [arXiv:1801.05235] [INSPIRE].

[4] A.M. Green and B.J. Kavanagh, *Primordial black holes as a dark matter candidate*, *J. Phys. G* **48** (2021) 4 [arXiv:2007.10722] [INSPIRE].

[5] V. Vaskonen and H. Veermäe, *Did NANOGrav see a signal from primordial black hole formation?*, *Phys. Rev. Lett.* **126** (2021) 051303 [arXiv:2009.07832] [INSPIRE].

[6] V. De Luca, G. Franciolini and A. Riotto, *NANOGrav data hints at primordial black holes as dark matter*, *Phys. Rev. Lett.* **126** (2021) 041303 [arXiv:2009.08268] [INSPIRE].

[7] K. Kohri and T. Terada, *Solar-mass primordial black holes explain NANOGrav hint of gravitational waves*, *Phys. Lett. B* **813** (2021) 136040 [arXiv:2009.11853] [INSPIRE].

[8] L. Bian, R.-G. Cai, J. Liu, X.-Y. Yang and R. Zhou, *Evidence for different gravitational-wave sources in the NANOGrav dataset*, *Phys. Rev. D* **103** (2021) L081301 [arXiv:2009.13893] [INSPIRE].

[9] S. Sugiyama, V. Takhistov, E. Vitagliano, A. Kusenko, M. Sasaki and M. Takada, *Testing stochastic gravitational wave signals from primordial black holes with optical telescopes*, *Phys. Lett. B* **814** (2021) 136097 [arXiv:2010.02189] [INSPIRE].

[10] G. Domènech and S. Pi, *NANOGrav hints on planet-mass primordial black holes*, arXiv:2010.03976 [INSPIRE].

[11] S. Bhattacharya, S. Mohanty and P. Parashari, *Implications of the NANOGrav result on primordial gravitational waves in nonstandard cosmologies*, *Phys. Rev. D* **103** (2021) 063532 [arXiv:2010.05071] [INSPIRE].

[12] K. Inomata, M. Kawasaki, K. Mukaida and T.T. Yanagida, *NANOGrav results and LIGO-Virgo primordial black holes in axionlike curvaton models*, *Phys. Rev. Lett.* **126** (2021) 131301 [arXiv:2011.01270] [INSPIRE].

[13] M. Raidal, V. Vaskonen and H. Veermäe, *Gravitational waves from primordial black hole mergers*, *JCAP* **09** (2017) 037 [arXiv:1707.01480] [INSPIRE].

[14] S. Wang, Y.-F. Wang, Q.-G. Huang and T.G.F. Li, *Constraints on the primordial black hole abundance from the first advanced LIGO observation run using the stochastic gravitational-wave background*, *Phys. Rev. Lett.* **120** (2018) 191102 [arXiv:1610.08725] [INSPIRE].

JCAP06(2021)022

[15] V. Mandic, S. Bird and I. Cholis, *Stochastic gravitational-wave background due to primordial binary black hole mergers*, *Phys. Rev. Lett.* **117** (2016) 201102 [arXiv:1608.06699] [INSPIRE].

[16] M. Rajagopal and R.W. Romani, *Ultralow frequency gravitational radiation from massive black hole binaries*, *Astrophys. J.* **446** (1995) 543 [astro-ph/9412038] [INSPIRE].

[17] E.S. Phinney, *A practical theorem on gravitational wave backgrounds*, astro-ph/0108028 [INSPIRE].

[18] H. Middleton, A. Sesana, S. Chen, A. Vecchio, W. Del Pozzo and P.A. Rosado, *Massive black hole binary systems and the NANOGrav* 12.5 *yr results*, *Mon. Not. Roy. Astron. Soc.* **502** (2021) L99 [arXiv:2011.01246] [INSPIRE].

[19] B. Carr, F. Kuhnel and L. Visinelli, *Constraints on stupendously large black holes*, *Mon. Not. Roy. Astron. Soc.* **501** (2021) 2029 [arXiv:2008.08077] [INSPIRE].

[20] T. Regimbau, *The astrophysical gravitational wave stochastic background*, *Res. Astron. Astrophys.* **11** (2011) 369 [arXiv:1101.2762] [INSPIRE].

[21] P. Ajith et al., *A template bank for gravitational waveforms from coalescing binary black holes. I. Non-spinning binaries*, *Phys. Rev. D* **77** (2008) 104017 [*Erratum ibid.* **79** (2009) 129901] [arXiv:0710.2335] [INSPIRE].

[22] Y. Ali-Haïmoud, *Correlation function of high-threshold regions and application to the initial small-scale clustering of primordial black holes*, *Phys. Rev. Lett.* **121** (2018) 081304 [arXiv:1805.05912] [INSPIRE].

[23] V. Desjacques and A. Riotto, *Spatial clustering of primordial black holes*, *Phys. Rev. D* **98** (2018) 123533 [arXiv:1806.10414] [INSPIRE].

[24] G. Ballesteros, P.D. Serpico and M. Taoso, *On the merger rate of primordial black holes: effects of nearest neighbours distribution and clustering*, *JCAP* **10** (2018) 043 [arXiv:1807.02084] [INSPIRE].

[25] Y. Tada and S. Yokoyama, *Primordial black holes as biased tracers*, *Phys. Rev. D* **91** (2015) 123534 [arXiv:1502.01124] [INSPIRE].

[26] S. Young and C.T. Byrnes, *Signatures of non-Gaussianity in the isocurvature modes of primordial black hole dark matter*, *JCAP* **04** (2015) 034 [arXiv:1503.01505] [INSPIRE].

[27] K.M. Belotsky et al., *Clusters of primordial black holes*, *Eur. Phys. J. C* **79** (2019) 246 [arXiv:1807.06590] [INSPIRE].

[28] T. Suyama and S. Yokoyama, *Clustering of primordial black holes with non-Gaussian initial fluctuations*, *PTEP* **2019** (2019) 103E02 [arXiv:1906.04958] [INSPIRE].

[29] S. Young and C.T. Byrnes, *Initial clustering and the primordial black hole merger rate*, *JCAP* **03** (2020) 004 [arXiv:1910.06077] [INSPIRE].

[30] V. Atal, A. Sanglas and N. Triantafyllou, *LIGO/Virgo black holes and dark matter: the effect of spatial clustering*, *JCAP* **11** (2020) 036 [arXiv:2007.07212] [INSPIRE].

[31] T. Nakamura, M. Sasaki, T. Tanaka and K.S. Thorne, *Gravitational waves from coalescing black hole MACHO binaries*, *Astrophys. J. Lett.* **487** (1997) L139 [astro-ph/9708060] [INSPIRE].

[32] P.C. Peters, *Gravitational radiation and the motion of two point masses*, *Phys. Rev.* **136** (1964) B1224 [INSPIRE].

[33] C. Boehm, A. Kobakhidze, C.A.J. O'hare, Z.S.C. Picker and M. Sakellariadou, *Eliminating the LIGO bounds on primordial black hole dark matter*, *JCAP* **03** (2021) 078 [arXiv:2008.10743] [INSPIRE].

[34] V. De Luca, V. Desjacques, G. Franciolini and A. Riotto, *The clustering evolution of primordial black holes*, *JCAP* **11** (2020) 028 [arXiv:2009.04731] [INSPIRE].

JCAP06(2021)022

[35] O. Shemmer et al., *Near infrared spectroscopy of high redshift active galactic nuclei. 1. A metallicity-accretion rate relationship*, *Astrophys. J.* **614** (2004) 547 [astro-ph/0406559] [INSPIRE].

[36] P. Natarajan and E. Treister, *Is there an upper limit to black hole masses?*, *Mon. Not. Roy. Astron. Soc.* **393** (2009) 838 [arXiv:0808.2813] [INSPIRE].

[37] J. Garriga, A. Vilenkin and J. Zhang, *Black holes and the multiverse*, *JCAP* **02** (2016) 064 [arXiv:1512.01819] [INSPIRE].

[38] H. Deng, J. Garriga and A. Vilenkin, *Primordial black hole and wormhole formation by domain walls*, *JCAP* **04** (2017) 050 [arXiv:1612.03753] [INSPIRE].

[39] D.J. Fixsen, E.S. Cheng, J.M. Gales, J.C. Mather, R.A. Shafer and E.L. Wright, *The Cosmic Microwave Background spectrum from the full COBE FIRAS data set*, *Astrophys. J.* **473** (1996) 576 [astro-ph/9605054] [INSPIRE].

[40] J. Chluba, A.L. Erickcek and I. Ben-Dayan, *Probing the inflaton: small-scale power spectrum constraints from measurements of the CMB energy spectrum*, *Astrophys. J.* **758** (2012) 76 [arXiv:1203.2681] [INSPIRE].

[41] K. Kohri, T. Nakama and T. Suyama, *Testing scenarios of primordial black holes being the seeds of supermassive black holes by ultracompact minihalos and CMB μ-distortions*, *Phys. Rev. D* **90** (2014) 083514 [arXiv:1405.5999] [INSPIRE].

[42] B.J. Carr and J.E. Lidsey, *Primordial black holes and generalized constraints on chaotic inflation*, *Phys. Rev. D* **48** (1993) 543 [INSPIRE].

[43] B.J. Carr, J.H. Gilbert and J.E. Lidsey, *Black hole relics and inflation: limits on blue perturbation spectra*, *Phys. Rev. D* **50** (1994) 4853 [astro-ph/9405027] [INSPIRE].

[44] T. Nakama, B. Carr and J. Silk, *Limits on primordial black holes from μ distortions in Cosmic Microwave Background*, *Phys. Rev. D* **97** (2018) 043525 [arXiv:1710.06945] [INSPIRE].

[45] C. Ünal, E.D. Kovetz and S.P. Patil, *Multimessenger probes of inflationary fluctuations and primordial black holes*, *Phys. Rev. D* **103** (2021) 063519 [arXiv:2008.11184] [INSPIRE].

[46] M. Shibata and M. Sasaki, *Black hole formation in the Friedmann universe: formulation and computation in numerical relativity*, *Phys. Rev. D* **60** (1999) 084002 [gr-qc/9905064] [INSPIRE].

[47] T. Harada, C.-M. Yoo, T. Nakama and Y. Koga, *Cosmological long-wavelength solutions and primordial black hole formation*, *Phys. Rev. D* **91** (2015) 084057 [arXiv:1503.03934] [INSPIRE].

[48] C.-M. Yoo, T. Harada, J. Garriga and K. Kohri, *Primordial black hole abundance from random Gaussian curvature perturbations and a local density threshold*, *PTEP* **2018** (2018) 123E01 [arXiv:1805.03946] [INSPIRE].

[49] C. Germani and I. Musco, *Abundance of primordial black holes depends on the shape of the inflationary power spectrum*, *Phys. Rev. Lett.* **122** (2019) 141302 [arXiv:1805.04087] [INSPIRE].

[50] I. Musco, *Threshold for primordial black holes: dependence on the shape of the cosmological perturbations*, *Phys. Rev. D* **100** (2019) 123524 [arXiv:1809.02127] [INSPIRE].

[51] A. Escrivà, *Simulation of primordial black hole formation using pseudo-spectral methods*, *Phys. Dark Univ.* **27** (2020) 100466 [arXiv:1907.13065] [INSPIRE].

[52] A. Escrivà, C. Germani and R.K. Sheth, *Universal threshold for primordial black hole formation*, *Phys. Rev. D* **101** (2020) 044022 [arXiv:1907.13311] [INSPIRE].

[53] V. Atal, J. Garriga and A. Marcos-Caballero, *Primordial black hole formation with non-Gaussian curvature perturbations*, *JCAP* **09** (2019) 073 [arXiv:1905.13202] [INSPIRE].

JCAP06(2021)022

[54] C.-M. Yoo, J.-O. Gong and S. Yokoyama, *Abundance of primordial black holes with local non-Gaussianity in peak theory*, *JCAP* **09** (2019) 033 [arXiv:1906.06790] [INSPIRE].

[55] A. Kehagias, I. Musco and A. Riotto, *Non-Gaussian formation of primordial black holes: effects on the threshold*, *JCAP* **12** (2019) 029 [arXiv:1906.07135] [INSPIRE].

[56] V. Atal, J. Cid, A. Escrivà and J. Garriga, *PBH in single field inflation: the effect of shape dispersion and non-Gaussianities*, *JCAP* **05** (2020) 022 [arXiv:1908.11357] [INSPIRE].

[57] J.M. Bardeen, J.R. Bond, N. Kaiser and A.S. Szalay, *The statistics of peaks of Gaussian random fields*, *Astrophys. J.* **304** (1986) 15 [INSPIRE].

[58] V. Atal and C. Germani, *The role of non-Gaussianities in primordial black hole formation*, *Phys. Dark Univ.* **24** (2019) 100275 [arXiv:1811.07857] [INSPIRE].

[59] C.T. Byrnes, P.S. Cole and S.P. Patil, *Steepest growth of the power spectrum and primordial black holes*, *JCAP* **06** (2019) 028 [arXiv:1811.11158] [INSPIRE].

[60] T. Nakama, J. Silk and M. Kamionkowski, *Stochastic gravitational waves associated with the formation of primordial black holes*, *Phys. Rev. D* **95** (2017) 043511 [arXiv:1612.06264] [INSPIRE].

[61] J.C. Niemeyer and K. Jedamzik, *Dynamics of primordial black hole formation*, *Phys. Rev. D* **59** (1999) 124013 [astro-ph/9901292] [INSPIRE].

[62] C. Germani and R.K. Sheth, *Nonlinear statistics of primordial black holes from Gaussian curvature perturbations*, *Phys. Rev. D* **101** (2020) 063520 [arXiv:1912.07072] [INSPIRE].

[63] W.H. Kinney, *Horizon crossing and inflation with large η*, *Phys. Rev. D* **72** (2005) 023515 [gr-qc/0503017] [INSPIRE].

[64] H. Deng, A. Vilenkin and M. Yamada, *CMB spectral distortions from black holes formed by vacuum bubbles*, *JCAP* **07** (2018) 059 [arXiv:1804.10059] [INSPIRE].

[65] B.J. Carr, *Pregalactic black hole accretion and the thermal history of the universe*, *Mon. Not. Roy. Astron. Soc.* **194** (1981) 639.

[66] M. Ricotti, J.P. Ostriker and K.J. Mack, *Effect of primordial black holes on the Cosmic Microwave Background and cosmological parameter estimates*, *Astrophys. J.* **680** (2008) 829 [arXiv:0709.0524] [INSPIRE].

[67] Y. Ali-Haïmoud and M. Kamionkowski, *Cosmic Microwave Background limits on accreting primordial black holes*, *Phys. Rev. D* **95** (2017) 043534 [arXiv:1612.05644] [INSPIRE].

[68] B.J. Carr and M. Sakellariadou, *Dynamical constraints on dark compact objects*, *Astrophys. J.* **516** (1999) 195 [INSPIRE].

[69] B. Carr and J. Silk, *Primordial black holes as generators of cosmic structures*, *Mon. Not. Roy. Astron. Soc.* **478** (2018) 3756 [arXiv:1801.00672] [INSPIRE].

[70] J. García-Bellido, M. Peloso and C. Unal, *Gravitational wave signatures of inflationary models from primordial black hole dark matter*, *JCAP* **09** (2017) 013 [arXiv:1707.02441] [INSPIRE].

[71] S. Mukherjee and J. Silk, *Can we distinguish astrophysical from primordial black holes via the stochastic gravitational wave background?*, arXiv:2105.11139 [INSPIRE].

JCAP06(2021)022

4 Conclusions and future prospects

Primordial black holes, particularly the ones that could originate from the collapse of non-linear perturbations at their horizon re-entry, constitute an excellent probe of the power spectrum at small scales and therefore could be used to partially reconstruct the inflationary potential beyond the ~ 7 *e-folds* constrained by measurements of CMB anisotropies and surveys of the large scale structure. Over the years, a number of possible mechanisms of formation have been proposed predicting a significant abundance of PBHs for a broad range of masses, from tiny ones, $10^{-18}\,\mathrm{M}_\odot$, up to stupendously massive ones with $\gtrsim 10^{10}\,\mathrm{M}_\odot$. In some cases, PBHs were even proposed to comprise the totality of DM, in the range of asteroid masses $10^{-16} \lesssim M_{PBH}/M_\odot \lesssim 10^{-10}$, after the reappraisal of the observational constraints on their abundance [117, 164].

These PBHs could have different observational signatures depending on their mass, or equivalently on the time of their formation; a population of evaporating light PBHs or one accreting at the *super-Eddington* limit at high redshifts, would alter the thermal and ionisation history of the Universe, whereas stellar PBHs could form binaries and merge within a Hubble time, thus emitting gravitational waves detectable by *LIGO/VIRGO*. These constraints, though, seem to overlook certain aspects of the formation and evolution of the PBHs, such as the fact that PBHs could be formed having a broad rather than a narrow mass function, being spatially clustered or that they could accrete from an early epoch, leading to ambiguous upper bounds on the fraction of dark matter in PBH. Accounting for any type of non-Gaussianities will also provide us with a more robust theoretical understanding of

the threshold of formation on different cosmological settings.

The work collected in Chapter 2 focuses on processes that could alter the evolution of $\mathcal{O}(10\ \mathrm{M}_\odot)$ PBH binaries with the subsequent reappraisal of the constraints on their abundances. More precisely, in [118], the effect of matter and radiation perturbations on the distribution of orbital parameters of PBH binaries, is investigated for three distinct profiles of an enhanced power spectrum at small scales. The first example is that of a scale-invariant power spectrum at the CMB scales, while the second template is an enhanced power spectrum at the intermediate scales, *i.e* at the comoving size of the binary at the time of its formation, and lastly a power spectrum that is considerably enhanced at comoving scales similar to the ones associated with the formation of $30\ \mathrm{M}_\odot$ PBHs. The effects of enhanced cosmological perturbations were neglected in previous analyses, resulting in more severe bounds on the abundance of PBHs in DM [165]. Their inclusion provides an extra source of torque to the binary, competing the one of the nearest PBH, leading to a different distribution of binary lifetimes and thus merging history. The effect of cosmological perturbations is shown to be prominent for lower abundances, relaxing the constraints on $30\ \mathrm{M}_\odot$ PBHs to $f \leq 0.1$ for an enhanced power spectrum at binary scales. Surprisingly, it is found to be subdominant for a power spectrum which is enhanced at PBH formation scales, unless this feature is rather broad. Note also that for $f \gtrsim 0.1$ binaries can be disrupted by collision with compact N-body systems [166], which may substantially deplete the population of primordial binaries. This effect could lead to the complete evasion of bounds on the abundance of PBHs. Further investigation of these effects seems to require numerical simulations, and remains a rather interesting line of research. Additionally, I introduce the *"universality" parameter* α, defined in [167], as an observational probe in order to disentangle the two channels for providing torque to the binary. The advent of ground-based gravitational wave detectors and the accumulation of reliable data of mergers in the next 5 years will result in an accurate, up to $\mathcal{O}(15\%)$, estimation of the parameter α, granting us the opportunity to explore the dynamical evolution of said binaries.

The second publication [119] presented in Chapter 2, studies the effect of a non-

Poissonian spatial distribution of PBHs on their merger rate distribution. By employing a simple phenomenological model of clustering, such as the one shown in Eq.(2.2), the merger rate actually is shown to drop really sharply for larger fractions of DM in PBHs ($f \gtrsim 10^{-3}$). The fact that the merger rate could be quenched at high abundances has been also reported in [166, 168]. There, by the use of numerical simulations also, they showed that their estimates for the rate could not be trusted for abundances $f > 0.1$, since the effect of PBH clusters that form even before matter-radiation equality [169, 149, 170] on the distribution of mergers cannot be neglected. This suppression for larger abundances f, leads to the appearance of degeneracies between the model's parameters, since two different populations of PBHs could yield the same merger rate. Two observational approaches that could disentangle any such degeneracies are explored; namely the evolution of merger rate with redshift probed by upcoming ground-based interferometers, such as the *Einstein Telescope* or *LISA* [171], up to $z \sim 30$ and the detection of the stochastic gravitational waves background by the *LIGO/VIRGO* collaboration.

The constraints on the abundance of PBHs with masses larger than the ones in the galactic centers, $M_{PBH} \gtrsim 10^5$ $M_\odot$, are mainly due to the spectral μ-distortions of the CMB. The physics of accretion, particularly for masses larger than 10^4 $M_\odot$ is not very well known. Whether the black hole is accreting via a disk [163, 172] or until redshifts smaller than $z \lesssim 300$ (when the CMB radiation is still sensitive to energy injections [163]), will affect the estimation of the abundances at the corresponding scales [173]. Additionally, in Chapter 3, I argue that a more thorough evaluation of these bounds is really relevant, since a population of such stupendously large PBHs could explain the isotropic signal detected by the *NANOGrav* collaboration. More precisely, the peak of the signal was fitted with the amplitude and spectral index of the stochastic background of gravitational waves from mergers of binaries systems of PBHs with masses $10^{11} - 10^{12}$ $M_\odot$, where it was found that an abundance $\sim 0.1\%$ could explain such signal. A non-Gaussian inflationary model with a constant roll phase could accommodate for a population of stupendously massive PBHs that evade the CMB spectral distortions. It is shown that for moderate values of f_{NL} ($f_{NL} \gtrsim 3$), the bounds from μ-distortions are evaded, given that for increasing f_{NL}

the threshold for formation is decreasing. These results are presented in [121]. Future experiments, such as *LISA* or the third generation of interferometric detectors *Einstein Telescope* and *Cosmic Explorer*, aim to detect the gravitational remnants of mergers of larger masses and at higher redshifts [174]. Mapping the spatial distribution of the coalescences and cross-correlating them with the positions of galaxies, using surveys of the large scale structures [175], or intensity mappings of the neutral hydrogen [176] from forthcoming experiments such as *Square Kilometer Array Observatory* [177] respectively, will yield insight into the nature of the progenitors (whether they are primordial or stellar). Furthermore, if any binary is observed to merge at redshifts higher than the appearance of the first population of stars (*PopIII*), around $z \sim 20$ [178], then this would be an irrefutable proof of their primordial origin. If such a primordial compact object is detected, then this would be an important milestone in early Universe cosmology.

The project that generated these results received support from a fellowship by ***la Caixa Foundation (ID 100010434)*** with code **LCF/BQ/IN17/11620034**. The project also received support from the European Union's Horizon 2020 research and innovation programme under the ***Marie Skłodowska-Curie*** grant agreement **No. 713673**.

Bibliography

[1] A. A. Penzias and R. W. Wilson, "A Measurement of excess antenna temperature at 4080-Mc/s," *Astrophys. J.*, vol. 142, pp. 419–421, 1965.

[2] G. F. Smoot *et al.*, "Structure in the COBE differential microwave radiometer first year maps," *Astrophys. J. Lett.*, vol. 396, pp. L1–L5, 1992.

[3] C. L. Bennett *et al.*, "Nine-Year Wilkinson Microwave Anisotropy Probe (WMAP) Observations: Final Maps and Results," *Astrophys. J. Suppl.*, vol. 208, p. 20, 2013.

[4] N. Aghanim *et al.*, "Planck 2018 results. VI. Cosmological parameters," *Astron. Astrophys.*, vol. 641, p. A6, 2020.

[5] N. Aghanim *et al.*, "Planck 2018 results. I. Overview and the cosmological legacy of Planck," *Astron. Astrophys.*, vol. 641, p. A1, 2020.

[6] D. J. Fixsen, "The Temperature of the Cosmic Microwave Background," *Astrophys. J.*, vol. 707, pp. 916–920, 2009.

[7] D. Baumann, "Inflation," in *Theoretical Advanced Study Institute in Elementary Particle Physics: Physics of the Large and the Small*, 2009. [arXiv:0907.5424 [hep-th]].

[8] A. H. Guth, "Inflationary universe: A possible solution to the horizon and flatness problems," *Phys. Rev. D*, vol. 23, pp. 347–356, Jan 1981.

[9] A. Albrecht and P. J. Steinhardt, "Cosmology for Grand Unified Theories with radiatively induced symmetry breaking," *Phys. Rev. Lett.*, vol. 48, pp. 1220–1223, Apr 1982.

[10] M. Giovannini, "Gravitational waves constraints on post-inflationary phases stiffer than radiation," *Phys. Rev. D*, vol. 58, p. 083504, 1998.

[11] L. A. Boyle and P. J. Steinhardt, "Probing the early universe with inflationary gravitational waves," *Phys. Rev. D*, vol. 77, p. 063504, 2008.

[12] L. A. Boyle and A. Buonanno, "Relating gravitational wave constraints from primordial nucleosynthesis, pulsar timing, laser interferometers, and the CMB: Implications for the early Universe," *Phys. Rev. D*, vol. 78, p. 043531, 2008.

[13] A. P. S. Yadav and B. D. Wandelt, "Primordial Non-Gaussianity in the Cosmic Microwave Background," *Adv. Astron.*, vol. 2010, p. 565248, 2010.

[14] V. F. Mukhanov, "The quantum theory of gauge-invariant cosmological perturbations," *Zhurnal Eksperimentalnoi i Teoreticheskoi Fiziki*, vol. 94, pp. 1–11, July 1988.

[15] M. Sasaki, "Large Scale Quantum Fluctuations in the Inflationary Universe," *Progress of Theoretical Physics*, vol. 76, no. 5, pp. 1036–1046, 1986.

[16] V. Mukhanov and S. Winitzki, *Introduction to quantum effects in gravity*. Cambridge University Press, 6 2007.

[17] Y. Akrami *et al.*, "Planck 2018 results. X. Constraints on inflation," *Astron. Astrophys.*, vol. 641, p. A10, 2020.

[18] P. A. R. Ade *et al.*, "BICEP2 / Keck Array x: Constraints on Primordial Gravitational Waves using Planck, WMAP, and New BICEP2/Keck Observations through the 2015 Season," *Phys. Rev. Lett.*, vol. 121, p. 221301, 2018.

[19] A. Kogut *et al.*, "The Primordial Inflation Explorer (PIXIE): A Nulling Polarimeter for Cosmic Microwave Background Observations," *JCAP*, vol. 07, p. 025, 2011.

[20] M. Hazumi *et al.*, "LiteBIRD: JAXA's new strategic L-class mission for all-sky surveys of cosmic microwave background polarization," *Proc. SPIE Int. Soc. Opt. Eng.*, vol. 11443, p. 114432F, 2020.

[21] F. Zwicky, "Republication of: The redshift of extragalactic nebulae," *General Relativity and Gravitation*, vol. 41, pp. 207–224, Jan. 2009.

[22] V. C. Rubin and W. K. Ford, Jr., "Rotation of the Andromeda Nebula from a Spectroscopic Survey of Emission Regions," *Astrophys. J.*, vol. 159, pp. 379–403, 1970.

[23] K. Freese, "Status of Dark Matter in the Universe," *Int. J. Mod. Phys.*, vol. 1, no. 06, pp. 325–355, 2017.

[24] U. G. Briel and J. P. Henry, "An x-ray temperature map of coma," 11 1997. astro-ph/9711237.

[25] D. Clowe, M. Bradac, A. H. Gonzalez, M. Markevitch, S. W. Randall, C. Jones, and D. Zaritsky, "A direct empirical proof of the existence of dark matter," *Astrophys. J. Lett.*, vol. 648, pp. L109–L113, 2006.

[26] N. Jeffrey *et al.*, "Dark Energy Survey Year 3 results: curved-sky weak lensing mass map reconstruction," 2021. [arXiv:2105.13539 [astro-ph.CO]].

[27] T. H. Reiprich *et al.*, "The Abell 3391/95 galaxy cluster system: A 15 Mpc intergalactic medium emission filament, a warm gas bridge, infalling matter clumps, and (re-) accelerated plasma discovered by combining SRG/eROSITA data with ASKAP/EMU and DECam data," *Astron. Astrophys.*, vol. 647, p. A2, 2021.

[28] S. E. Hong, D. Jeong, H. Seong Hwang, and J. Kim, "Revealing the Local Cosmic Web from galaxies by deep learning," *The Astrophysical Journal*, vol. 913, p. 76, May 2021.

[29] V. Mukhanov, *Physical Foundations of Cosmology*. Oxford: Cambridge University Press, 2005.

[30] M. Davis, G. Efstathiou, C. S. Frenk, and S. D. M. White, "The evolution of large-scale structure in a universe dominated by cold dark matter," *The Astrophysical Journal*, vol. 292, p. 371, May 1985.

[31] P. A. R. Ade *et al.*, "Planck 2013 results. XV. CMB power spectra and likelihood," *Astron. Astrophys.*, vol. 571, p. A15, 2014.

[32] N. Aghanim *et al.*, "Planck 2018 results. V. CMB power spectra and likelihoods," *Astron. Astrophys.*, vol. 641, p. A5, 2020.

[33] G. Steigman, B. Dasgupta, and J. F. Beacom, "Precise Relic WIMP Abundance and its Impact on Searches for Dark Matter Annihilation," *Phys. Rev. D*, vol. 86, p. 023506, 2012.

[34] G. Arcadi, M. Dutra, P. Ghosh, M. Lindner, Y. Mambrini, M. Pierre, S. Profumo, and F. S. Queiroz, "The waning of the WIMP? A review of models, searches, and constraints," *Eur. Phys. J. C*, vol. 78, no. 3, p. 203, 2018.

[35] R. D. Peccei and H. R. Quinn, "Constraints imposed by CP conservation in the presence of pseudoparticles," *Phys. Rev. D*, vol. 16, pp. 1791–1797, Sep 1977.

[36] A. Arvanitaki, S. Dimopoulos, S. Dubovsky, N. Kaloper, and J. March-Russell, "String Axiverse," *Phys. Rev. D*, vol. 81, p. 123530, 2010.

[37] K. Choi, S. H. Im, and C. S. Shin, "Recent progress in the physics of axions and axion-like particles," *Annual Review of Nuclear and Particle Science*, vol. 71, Jun 2021.

[38] P. Sikivie, "Experimental tests of the "invisible" axion," *Phys. Rev. Lett.*, vol. 51, pp. 1415–1417, Oct 1983.

[39] S. J. Asztalos *et al.*, "An Improved RF cavity search for halo axions," *Phys. Rev. D*, vol. 69, p. 011101, 2004.

[40] E. Aprile *et al.*, "First Axion Results from the XENON100 Experiment," *Phys. Rev. D*, vol. 90, no. 6, p. 062009, 2014. [Erratum: Phys.Rev.D 95, 029904 (2017)].

[41] P. W. Graham, I. G. Irastorza, S. K. Lamoreaux, A. Lindner, and K. A. van Bibber, "Experimental Searches for the Axion and Axion-Like Particles," *Ann. Rev. Nucl. Part. Sci.*, vol. 65, pp. 485–514, 2015.

[42] L. Di Luzio, M. Giannotti, E. Nardi, and L. Visinelli, "The landscape of QCD axion models," *Physics Reports*, vol. 870, p. 1–117, Jul 2020.

[43] B. Paczynski, "Gravitational microlensing by the galactic halo," *Astrophys. J.*, vol. 304, pp. 1–5, 1986.

[44] P. Tisserand *et al.*, "Limits on the Macho Content of the Galactic Halo from the EROS-2 Survey of the Magellanic Clouds," *Astron. Astrophys.*, vol. 469, pp. 387–404, 2007.

[45] R. A. Allsman *et al.*, "MACHO project limits on black hole dark matter in the 1-30 solar mass range," *Astrophys. J. Lett.*, vol. 550, p. L169, 2001.

[46] C. Alcock *et al.*, "EROS and MACHO combined limits on planetary mass dark matter in the galactic halo," *Astrophys. J. Lett.*, vol. 499, p. L9, 1998.

[47] B. P. Abbott and et al., "Observation of gravitational waves from a binary black hole merger," *Phys. Rev. Lett.*, vol. 116, p. 061102, Feb 2016.

[48] Y. B. Zel'dovich and I. D. Novikov, "The Hypothesis of Cores Retarded during Expansion and the Hot Cosmological Model," *Soviet Astronomy*, vol. 10, p. 602, Feb. 1967.

[49] S. Hawking, "Gravitationally collapsed objects of very low mass," *Mon. Not. Roy. Astron. Soc.*, vol. 152, p. 75, 1971.

[50] B. J. Carr and S. W. Hawking, "Black holes in the early Universe," *Mon. Not. Roy. Astron. Soc.*, vol. 168, pp. 399–415, 1974.

[51] B. J. Carr, "The Primordial black hole mass spectrum," *Astrophys. J.*, vol. 201, pp. 1–19, 1975.

[52] B. Carr and F. Kühnel, "Primordial black holes as dark matter: Recent developments," *Annual Review of Nuclear and Particle Science*, vol. 70, p. 355–394, Oct 2020.

[53] S. W. Hawking, "Particle Creation by Black Holes," *Commun. Math. Phys.*, vol. 43, pp. 199–220, 1975. [Erratum: Commun.Math.Phys. 46, 206 (1976)].

[54] R. Abbott *et al.*, "Properties and Astrophysical Implications of the 150 $M_\odot$ Binary Black Hole Merger GW190521," *Astrophys. J. Lett.*, vol. 900, no. 1, p. L13, 2020.

[55] R. Abbott *et al.*, "GW190814: Gravitational Waves from the Coalescence of a 23 Solar Mass Black Hole with a 2.6 Solar Mass Compact Object," *Astrophys. J. Lett.*, vol. 896, no. 2, p. L44, 2020.

[56] W. A. Fowler and F. Hoyle, "Neutrino Processes and Pair Formation in Massive Stars and Supernovae," *Astrophys. J. Suppl.*, vol. 9, pp. 201–319, 1964.

[57] K. Belczynski *et al.*, "The Effect of Pair-Instability Mass Loss on Black Hole Mergers," *Astron. Astrophys.*, vol. 594, p. A97, 2016.

[58] K. Vattis, I. S. Goldstein, and S. M. Koushiappas, "Could the 2.6 $M_\odot$ object in GW190814 be a primordial black hole?," *Phys. Rev. D*, vol. 102, no. 6, p. 061301, 2020.

[59] A. Gupta, D. Gerosa, K. G. Arun, E. Berti, W. M. Farr, and B. S. Sathyaprakash, "Black holes in the low mass gap: Implications for gravitational wave observations," *Phys. Rev. D*, vol. 101, no. 10, p. 103036, 2020.

[60] B. P. Abbott *et al.*, "GW190425: Observation of a Compact Binary Coalescence with Total Mass $\sim 3.4 M_\odot$," *Astrophys. J. Lett.*, vol. 892, no. 1, p. L3, 2020.

[61] R. Abbott, T. D. Abbott, S. Abraham, F. Acernese, K. Ackley, C. Adams, R. X. Adhikari, V. B. Adya, C. Affeldt, M. Agathos, and et al., "Properties and astrophysical implications of the 150 $M_\odot$ binary black hole merger GW190521," *The Astrophysical Journal*, vol. 900, p. L13, Sep 2020.

[62] T. Harada, C.-M. Yoo, K. Kohri, K.-i. Nakao, and S. Jhingan, "Primordial black hole formation in the matter-dominated phase of the Universe," *Astrophys. J.*, vol. 833, no. 1, p. 61, 2016.

[63] B. Carr, T. Tenkanen, and V. Vaskonen, "Primordial black holes from inflaton and spectator field perturbations in a matter-dominated era," *Phys. Rev. D*, vol. 96, no. 6, p. 063507, 2017.

[64] P. Ivanov, P. Naselsky, and I. Novikov, "Inflation and primordial black holes as dark matter," *Phys. Rev. D*, vol. 50, pp. 7173–7178, Dec 1994.

[65] J. Garcia-Bellido, A. D. Linde, and D. Wands, "Density perturbations and black hole formation in hybrid inflation," *Phys. Rev. D*, vol. 54, pp. 6040–6058, 1996.

[66] J. Yokoyama, "Formation of MACHO primordial black holes in inflationary cosmology," *Astron. Astrophys.*, vol. 318, p. 673, 1997.

[67] S. Clesse and J. García-Bellido, "Massive Primordial Black Holes from Hybrid Inflation as Dark Matter and the seeds of Galaxies," *Phys. Rev. D*, vol. 92, no. 2, p. 023524, 2015.

[68] B. Carr, S. Clesse, J. García-Bellido, and F. Kühnel, "Cosmic conundra explained by thermal history and primordial black holes," *Phys. Dark Univ.*, vol. 31, p. 100755, 2021.

[69] K. Jedamzik, "Primordial black hole formation during the QCD epoch," *Phys. Rev. D*, vol. 55, pp. 5871–5875, 1997.

[70] M. Y. Khlopov, R. V. Konoplich, S. G. Rubin, and A. S. Sakharov, "First-order phase transitions as a source of black holes in the early universe," *Grav. Cosmol.*, vol. 6, pp. 153–156, 2000.

[71] V. A. Berezin, V. A. Kuzmin, and I. I. Tkachev, "Thin wall vacuum domains evolution," *Phys. Lett. B*, vol. 120, pp. 91–96, 1983.

[72] S. G. Rubin, M. Y. Khlopov, and A. S. Sakharov, "Primordial black holes from nonequilibrium second order phase transition," *Grav. Cosmol.*, vol. 6, pp. 51–58, 2000.

[73] H. Deng, J. Garriga, and A. Vilenkin, "Primordial black hole and wormhole formation by domain walls," *JCAP*, vol. 04, p. 050, 2017.

[74] F. Ferrer, E. Masso, G. Panico, O. Pujolas, and F. Rompineve, "Primordial Black Holes from the QCD axion," *Phys. Rev. Lett.*, vol. 122, no. 10, p. 101301, 2019.

[75] S. W. Hawking, I. G. Moss, and J. M. Stewart, "Bubble collisions in the very early universe," *Phys. Rev. D*, vol. 26, pp. 2681–2693, Nov 1982.

[76] M. Lewicki and V. Vaskonen, "On bubble collisions in strongly supercooled phase transitions," *Phys. Dark Univ.*, vol. 30, p. 100672, 2020.

[77] H. Kodama, M. Sasaki, and K. Sato, "Abundance of Primordial Holes Produced by Cosmological First-Order Phase Transition," *Progress of Theoretical Physics*, vol. 68, no. 6, pp. 1979–1998, 1982.

[78] C. Germani and I. Musco, "Abundance of Primordial Black Holes Depends on the Shape of the Inflationary Power Spectrum," *Phys. Rev. Lett.*, vol. 122, no. 14, p. 141302, 2019.

[79] B. J. Carr, K. Kohri, Y. Sendouda, and J. Yokoyama, "New cosmological constraints on primordial black holes," *Phys. Rev. D*, vol. 81, p. 104019, 2010.

[80] C. T. Byrnes, P. S. Cole, and S. P. Patil, "Steepest growth of the power spectrum and primordial black holes," *JCAP*, vol. 06, p. 028, 2019.

[81] C. Germani and T. Prokopec, "On primordial black holes from an inflection point," *Phys. Dark Univ.*, vol. 18, pp. 6–10, 2017.

[82] G. Ballesteros and M. Taoso, "Primordial black hole dark matter from single field inflation," *Phys. Rev. D*, vol. 97, p. 023501, Jan 2018.

[83] M. P. Hertzberg and M. Yamada, "Primordial black holes from polynomial potentials in single field inflation," *Phys. Rev. D*, vol. 97, p. 083509, Apr 2018.

[84] J. Martin, H. Motohashi, and T. Suyama, "Ultra Slow-Roll Inflation and the non-Gaussianity Consistency Relation," *Phys. Rev. D*, vol. 87, no. 2, p. 023514, 2013.

[85] M. H. Namjoo, H. Firouzjahi, and M. Sasaki, "Violation of non-Gaussianity consistency relation in a single field inflationary model," *EPL*, vol. 101, no. 3, p. 39001, 2013.

[86] V. Atal, J. Garriga, and A. Marcos-Caballero, "Primordial black hole formation with non-Gaussian curvature perturbations," *JCAP*, vol. 09, p. 073, 2019.

[87] H. Motohashi and W. Hu, "Primordial Black Holes and Slow-Roll Violation," *Phys. Rev. D*, vol. 96, no. 6, p. 063503, 2017.

[88] S. Chongchitnan and G. Efstathiou, "Accuracy of slow-roll formulae for inflationary perturbations: implications for primordial black hole formation," *JCAP*, vol. 2007, p. 011–011, Jan 2007.

[89] G. Ballesteros, J. Rey, M. Taoso, and A. Urbano, "Primordial black holes as dark matter and gravitational waves from single-field polynomial inflation," *JCAP*, vol. 2020, p. 025–025, Jul 2020.

[90] K. Dimopoulos, "Ultra slow-roll inflation demystified," *Phys. Lett. B*, vol. 775, pp. 262–265, 2017.

[91] J. M. Bardeen, J. R. Bond, N. Kaiser, and A. S. Szalay, "The Statistics of Peaks of Gaussian Random Fields," *Astrophys. J.*, vol. 304, pp. 15–61, 1986.

[92] V. Atal, J. Cid, A. Escrivà, and J. Garriga, "PBH in single field inflation: the effect of shape dispersion and non-gaussianities," *JCAP*, vol. 2020, p. 022–022, May 2020.

[93] V. Atal and C. Germani, "The role of non-gaussianities in Primordial Black Hole formation," *Phys. Dark Univ.*, vol. 24, p. 100275, 2019.

[94] Y.-F. Cai, X. Chen, M. H. Namjoo, M. Sasaki, D.-G. Wang, and Z. Wang, "Revisiting non-Gaussianity from non-attractor inflation models," *JCAP*, vol. 05, p. 012, 2018.

[95] M. Shibata and M. Sasaki, "Black hole formation in the friedmann universe: Formulation and computation in numerical relativity," *Phys. Rev. D*, vol. 60, p. 084002, Sep 1999.

[96] S. Young, I. Musco, and C. T. Byrnes, "Primordial black hole formation and abundance: contribution from the non-linear relation between the density and curvature perturbation," *JCAP*, vol. 11, p. 012, 2019.

[97] I. Musco, "Threshold for primordial black holes: Dependence on the shape of the cosmological perturbations," *Phys. Rev. D*, vol. 100, p. 123524, Dec 2019.

[98] M. W. Choptuik, "Universality and scaling in gravitational collapse of a massless scalar field," *Phys. Rev. Lett.*, vol. 70, pp. 9–12, Jan 1993.

[99] J. C. Niemeyer and K. Jedamzik, "Near-critical gravitational collapse and the initial mass function of primordial black holes," *Phys. Rev. Lett.*, vol. 80, pp. 5481–5484, Jun 1998.

[100] I. Musco, V. De Luca, G. Franciolini, and A. Riotto, "Threshold for primordial black holes. II. A simple analytic prescription," *Phys. Rev. D*, vol. 103, no. 6, p. 063538, 2021.

[101] T. Harada, C.-M. Yoo, and K. Kohri, "Threshold of primordial black hole formation," *Phys. Rev. D*, vol. 88, no. 8, p. 084051, 2013. [Erratum: Phys.Rev.D 89, 029903 (2014)].

[102] A. Escrivà, C. Germani, and R. K. Sheth, "Universal threshold for primordial black hole formation," *Phys. Rev. D*, vol. 101, no. 4, p. 044022, 2020.

[103] J. C. Niemeyer and K. Jedamzik, "Dynamics of primordial black hole formation," *Phys. Rev. D*, vol. 59, p. 124013, May 1999.

[104] I. Musco, J. C. Miller, and L. Rezzolla, "Computations of primordial black hole formation," *Class. Quant. Grav.*, vol. 22, pp. 1405–1424, 2005.

[105] M. Sasaki, T. Suyama, T. Tanaka, and S. Yokoyama, "Primordial black holes -perspectives in gravitational wave astronomy-," *Class. Quant. Grav.*, vol. 35, no. 6, p. 063001, 2018.

[106] R. Kimura, T. Suyama, M. Yamaguchi, and Y.-L. Zhang, "Reconstruction of Primordial Power Spectrum of curvature perturbation from the merger rate of Primordial Black Hole Binaries," *JCAP*, vol. 04, p. 031, 2021.

[107] A. D. Gow, C. T. Byrnes, P. S. Cole, and S. Young, "The power spectrum on small scales: Robust constraints and comparing PBH methodologies," *JCAP*, vol. 02, p. 002, 2021.

[108] A. Dolgov and J. Silk, "Baryon isocurvature fluctuations at small scales and baryonic dark matter," *Phys. Rev. D*, vol. 47, pp. 4244–4255, May 1993.

[109] B. Carr, M. Raidal, T. Tenkanen, V. Vaskonen, and H. Veermäe, "Primordial black hole constraints for extended mass functions," *Phys. Rev. D*, vol. 96, no. 2, p. 023514, 2017.

[110] A. M. Green, "Microlensing and dynamical constraints on primordial black hole dark matter with an extended mass function," *Phys. Rev. D*, vol. 94, no. 6, p. 063530, 2016.

[111] B. Carr and F. Kuhnel, "Primordial Black Holes as Dark Matter: Recent Developments," *Ann. Rev. Nucl. Part. Sci.*, vol. 70, pp. 355–394, 2020.

[112] A. Polnarev and R. Zembowicz, "Formation of primordial black holes by cosmic strings," *Phys. Rev. D*, vol. 43, pp. 1106–1109, Feb 1991.

[113] B. Carr, K. Kohri, Y. Sendouda, and J. Yokoyama, "Constraints on Primordial Black Holes," 2020. [arXiv:2002.12778 [astro-ph.CO]].

[114] A. M. Green and B. J. Kavanagh, "Primordial Black Holes as a dark matter candidate," *J. Phys. G*, vol. 48, no. 4, p. 4, 2021.

[115] A. Katz, J. Kopp, S. Sibiryakov, and W. Xue, "Femtolensing by Dark Matter Revisited," *JCAP*, vol. 12, p. 005, 2018.

[116] A. M. Green, "Astrophysical uncertainties on stellar microlensing constraints on multi-Solar mass primordial black hole dark matter," *Phys. Rev. D*, vol. 96, no. 4, p. 043020, 2017.

[117] P. Montero-Camacho, X. Fang, G. Vasquez, M. Silva, and C. M. Hirata, "Revisiting constraints on asteroid-mass primordial black holes as dark matter candidates," *JCAP*, vol. 08, p. 031, 2019.

[118] J. Garriga and N. Triantafyllou, "Enhanced cosmological perturbations and the merger rate of PBH binaries," *JCAP*, vol. 2019, p. 043–043, Sep 2019.

[119] V. Atal, A. Sanglas, and N. Triantafyllou, "LIGO/VIRGO black holes and dark matter: the effect of spatial clustering," *JCAP*, vol. 2020, p. 036–036, Nov 2020.

[120] Z. Arzoumanian *et al.*, "The NANOGrav 12.5 yr Data Set: Search for an Isotropic Stochastic Gravitational-wave Background," *Astrophys. J. Lett.*, vol. 905, no. 2, p. L34, 2020.

[121] V. Atal, A. Sanglas, and N. Triantafyllou, "NANOGrav signal as mergers of Stupendously Large Primordial Black Holes," *JCAP*, vol. 06, p. 022, 2021.

[122] B. P. Abbott *et al.*, "GWTC-1: A Gravitational-Wave Transient Catalog of Compact Binary Mergers Observed by LIGO and Virgo during the First and Second Observing Runs," *Phys. Rev. X*, vol. 9, no. 3, p. 031040, 2019.

[123] R. Abbott *et al.*, "GWTC-2: Compact Binary Coalescences Observed by LIGO and Virgo During the First Half of the Third Observing Run," *Phys. Rev. X*, vol. 11, p. 021053, 2021.

[124] B. Zackay, T. Venumadhav, L. Dai, J. Roulet, and M. Zaldarriaga, "Highly spinning and aligned binary black hole merger in the Advanced LIGO first observing run," *Phys. Rev. D*, vol. 100, no. 2, p. 023007, 2019.

[125] T. Venumadhav, B. Zackay, J. Roulet, L. Dai, and M. Zaldarriaga, "New binary black hole mergers in the second observing run of Advanced LIGO and Advanced Virgo," *Phys. Rev. D*, vol. 101, no. 8, p. 083030, 2020.

[126] A. H. Nitz, T. Dent, G. S. Davies, S. Kumar, C. D. Capano, I. Harry, S. Mozzon, L. Nuttall, A. Lundgren, and M. Tápai, "2-OGC: Open Gravitational-wave Catalog of binary mergers from analysis of public Advanced LIGO and Virgo data," *Astrophys. J.*, vol. 891, p. 123, 3 2020.

[127] V. De Luca, G. Franciolini, P. Pani, and A. Riotto, "The evolution of primordial black holes and their final observable spins," *JCAP*, vol. 04, p. 052, 2020.

[128] S. Miller, T. A. Callister, and W. M. Farr, "The low effective spin of binary black holes and implications for individual gravitational-wave events," *The Astrophysical Journal*, vol. 895, p. 128, Jun 2020.

[129] K. Belczynski *et al.*, "Evolutionary roads leading to low effective spins, high black hole masses, and O1/O2 rates for LIGO/Virgo binary black holes," *Astron. Astrophys.*, vol. 636, p. A104, 2020.

[130] Y. Huang, C.-J. Haster, S. Vitale, A. Zimmerman, J. Roulet, T. Venumadhav, B. Zackay, L. Dai, and M. Zaldarriaga, "Source properties of the lowest signal-to-noise-ratio binary black hole detections," *Phys. Rev. D*, vol. 102, no. 10, p. 103024, 2020.

[131] B. P. Abbott *et al.*, "Binary Black Hole Population Properties Inferred from the First and Second Observing Runs of Advanced LIGO and Advanced Virgo," *Astrophys. J. Lett.*, vol. 882, no. 2, p. L24, 2019.

[132] K. K. Y. Ng, S. Vitale, A. Zimmerman, K. Chatziioannou, D. Gerosa, and C.-J. Haster, "Gravitational-wave astrophysics with effective-spin measurements: asymmetries and selection biases," *Phys. Rev. D*, vol. 98, no. 8, p. 083007, 2018.

[133] V. De Luca, V. Desjacques, G. Franciolini, A. Malhotra, and A. Riotto, "The initial spin probability distribution of primordial black holes," *JCAP*, vol. 05, p. 018, 2019.

[134] M. Mirbabayi, A. Gruzinov, and J. Noreña, "Spin of Primordial Black Holes," *JCAP*, vol. 03, p. 017, 2020.

[135] A. Hall, A. D. Gow, and C. T. Byrnes, "Bayesian analysis of LIGO-Virgo mergers: Primordial vs. astrophysical black hole populations," *Phys. Rev. D*, vol. 102, p. 123524, 2020.

[136] G. Hütsi, M. Raidal, V. Vaskonen, and H. Veermäe, "Two populations of LIGO-Virgo black holes," *JCAP*, vol. 03, p. 068, 2021.

[137] M. Zevin, S. S. Bavera, C. P. L. Berry, V. Kalogera, T. Fragos, P. Marchant, C. L. Rodriguez, F. Antonini, D. E. Holz, and C. Pankow, "One Channel to Rule Them All? Constraining the Origins of Binary Black Holes Using Multiple Formation Pathways," *Astrophys. J.*, vol. 910, no. 2, p. 152, 2021.

[138] H. Tashiro and K. Kadota, "Constraining Mixed Dark-Matter Scenarios of WIMPs and Primordial Black Holes from CMB and 21-cm observations," *Phys. Rev. D*, vol. 103, no. 12, p. 123532, 2021.

[139] S. M. Boucenna, F. Kuhnel, T. Ohlsson, and L. Visinelli, "Novel Constraints on Mixed Dark-Matter Scenarios of Primordial Black Holes and WIMPs," *JCAP*, vol. 07, p. 003, 2018.

[140] J. Adamek, C. T. Byrnes, M. Gosenca, and S. Hotchkiss, "WIMPs and stellar-mass primordial black holes are incompatible," *Phys. Rev. D*, vol. 100, no. 2, p. 023506, 2019.

[141] G. Franciolini, V. Baibhav, V. De Luca, K. K. Y. Ng, K. W. K. Wong, E. Berti, P. Pani, A. Riotto, and S. Vitale, "Quantifying the evidence for primordial black holes in LIGO/Virgo gravitational-wave data," 2021. [arXiv:2105.03349 [gr-qc]].

[142] J. García-Bellido, J. F. Nuño Siles, and E. Ruiz Morales, "Bayesian analysis of the spin distribution of ligo/virgo black holes," *Physics of the Dark Universe*, vol. 31, p. 100791, Jan 2021.

[143] V. De Luca, G. Franciolini, P. Pani, and A. Riotto, "Bayesian Evidence for Both Astrophysical and Primordial Black Holes: Mapping the GWTC-2 Catalog to Third-Generation Detectors," *JCAP*, vol. 05, p. 003, 2021.

[144] T. Hartwig, M. Volonteri, V. Bromm, R. S. Klessen, E. Barausse, M. Magg, and A. Stacy, "Gravitational Waves from the Remnants of the First Stars," *Mon. Not. Roy. Astron. Soc.*, vol. 460, no. 1, pp. L74–L78, 2016.

[145] M. Punturo *et al.*, "The Einstein Telescope: A third-generation gravitational wave observatory," *Class. Quant. Grav.*, vol. 27, p. 194002, 2010.

[146] S. Dwyer, D. Sigg, S. W. Ballmer, L. Barsotti, N. Mavalvala, and M. Evans, "Gravitational wave detector with cosmological reach," *Phys. Rev. D*, vol. 91, no. 8, p. 082001, 2015.

[147] K. K. Y. Ng, S. Vitale, W. M. Farr, and C. L. Rodriguez, "Probing multiple populations of compact binaries with third-generation gravitational-wave detectors," *Astrophys. J. Lett.*, vol. 913, no. 1, p. L5, 2021.

[148] B. J. Kavanagh, D. Gaggero, and G. Bertone, "Merger rate of a subdominant population of primordial black holes," *Phys. Rev. D*, vol. 98, Jul 2018.

[149] D. Inman and Y. Ali-Haïmoud, "Early structure formation in primordial black hole cosmologies," *Phys. Rev. D*, vol. 100, no. 8, p. 083528, 2019.

[150] K. M. Belotsky, V. I. Dokuchaev, Y. N. Eroshenko, E. A. Esipova, M. Y. Khlopov, L. A. Khromykh, A. A. Kirillov, V. V. Nikulin, S. G. Rubin, and I. V. Svadkovsky, "Clusters of primordial black holes," *Eur. Phys. J. C*, vol. 79, no. 3, p. 246, 2019.

[151] M. Trashorras, J. García-Bellido, and S. Nesseris, "The clustering dynamics of primordial black boles in N-body simulations," *Universe*, vol. 7, no. 1, p. 18, 2021.

[152] V. De Luca, G. Franciolini, P. Pani, and A. Riotto, "The evolution of primordial black holes and their final observable spins," *JCAP*, vol. 04, p. 052, 2020.

[153] S. Bhagwat, V. De Luca, G. Franciolini, P. Pani, and A. Riotto, "The importance of priors on LIGO-Virgo parameter estimation: the case of primordial black holes," *JCAP*, vol. 01, p. 037, 2021.

[154] K. Kritos, V. De Luca, G. Franciolini, A. Kehagias, and A. Riotto, "The Astro-Primordial Black Hole Merger Rates: a Reappraisal," *JCAP*, vol. 05, p. 039, 2021.

[155] S. Clesse and J. García-Bellido, "Seven Hints for Primordial Black Hole Dark Matter," *Phys. Dark Univ.*, vol. 22, pp. 137–146, 2018.

[156] E. Banados *et al.*, "An 800-million-solar-mass black hole in a significantly neutral Universe at redshift 7.5," *Nature*, vol. 553, no. 7689, pp. 473–476, 2018.

[157] K. Inayoshi, E. Visbal, and Z. Haiman, "The Assembly of the First Massive Black Holes," *Ann. Rev. Astron. Astrophys.*, vol. 58, pp. 27–97, 2020.

[158] M. Volonteri and J. Bellovary, "Black Holes in the Early Universe," *Rept. Prog. Phys.*, vol. 75, p. 124901, 2012.

[159] R. Salvaterra, F. Haardt, M. Volonteri, and A. Moretti, "Limits on the high redshift growth of massive black holes," *Astron. Astrophys.*, vol. 545, p. L6, 2012.

[160] T. Nakama, T. Suyama, and J. Yokoyama, "Supermassive black holes formed by direct collapse of inflationary perturbations," *Phys. Rev. D*, vol. 94, no. 10, p. 103522, 2016.

[161] T. Nakama, B. Carr, and J. Silk, "Limits on primordial black holes from μ distortions in cosmic microwave background," *Phys. Rev. D*, vol. 97, no. 4, p. 043525, 2018.

[162] K. Kohri, T. Nakama, and T. Suyama, "Testing scenarios of primordial black holes being the seeds of supermassive black holes by ultracompact minihalos and CMB μ-distortions," *Phys. Rev. D*, vol. 90, no. 8, p. 083514, 2014.

[163] P. D. Serpico, V. Poulin, D. Inman, and K. Kohri, "Cosmic microwave background bounds on primordial black holes including dark matter halo accretion," *Phys. Rev. Res.*, vol. 2, no. 2, p. 023204, 2020.

[164] N. Smyth, S. Profumo, S. English, T. Jeltema, K. McKinnon, and P. Guhathakurta, "Updated Constraints on Asteroid-Mass Primordial Black Holes as Dark Matter," *Phys. Rev. D*, vol. 101, no. 6, p. 063005, 2020.

[165] Y. Ali-Haïmoud, E. D. Kovetz, and M. Kamionkowski, "Merger rate of primordial black-hole binaries," *Phys. Rev. D*, vol. 96, no. 12, p. 123523, 2017.

[166] M. Raidal, C. Spethmann, V. Vaskonen, and H. Veermäe, "Formation and Evolution of Primordial Black Hole Binaries in the Early Universe," *JCAP*, vol. 02, p. 018, 2019.

[167] B. Kocsis, T. Suyama, T. Tanaka, and S. Yokoyama, "Hidden universality in the merger rate distribution in the primordial black hole scenario," *Astrophys. J.*, vol. 854, no. 1, p. 41, 2018.

[168] S. Young and C. T. Byrnes, "Initial clustering and the primordial black hole merger rate," *JCAP*, vol. 03, p. 004, 2020.

[169] M. Ricotti and A. Gould, "A New Probe of Dark Matter and High-Energy Universe Using Microlensing," *Astrophys. J.*, vol. 707, pp. 979–987, 2009.

[170] M. V. Tkachev, S. V. Pilipenko, and G. Yepes, "Dark matter simulations with primordial black holes in the early universe," *Monthly Notices of the Royal Astronomical Society*, vol. 499, p. 4854–4862, Oct 2020.

[171] K. Danzmann and A. R. Diger, "LISA technology concept, status, prospects," *Classical and Quantum Gravity*, vol. 20, pp. S1–S9, apr 2003.

[172] V. Poulin, P. D. Serpico, F. Calore, S. Clesse, and K. Kohri, "CMB bounds on disk-accreting massive primordial black holes," *Phys. Rev. D*, vol. 96, no. 8, p. 083524, 2017.

[173] V. De Luca, G. Franciolini, P. Pani, and A. Riotto, "Constraints on Primordial Black Holes: the Importance of Accretion," *Phys. Rev. D*, vol. 102, no. 4, p. 043505, 2020.

[174] O. Pujolas, V. Vaskonen, and H. Veermäe, "Prospects for probing gravitational waves from primordial black hole binaries," 2021. [arXiv:2107.03379 [astro-ph.CO]].

[175] G. Scelfo, N. Bellomo, A. Raccanelli, S. Matarrese, and L. Verde, "GW×LSS: chasing the progenitors of merging binary black holes," *Journal of Cosmology and Astroparticle Physics*, vol. 2018, p. 039–039, Sep 2018.

[176] G. Scelfo, M. Spinelli, A. Raccanelli, L. Boco, A. Lapi, and M. Viel, "Gravitational waves × HI intensity mapping: cosmological and astrophysical applications," 2021. [arXiv:2106.09786 [astro-ph.CO]].

[177] R. Braun, T. Bourke, J. A. Green, E. Keane, and J. Wagg, "Advancing Astrophysics with the Square Kilometre Array," *PoS*, vol. AASKA14, p. 174, 2015.

[178] L. Haemmerlé, L. Mayer, R. S. Klessen, T. Hosokawa, P. Madau, and V. Bromm, "Formation of the first stars and black holes," *Space Sci. Rev.*, vol. 216, no. 4, p. 48, 2020.